Multi-Hazard Damage Mitigation for Low-Rise Wood-Framed Structures using a CarbonFlex Composite

by

Kittinan Dhiradhamvit

A Dissertation Presented in Partial Fulfillment
of the Requirements for the Degree
Doctor of Philosophy

Approved November 2013 by the
Graduate Supervisory Committee:

Thomas Attard, Co-Chair
Apostolos Fafitis, Co-Chair
Narayanan Neithalath
Benjamin Thomas

ARIZONA STATE UNIVERSITY

December 2013

ABSTRACT

This study focused on investigating the ability of a polymeric-enhanced high-tenacity fabric composite called CarbonFlex to mitigate damages from multi-natural hazards, which are earthquakes and tornadoes, in wood-framed structures. Typically, wood-framed shear wall is a seismic protection system used in low-rise wood structures. It is well-known that the main energy dissipation of the system is its fasteners (nails) which are not enough to dissipate energy leading to decreasing of structure's integrity. Moreover, wood shear walls could not sustain their stiffness after experiencing moderate wall drift which made them susceptible to strong aftershocks. Therefore, CarbonFlex shear wall system was proposed to be used in the wood-framed structures. Seven full-size CarbonFlex shear walls and a CarbonFlex wrapped structures were tested. The results were compared to those of conventional wood-framed shear walls and a wood structure. The comparisons indicated that CarbonFlex specimens could sustain their strength and fully recover their initial stiffness although they experienced four percent story drift while the stiffness of the conventional structure dramatically degraded. This indicated that CarbonFlex shear wall systems provided a better seismic protection to wood-framed structures. To evaluate capability of CarbonFlex to resist impact damages from wind-borne debris in tornadoes, several debris impact tests of CarbonFlex and a carbon fiber reinforced storm shelter's wall panels were conducted. The results showed that three CarbonFlex wall panels passed the test at the highest debris impact speed and the other two passed the test at the second highest speed while the carbon fiber panel failed both impact speeds.

DEDICATION

For My Parents, Family, and Asst. Prof. Yenhatai Nanna.

ACKNOWLEDGMENTS

First, I would like to give my sincere thanks to all members of my dissertation committee for their valuable time, suggestions, and many hours of assistance: Dr. Thomas Attard, Dr. Apostolos Fafitis, Dr. Benjamin Thomas, and Dr. Narayanan Neithalath.

I would like to thank Dr. Thomas Attard, my advisor, for helpful guidance, suggestions, and supports that made this dissertation possible to be done. In addition, I am really indebted to him for his friendly helps and concerns that made my hard foreign student life a lot easier. For example, he let me live in his house for free for one semester when I transferred from University of Tennessee to Arizona State University and countless helps.

I am also grateful to my family, especially, my parents who have worked at least 12 hours a day, seven days a week to support me while I was studying and preparing this dissertation.

I would like to extend my thanks to Mr. Dhiraphol Dhiradhamvit and Mr. Worrawat Yingmanokij, my brothers, who helped prepare some specimens and provided transportation. In addition, I am appreciative Mr. Hongyu Zhou for his helps, suggestions, and supports. I appreciate my friends, Mr. Suphajon Klinsuwan and Mr. Krib Sitathani, for their valuable suggestions. I also would like to thank Mr. Chase Wharton and his wife, Brittney, for their helps, lunches, and the most delicious cookies.

I am thankful to Dr. Edwin Burdette for his fellowship, kindness, and supports. Also, I would like to thank my friends in Tennessee, Dr. Akawut Siriruk and Nancy Robert, for their helps.

My experiments could not be done without helps from Joseph Williams, Isaias Martinez, Luis Bonilla, Matthew Carroll, Jessica Jia, Michael Munger, Anirudh Kumar, Joshua Anderson, Marc Tuiteleleapaga, Cory Russel, Alex Links, Francesco Kupta, and Kevin Burnish.

I would like to extend my thanks to Peter Goguen, Tyler Harris, and Kenneth Witczak for their hard work and helps. The experiments would not be success without them.

I would like to thanks Dr. Edward Gibson for his valuable suggestions and reviews of the first draft of this dissertation.

This research was funded by Department of Homeland Security sponsored Southeast Region Research Initiative (SERRI) at the Department of Energy's Oak Ridge National Laboratory.

TABLE OF CONTENTS

Page

CHAPTER Page

LIST OF TABLES

LIST OF FIGURES

Figure Page

Figure Page

Figure Page

Figure Page

LIST OF ABBREVIATIONS

μm	Micro-meter
ADR	Average Damping Ratio
APA	The Engineered Wood Association
ASCE	American Society of Civil Engineers
ASTM	American Society for Testing and Materials
BIP	Buckling Induced Pinching
CF	CarbonFlex
CFFW1	CarbonFlex Fully Wrapped Wall Number One
CFFW2	CarbonFlex Fully Wrapped Wall Number Two
CFFW3	CarbonFlex Fully Wrapped Wall Number Three
CFOW	CarbonFlex Wrapped Wall with Opening
CFPW	CarbonFlex Fully Wrapped Plywood Shear Wall
CFRP	Carbon Fiber Reinforced Polymer
CFSBW	CarbonFlex Strip Bracing Wall
CFSPW	CarbonFlex Strip Bracing with Plywood Wall
CMU	Concrete Masonry Unit
DHS	Department of Homeland Security
DMI	Damping Ratio per Square Inch
EF	Enhanced Fujita Scale
FEMA	Federal Emergency Management Agency
FRP	Fiber Reinforced Polymer
ft	foot

HPD	High Peak Displacement Time History Record
hr	Hour
ICC	International Code Council
in.	Inch
ksi	Kips per square inch
lb	Pound
in^2	Inch square
LPD	Low Peak Displacement Time History Record
MPD	Moderate Peak Displacement Time History Record
mph	Miles per hour
mm	Millimeter
NAHB	National Association of Home Builders
NOAA	National Oceanic and Atmospheric Administration
NSSA	National Storm Shelter Association
OC	On Center
OSB	Oriented Strand Board
PAN	Polyacrylonitrile
PLW	Parallel Wall (a wall subjected to the loads that are parallel to the wall's plane)
PPD-T	Poly Para-Phenyleneterephthalamide
PPW	Perpendicular Wall (a wall subjected to the loads that are perpendicular to the wall's plane)
psi	Pounds per square inch

PW1	Plywood Shear Wall Number One
PW2	Plywood Shear Wall Number Two
PYL	Post-Yield Length
SDPWS	Special Design Provisions for Wind and Seismic
sec	Second
SPSW	Steel Plate Shear Wall
TBS	Tension and Buckling Strip
WBD	Wind-Borne Debris
WiSE	Wind Science and Engineering center
USGS	United State Geological Survey

LIST OF SYMBOLS

α	Ratio of opening area to the total wall area
α_h	The average modulus degradation
α_i	A parameter defining the slope of each linear interpolation step
β	Ratio of the summation of lengths of fully sheathed segments to the total length of the wall
Δ	Beam's displacement
$\Delta\phi$	Post-yield curvature
Δ_{bend}	Deflections of framing members
Δ_{bPW1}	Bending deflection of PW1
Δ_{bPW2}	Bending deflection of PW2
Δ_{holddown}	Deformations due to slip of hold-down
Δ_{in}	Indentation created by a debris impact test missile
Δ_{nail}	Deformations due to nails' slip
Δ_p	Post-yield displacement
Δ_{pw}	Shear wall's deflection
Δ_{shear}	Through thickness shear deformations of sheathing panels
Δ_ε	A constant defining the post-yield strains
ε_F	Mean of the measured strains at fracture
ε_m	Strain at maximum strength
$\varepsilon_{\max}$	Strain at the extreme fiber of the cross-section

ε_x	Strain at some distance y
ε_Y	Mean of the yield strains
ε_{Yield}	Yield strain
θ	Beam's rotation
μ	Ductility
$\sum L_i$	Summation of lengths of fully sheathed segments
ρ_a	Air density
σ_m	Stress at maximum strength
σ_x	Stress at some distance y
σ_{yield}	Yield stress
A	Cross-section area of boundary elements (end-studs)
A_0	Area of openings
A_d	Plane area of the debris
b	Width of a shear wall
C	Shape coefficient of debris
C_0	Shear capacity adjustment factor
C-C	Carbon-to-Carbon (link)
d_a	Hold-down slip
D_{HM}	Maximum hysteretic energy dissipation
E	Modulus of elasticity
e	Vertical distance from the neutral axis of the beam to the yielding beam's fiber

E_k	Kinetic energy
e_n	Nail slip
F	Force acting on a beam
^oF	Degree Fahrenheit
F_s	Shear capacity ratio
g	Gravity
Gt	Through thickness rigidity of a sheathing panel
h	Height of a shear wall
h_p	Thickness of the polymeric constituent, which relates to its volumetric fraction, in CarbonFlex.
K_{eff}	Effective stiffness
k_{pw1}	Calculated initial stiffness of PW1
k_{pw2}	Calculated initial stiffness of PW2
L	Beam's span length
L_{tot}	Total length of a shear wall with opening
L_{CF}	Length of CarbonFlex strips used in joint wrapped PPW
M	Fixed-end moment
m	Mass
M_E	Moment at mid-span for a simple supported beam
M_{yield}	Yielding moment
n	A number of linear interpolation steps after maximum stress occurred
P_M	Maximum load
P_{MD}	Load at maximum displacement

r	Sheathed area ratio
T_a	Tachikawa Number
t_c	Curing time of the saturant resin before applying the polymeric constituent which controls the quality of bonding between the saturant resin and the polymeric constituent.
U	Wind speed
UE	Unit energy
u	Horizontal velocity of debris
v	Shear force at the top of a shear wall
v_0	Velocity
V_P	Volumetric fraction of the polymeric constituent
x	Horizontal traveling displacement of the debris
y	Vertical distance from the neutral axis of a beam

CHAPTER 1

Introduction

CarbonFlex, a new carbon fiber-based composite, was initially conceptualized and developed in 2009 by Dr. Thomas Attard and his research team starting at the University of Tennessee. The motivation for developing this innovative material originated out of a need to incorporate a structural protection material having high strength, stiffness, and ductility into various infrastructure and structural systems. CarbonFlex is composed of three constituents, which are carbon fibers (or other high tenacity fibrous systems), epoxy saturant, and a unique polymer. Each component has different roles which make CarbonFlex strong and ductile. The interfacial cohesive interaction of the three materials at the molecular levels ultimately gives CarbonFlex its unique properties such as impact resistance, damping, and energy dissipation. The carbon fiber, which has a very high strength to weight ratio, provides strength and load-bearing capacity to the system. The epoxy saturant acts as a binder for the carbon fibers and provides substrate-bonding ability while the polymer provides a measure of ductility.

A previous study (Dhiradhamvit et al. 2011) showed the positive attributes of CarbonFlex in wood-framed constructions and general structural-protection applications. The composite not only increased stiffness, but also provided tremendous ductility to structural components (e.g., wood beams) via a new concept called “sustainable negative stiffness,” where the stiffness of a CarbonFlex-wrapped wood beam became “less” negative after the peak load had been reached. This became one of the motivations behind conceptualizing idea of CarbonFlex: to protect wood-framed structures from natural hazards that induce high energy excitation or impact loading such as earthquakes

and tornadoes. In this study, the concept of CarbonFlex in wood-framed structures was implemented. Experimental tests using the CarbonFlex composite to design shear walls to add energy dissipation and damping, provide in-plane racking, provide ductility and increased R-factor, reduce displacements and accelerations resulting in a reduction in structural and non-structural damage to wood-framed constructions, and provide a path for load transfer and alleviate soft-story collapse during earthquakes, were conducted. In addition, CarbonFlex-designed storm rooms were tested under level-5 tornadoes to improve impact resistance.

Problem Statement

According to United State Geological Survey (USGS), natural hazard events are responsible for lives and billions of dollars of damages, every year in the U.S. There are many types of natural hazards that occur in the U.S. such as earthquake, flood, hurricane, thunder storm, tornado, and wild fire. One of the natural hazards that causes many lives and multi-million dollar damages is earthquake. In 1989, the Loma Prieta earthquake occurred in San Francisco. It caused more than 5.9 billion dollars in direct property damages (Nigg & Mileti, 1998). On Monday, January 17, 1994, the Northridge earthquake struck three counties (Los Angeles, Ventura and Orange) in California causing 72 deaths and 41.8 billion US dollars of direct loss (Petak & Elahi, 2000).

As an example of potential hazard, in the San Francisco Bay Area, approximately 75 percent of residents live in family-style light-frame residential wood structures in active seismic zones (Residential Building Committee, 2006; Lyons, 1998; International Code Council, 2006; International Code Council, 2007; International Code Council, 2009). The main structural component in light-frame buildings, that resists lateral forces,

is wood shear wall (NAHB Research Center, Inc., 2001; van de Lindt, 2004). Exterior wood shear walls ("shear walls") are used to increase the stiffness in structures and to reduce displacements (Lyons, 1998).

A shear wall is a wall designed to resist lateral forces which are parallel to the plane of the wall (International Code Council, 2009). In a building with a shear wall system, lateral loads created by wind or earthquake will be transferred from floors to the foundation by shear walls. There are many types of shear walls depending on construction materials. For example, steel plate shear wall consists of a steel plate welded to the boundary elements which are columns and beams (Astaneh‐Asl, 2008). A wood shear wall is composed of sheathing materials, which are plywood, gypsum board, or oriented strand board (OSB), fastened to wood framings using appropriate nailing schedules and properly secured to roof and foundation as shown in figure 1 (APA – The Engineered Wood Association, 2007).

The high in-plane shear force resistance (APA – The Engineered Wood Association, 2007) enables shear walls to provide structural rigidity and reduce deflections and inter-story drifts (van de Lindt, 2004; Filiatrault, Isoda, & Folz, 2003; Tuomi & McCutcheon, 1978). In addition, nail fasteners provide hysteretic damping to the framing members (Robert H. Falk & Itani, 1987; Serrette et al., 1997) for additional side-sway resistance. This "rigid" design philosophy allows a shear transfer of lateral loads to the foundations and prevents panel buckling in conventional light frame construction, including homes, apartment complexes, and commercial buildings. However, light-frame residential wood structures having symmetrical floor plans are susceptible to earthquake damage (R.H. Falk & Soltis, 1988) even though wood

inherently flexes and provides natural energy dissipation (Homeland Security Department, 2006).

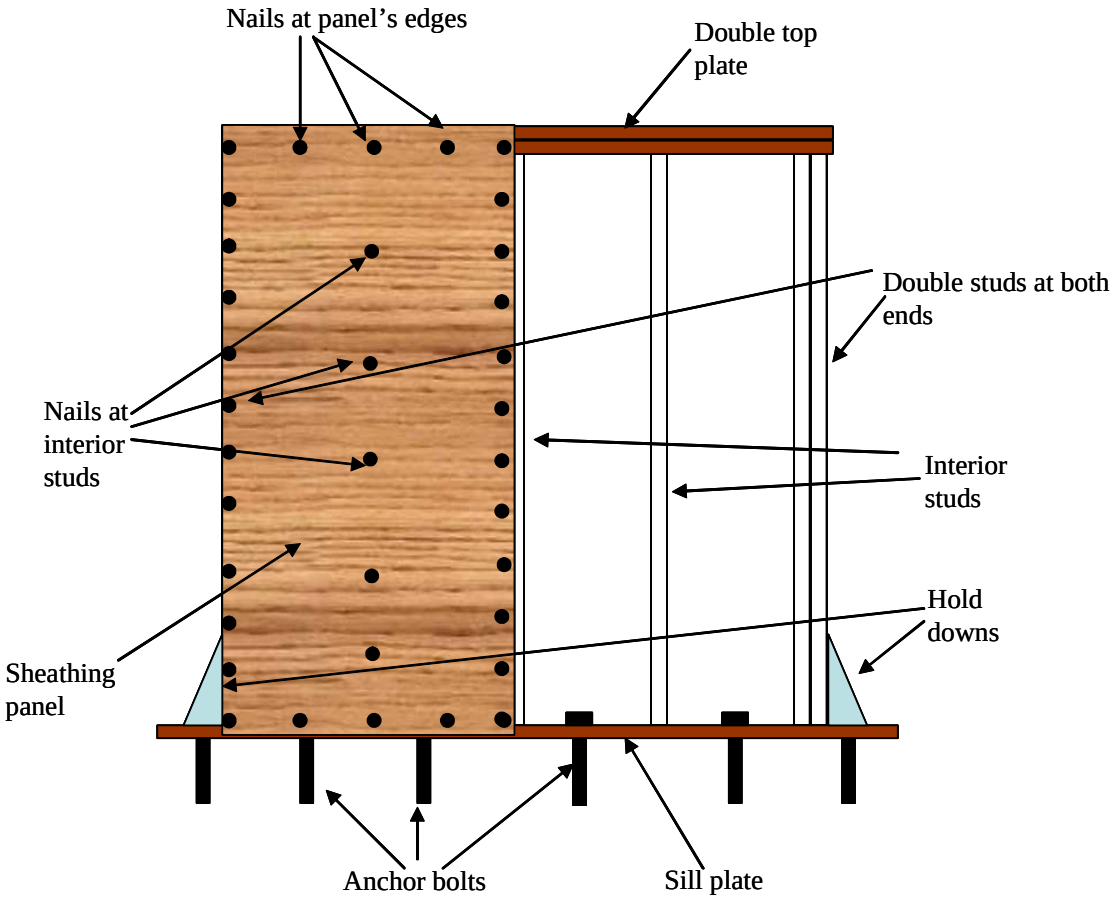

Figure 1. Diagram of shear wall.

Shaking table tests indicated that traditional shear walls may not provide a sufficient energy release mechanism, resulting in large accelerations and displacements (Dhiradhamvit et al., 2011). In addition, racking strength in this light becomes a very important consideration. Too little deflection of the shear wall assemblies provided by racking results in a concentration of forces in the panel where shear failure can occur, whereas too much deflection leads to a greater loss of fastener integrity (Beall et al., 2006).

Current design standards rely too heavily on the hysteretic damping of fasteners which (1) provide minimal viscous-type damping necessary to dissipate energy, and (2) have shown a propensity for pulling though sheathing or withdrawing from the frame resulting in sheathing failures, which often occurs at moderate wall drift as nail connections undergo extensive deformations (Seaders et al., 2009). Shaking table tests conducted by Attard (Dhiradhamvit et al., 2011) as well as by other studies (Xu & Mishra, 2004; Lebeda, Gupta, Rosowsky, & Dolan, 2005) confirm these findings and identify a common problem with current code-designed shear walls, which are over-rigidly designed and provide insufficient viscous-type damping and energy dissipation (that may result in shear panel failure, wall softening, uplift, and excessive drifts).

ASCE 7-10 (American Society of Civil Engineers, 2010) defined a story that has lateral stiffness less than 70 percent of that of the story above or less than 80 percent of the average stiffness of three stories above as a “soft-story.” A good example of a soft-story is a garage that has rooms above it. The soft-story is a serious problem that can cause a structure to collapse (Misam & Mangulkar Madhuri, 2012; Fakhouri, & Igarashi, 2012). Due to insufficient energy dissipation of nails in wood shear walls, damages, such as nail pulled out, nail sheared off, and detaching of the plywood panels, can occur during seismic events. Consequently, shear wall damages can dramatically decrease the stiffness and strength of low-rise wood-framed constructions, resulting in “earthquake induced” soft-story collapse.

Earthquake aftershocks, i.e., shaking motion occurring after the main seismic event (Yin & Li, 2011), may also have large magnitude (although typically less than the main shock event. The main shock, in fact, of the magnitude 6.7 earthquake in

Northridge, California, that remains the largest earthquake in US history, economic-wise, was followed by thousands of aftershocks. The largest measured magnitude of these aftershocks is 5.9 (McDonald, Bozorgnia, & Osteraas, 2000). In 2008, after the magnitude 8.0, Wenchuan earthquake, 86,403 aftershocks (eight aftershocks have magnitude greater than 6.0 and 40 aftershocks have magnitude greater than 5.0) struck structures that had already experienced damages by the main shock, elevating the severity of damage and subsequent collapses (Huang, Qian, & Fu, 2012). In 2003, the Berkeley Seismological Laboratory (2003) determined that there is 32 percent probability that a magnitude 7.0 earthquake will occur along the Hayward Fault in the San Francisco Bay Area within the next 30 years. Projected damages are expected to exceed the U.S. record $6.3 billion losses from the 1994 Northridge earthquake (Kircher, 2003).

Therefore, a seismic protection system which can sustain its stiffness, provide a significant increase in energy dissipation (that does not rely on the minimal hysteretic energy provided by nails), and provide sustainable high strength is desired. According to preliminary experimental tests, CarbonFlex appears to be a viable solution to this need by providing additional requisite energy dissipation, enhancing ductility and providing a stable crack growth mechanism in wood substrates so that nail pull-out or mail withdrawal occurrences (also resulting in cracking in plywood sheathing) otherwise common in plywood, or OSB, shear wall systems, is minimized thus alleviating potential soft-story collapse. Therefore, the idea of a CarbonFlex shear wall system that could be used as a sheathing material in lieu of conventional plywood sheets emerged.

The proposed CarbonFlex is used to tightly wrap the exterior side of the wood structure to create a CarbonFlex shear wall system providing lateral resistance and energy

dissipation to the structure. Instead of using nails as is the case in conventional wood shear wall constructions, CarbonFlex is attached to wood 2 x 4 studs using epoxy that is designed to provide good bonding strength with various types of substrates. The epoxy is continuously spread on to the attaching exterior faces of studs providing continuous load transferring paths from the final CarbonFlex panel to the wood framings. In contrast, in traditional wood shear walls, the load is transferred through discrete fasteners resulting in increased stress concentrations on the fasteners which lead to failure of the fasteners and detaching of the sheathing panels also through increased cracking. Therefore, using CarbonFlex shear walls in low-rise wood structures will expectedly sustain strength and stiffness of the buildings at higher structural demands while also reducing accelerations.

In addressing other natural hazard risks, severe storms, such as tornadoes and hurricanes, also cause catastrophic losses. Allstate, the largest publicly insurer, lost about two billion dollars due to tornadoes during spring 2011 (Berkowitz, 2012). “Deaths caused by tornadoes were 38, 67, and 81 for 2005, 2006, and 2007, respectively. As of May 2008, 110 deaths have been caused by tornadoes” (Federal Emergency Management Agency, 2008). Federal Emergency Management Agency (FEMA) released the first edition of FEMA P-320 Taking Shelter from the Storm: Building a Safe Room for Your Home or Small Business in August 1998. Since then, tens of thousands of safe rooms have been built (Federal Emergency Management Agency, 2008). In August 2012, Hurricane Isaac went across New Orleans. The range of on shore damages were estimated to be 500 million to 1.5 billion dollars (Liberto, 2012).

In August 2008, the International Code Council® (ICC®) and the National Storm Shelter Association (NSSA) issued the ICC/NSSA Standard for the Design and

Construction of Storm Shelters (ICC-500). The ICC-500 requires that all the shelters must be designed to withstand the impact of wind-borne debris. It also provides impact testing criteria for both tornado and hurricane shelters.

In August 2008, FEMA issued the third edition of FEMA P-320 which provides several construction plans for various types of safe rooms that meet or exceed the requirements of ICC-500. Two of the plans in the FEMA P-320 that relate to the wood frame structures are 1) drawing AG-05: Wood-Frame Safe Room Plan – Plywood Sheathing with Concrete Masonry Unit (CMU) Infill and 2) drawing AG-06: Wood-Frame Safe Room Plan – Plywood and Steel Wall Sheathing. According to drawing AG-05, the envelope elements of the safe room (walls) include the CMUs fill in between the double wood studs. Then, the exterior side of the wall is sheathed by double layers of 3/4 inch thick plywood. In stead of utilizing CMU, the drawing AG-06 uses a 14 gauge steel panel to attach to the double studs and double layers of 3/4 inch thick plywood is placed on top of the steel plate. However, the CMU and steel plate are heavy and difficult to work with (nailing or screwing the plywood through the 14 gauge steel).

This, therefore, served as the motivation behind using CarbonFlex in safe room construction. CarbonFlex sheathing was used to supplant the steel plate in drawing AG-06. Several 4 ft x 4 ft wall panels were built and tested to study their capability to absorb the impact energy from wind-borne debris. In addition, three steel door assemblies were modified by CarbonFlex and tested. The missile impact tests were conducted at Debris Impact Testing Facility, Wind Science and Engineering Research Center, Texas Tech University.

Study Objectives

This study has two objectives. The first objective is to create a new seismic protection system for residential wood structures that has better stiffness and strength sustainability so that the earthquake damage can be reduced. The proposed system is the CarbonFlex shear wall. To investigate the ability to maintain stiffness and strength, several CarbonFlex shear walls and a structure were tested using three modified earthquake displacement-time histories having low, moderate, and high peak displacement (LPD, MPD, and HPD). Stiffness and strength of specimens quantified from the HPD test (details discussed in chapter 5) was compared to that quantified from MPD test. From this comparison, the stiffness sustainability can be expressed. In addition, the results were compared to those of conventional plywood shear wall specimens to illustrate improvement of structural performance using CarbonFlex. Moreover, some guidelines for constructing a CarbonFlex shear wall were suggested.

The other objective is to expand the application of CarbonFlex so that it may represent a viable solution in the design of above-ground storm shelters for residential wood structures. This study provided pioneer work that will support the design of CarbonFlex-storm shelters in the future. To obtain the information, several debris impact testes were conducted on four CarbonFlex-storm shelter designs. In addition, three door assemblies modified by CarbonFlex were also tested. The information included suitable parameters that control impact resistance of CarbonFlex-storm shelters, allowable wind speeds for each design, and some construction recommendations.

Therefore, the study as presented herein focuses on the ability of a polymeric-enhanced high-tenacity fabric composite, CarbonFlex, to mitigate multi-natural hazard

damage in wood-framed structures. Improved structural performance in two natural hazard environments, namely earthquakes and tornadoes, were thoroughly investigated.

Outline of Dissertation

In Chapter 2, a brief discussion of fiber reinforced polymers, types of fibers, and matrix, was provided. Then, information of materials used in manufacturing of CarbonFlex was discussed. Finally, the manufacturing processes of CarbonFlex with and without substrates were explained in details.

Experimental test results from preliminary analyses of CarbonFlex were presented in Chapter 3. The experimental tests included tensile, cyclic-loading, free-vibration tests of CarbonFlex coupons, and flexural test of CarbonFlex wrapped wood beams. In addition, a numerical model of CarbonFlex wrapped wood beam was proposed.

Chapter 4 provided the details of wood-framed specimens. The chapter was separated into three sections describing the specimens tested in each experimental phase. Phase 1 included six walls subjected to perpendicular (out of plane) loads and six walls subjected to parallel (in plane) loads. Phase 2 consisted of four CarbonFlex shear walls. Phase 3 composed of two-8 ft x 8 ft x 9 ft single story structures. One structure was equipped with conventional shear walls. The other was wrapped by CarbonFlex.

The results of seismic testing were presented in Chapter 5. The chapter was also separated into three sections. The results from walls subjected to perpendicular loads were presented followed by a selection of an ideal CarbonFlex-wrapping scheme. Then, behaviors of a CarbonFlex shear wall were discussed in details. The possibility of using CarbonFlex strips as a hold-down to resist the wall's overturning moment was studied. The method to estimate strength of CarbonFlex shear wall with opening was suggested.

Finally, the results from a structure protected by conventional plywood shear walls were compared to those of a structure wrapped by CarbonFlex and ability to sustain stiffness and strength of CarbonFlex structure was shown.

Chapter 6 started with a short discussion of tornadoes and wind induced structural damage. Then, the background of wind-borne debris was discussed followed by an introduction of storm shelters for homes. After that, details of debris impact test and specimens were provided. Finally, the results from debris impact testing of six wall panels and three door assemblies were presented.

Chapter 7 provided conclusions of the CarbonFlex shear wall and debris impact tests. Moreover, the construction guideline for CarbonFlex shear walls was recommended. Finally, suggestions for future studies were provided.

CHAPTER 2

Materials and Manufacturing Processes of CarbonFlex

CarbonFlex can be categorized as a fiber reinforced polymer (FRP) composite material because it is composed of carbon fibers that strengthen a special polymer matrix (combination of an epoxy and a unique rubberizing polymer). A brief discussion of FRPs was provided in this chapter followed by information of raw materials used in production of CarbonFlex. Then, the manufacturing processes of CarbonFlex were discussed in detail.

Fiber Reinforced Polymer

A fiber reinforced polymer (FRP) is a material constituted using a combination of two or more constituents to achieve either improved and/ or desired properties (Campbell, 2010; Tuakta, 2005). FRPs have two main components, which are the reinforcement (fibers) and the matrix (polymer) as shown in figure 2. Normally, reinforcement fibers have a far greater tensile strength than that of the matrix. Therefore, the reinforcement fibers provide strength and stiffness to the FRP system, whereas the matrix provides environmental protection and serves to unify the fibers. FRPs have a wide field of application, including automobile, aerospace, and civil engineering, for structural modifications and improvements.

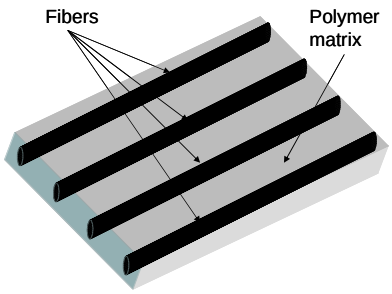

Figure 2. Diagram of FRP.

FRPs have been particularly utilized in structural systems such as bridges, highways, pipelines, and buildings for several years because of the versatile properties that they possess. For example, the properties of FRPs may be tailor-designed, by adjusting the volume fractions, curing conditions, temperature, etc. of the constituents, in order to satisfy specific structural requirements while providing a low-cost life-cycle solution to various problems (Van Den Einde, Zhao, & Seible, 2003). Furthermore, FRPs may have higher strength-to-weight ratios and may be considered "greener" in terms of embodied energy than conventional materials (Hota & Liang, 2011). Embodied energy is defined as an energy consumption factor in the manufacturing processes such as the amount of heat used to melt raw materials in fiber glass manufacturing. Cumming-Saxton (1981) compared embodied energy of three materials used in manufacturing of automotive parts. The materials are fiber glass, steel, and aluminum. The study showed that the embodied energy was reduced by 40 and 75 percent by using fiber glass instead of steel and aluminum, respectively.

Applications of FRPs can be found in both new constructions and in retrofitting projects. For instance, they have been used as the rebar designed for reinforced concrete structures (Gangone, Kroening, Minnetyan, Janoyan, & Grimmke, 2005). Thippeswamy, GangaRao, and Craigo (2000) discussed the production, development, and testing of several types of bridge decks in the United States that utilized FRPs. They concluded that FRP-designed bride decks are suitable for mass production, have good energy absorption, are able to improve fatigue and corrosion resistance properties, and may help to reduce the erection time of a structure. Moreover, FRPs have been used to strengthen deteriorated structures so that they may achieve a certain desired strength and to provide

specific capabilities such as seismic resistance. In civil engineering applications, three commonly used fibers are glass, aramid, and carbon fibers (Tuakta, 2005).

Reinforcements (Fibers)

Glass fiber. Glass fiber is made of various grades of glass. Raw materials, such as silica sand, limestone, clay, and kaolin, are heat melted mixed together in the furnace at a temperature of approximately 2200 ºF (Campbell, 2010). The melted conglomerate of materials is then drawn through a bushing process to form the small diameter (5 to 24 μm.) filaments. Finally, these filaments are processed and shaped to form the desired forms, such as chopped or continuous fibers, or are woven into fabrics. There are several types of glass fiber, including A-glass, C-glass, D-glass, and E-glass. A-glass (alkali) is made from materials that have a high alkali-content. C-glass (chemical) has a good chemical resistance. D-glass (dielectric) has a dielectric property which is mainly used in the electronic industries. E-glass (electrical) has a lower alkali content and is stronger than A-glass (Rosato, 2004). Due to its relatively low cost, the most commonly used glass fiber used in civil engineering applications is E-glass (Tuakta, 2005). However, E-glass is susceptible to chemical corrosion (Jones & Chandler, 1986; Li et al., 2011), and therefore, a single layer of C-glass, which is more expensive than E-glass, is usually needed as a protector against corrosion (Rosato, 2004).

Aramid fiber. Aramid fiber or Kevlar™ (DuPont's trade name) is made from a reaction of Paraphenylene Diamine and Terephthaloyl Chloride which yields a polymer called Poly Para-Phenyleneterephthalamide (PPD-T) (ASM International, 1990). The PPD-T is then dissolved in 100 percent sulfuric acid to generate liquid crystals that are extruded through a hot spinneret (Kalsbeek & Bruining 2012). The extruded fibers are

subsequently moved through cold water in order to remove the acidic overlay (Middleton, 1990). The fibers are then dried and wound up (Campbell, 2010). During these processes, molecules of aramid are oriented along the fiber direction resulting in the final anisotropic properties (Tuakta, 2005). Because aramid fiber has a high tensile strength and a low density, it is attractive to the aircraft and aerospace industries. In addition, it has energy absorption capability and has therefore been widely used in ballistic applications (Lee, 1993).

Carbon fiber. Carbon fiber is manufactured through a carbonization process. During this process, the precursor (feed-stock) is heated at temperatures above 3600 ºF, resulting in forming of carbon crystallites along the fiber axis (Tuakta, 2005). There are three precursors mainly used in the industries which are rayon, petroleum (pitch), and polyacrylonitrile (PAN).

Rayon precursor is made from cellulose material. It is considered to be a "pioneer" precursor used in the early development of carbon fiber manufacturing. However, there is a large amount of weight loss during the carbonization of rayon-based carbon fiber resulting in higher manufacturing costs than carbon fibers that are made from other precursors such as petroleum, and polyacrylonitrile. (Balaguru, Giancaspro, & Nanni, 2009).

Pitch precursor has relatively low cost compared to the PAN, or polyacrylonitrile, precursor because it is made using a by-product from petroleum refinery. The weight loss during the carbonization of the pitch-based carbon fiber is lower than that of rayon and PAN precursors. However, it has less uniformity during production (Balaguru et al., 2009; Tuakta, 2005). According to Huang (2009), pitch-based carbon fiber has larger

crystallites than PAN-based resulting in higher stress concentration at grain boundaries. Therefore, it usually has lower tensile strength than PAN-based carbon fiber that has smaller crystallites.

Although PAN-based carbon fiber has moderate weight loss (about 50 percent) during carbonization, it has higher tensile strength than other precursor-based carbon fibers because it has less surface defects. Therefore, currently, most of carbon fibers are made of PAN precursor (Balaguru et al., 2009).

Carbon fiber has many advantages. It has not only a high tensile strength to weight ratio but also high fatigue strength. In addition, it is not susceptible to corrosion or oxidation at temperatures below 750 ^{o}F (Balaguru et al., 2009). Even though carbon fiber is more expensive than other conventional construction materials, many studies have shown that using carbon fiber is more effective through the life cycle of structures. For example, Eamon, Jensen, Grace, and Shi (2012) analyzed the life cycle cost of prestressed concrete bridge superstructures reinforced by various types of reinforcements which are: 1) uncoated steel with cathodic protection, 2) epoxy coated steel, and 3) carbon fiber reinforced polymer (CFRP). They concluded that CFRP reinforcement has the highest reduction of life cycle cost when used in high traffic areas, and CFRP reinforcement will be the least expensive choice when a structure's age reaches 23 to 77 years.

Matrix

In general, the matrix used in composite materials can be metallic, ceramic, or polymeric in nature. FRP is a composite material that has a polymeric matrix as shown in

figure 2. The polymeric matrix can be separated into two main types: thermoplastic and thermoset polymers.

Thermoplastic polymer. Thermoplastic polymers have longer molecule chains than thermoset polymers. Each molecule is composed of many carbon-to-carbon (C-C) links ranging from several hundred to several thousands of links. The long molecular chain lengths preclude easy movement. As a result, thermoplastic polymers remain in a solid state at room temperatures to moderate temperatures (Hoa, 2009). To lower their viscosity (i.e., to 'soften' them), heat is needed. Following the application of heat, the viscosity increases, and the polymers achieve a solid state (after they cool down). An important characteristic of thermoplastic polymers is that they may be repeatedly softened by reheating (Rosato, 2004), resulting in a back and forth transition between states. There are many thermoplastic polymers available on the market, including acetal, nylon, polyester, polypropylene, polyetheretherketine, and polycarbonate.

Thermoset polymer. Molecules of thermoset polymers have less C-C links than those of thermoplastic polymers. Because of their short molecular chains, thermoset polymers are usually found in a liquid state at room temperatures. In order to change thermoset polymers from a liquid to a solid state, a curing agent is used (Hoa, 2009) to invoke a chemical reaction called polymerization where molecules form cross-linked structures in which molecules of polymers linked one another in two dimensions (like a cloth). Due to their tight cross-linked structure, thermoset polymers usually have better dimensional stability (e.g., less shrinkage), higher strength, a larger range of temperature resistance, and stronger electrical and chemical resistances than most thermoplastic polymers (Akovalł, 2001; Rosato, 2004; Tuakta, 2005) although thermoset polymers

cannot transition between states. As such, unlike thermoplastic polymers, following the curing process, the form of thermoset polymers cannot be changed. Some common thermoset polymers used in FRPs are epoxies, polyesters, polyimides, and bismaleimides (Akovalł, 2001). Because epoxies are used in the production of CarbonFlex, a brief discussion follows.

Epoxy. An epoxy is an adhesive widely used in many industries, such as the automotive, aerospace, and construction fields, and are classified as either structural and nonstructural adhesives. It was first introduced commercially in 1946, and is considered highly desirable because it bonds well to various types of substrates and can be modified to obtain numerous desired properties by adding fillers or by selecting an appropriate combination of resins and curing agents. Typically, epoxies that are used in structural applications have tensile strengths greater than 1000 psi and properties that do not change significantly during service life (Petrie, 2007) within certain temperature ranges depending on their designed working temperatures. Among thermoset polymers, epoxies offer the highest performance (Rosato, 2004).

CarbonFlex

CarbonFlex is a newly developed carbon fiber based material. The motivation behind the development of CarbonFlex emerged from the concept of having a material that has both high strength and high ductility (high-energy dissipation) that can be used as a structural seismic protection system. CarbonFlex is composed of three main constituents which are carbon fiber (strength provider), an epoxy resin or saturant (carbon fiber protector and binder), and a rubber-like polymer. Although carbon fiber is more

expensive than glass fiber, there are many reasons for selecting carbon fibers as the reinforcement system for CarbonFlex:

1. Carbon fibers have higher strength than glass fibers and are generally non-corrosive. To achieve the same strength, more layers of glass fiber would be needed, and consequently, labor costs and construction time would be increased.
2. Glass fibers (E-glass) are more vulnerable to corrosion. Therefore, a layer of C-glass might be needed resulting in more complicated manufacturing.
3. Many studies and articles show that the price of carbon fiber will be reduced due to increases in demands (Ashley, 2012).
4. Carbon fibers have a better service life (Tuakta, 2005) than aramid and glass fibers due to their higher fatigue strength (Taerwe, 1995).

Materials Used in Manufacturing of CarbonFlex

Carbon fiber. The unidirectional MBrace® CF-130 carbon fiber from BASF – The Chemical Company is used as a strength provider for CarbonFlex. MBrace® CF-130 is a polyacrylonitrile (PAN) based carbon fiber (Miyagawa, Jurek, Mohanty, Misra, & Drzal, 2006). MBrace® CF-130 is available in a fabric form. One conventional roll of MBrace® CF-130 can cover about 269 ft^2. It can be easily applied on the substrate because the pre-wet process is not required. According to the product data sheet, the ultimate tensile strength of MBrace® CF-130 is 550 ksi. The tensile modulus is 33,000 ksi. The actual cured thickness (fiber and saturant (epoxy) resin) is 0.02 to 0.04 inch, and the areal weight is 0.062 lb/ft^2.

Epoxy. There are two types of epoxy used in CarbonFlex production which are MBrace® Saturant resin and MBrace® Primer. Both are products from BASF – The Chemical Company. The primer is used in substrate's surface preparation process. It will be applied onto surfaces of the substrate prior applying the saturant and installation of MBrace® CF-130. It is designed to be able to penetrate the pores of substrates and provides a good and smooth bonding base to the saturant. It can be applied on various types of substrates such as steel, wood, concrete, and masonry. Yield stress and modulus in tension of the primer are 2100 psi and 105 ksi, respectively. In compression, yield stress and modulus are 3800 psi and 410 ksi, respectively.

The saturant resin is used to encapsulate fiber fabrics to provide protection from environment. It can be used with glass, carbon, and aramid fabrics. The 'pot-life' (working time) varies depending on the temperature. For example, the pot-life is 200 minutes at 50 ºF and 15 minutes at 90 ºF. Yield stress and modulus in tension of the saturant are 7900 psi and 440 ksi, respectively. In compression, yield stress and modulus are 12500 psi and 380 ksi, respectively.

Rubberized polymer. This special polymer is a product of the chemical reaction between an isocyanate component and primary or secondary amineterminated material (Primeaux II, 1989). It is a two-component spray-able elastomer. It has a very fast curing time (dry with in 5 to 10 minutes and achieve full strength with in seven days). Due to its chemical, environmental, and impact resistance, it has been widely used in spray-coating industries for decades. For instance, it has been used as a truck liner and roof coating. It is strongly believed that mechanical behaviors of CarbonFlex depend on the thickness (h_p) of this polymer and the interfacial bonding between this polymer and the saturant resin

generally applied to the MBrace® CF-130 to manufacture CFRP. The reaction between the polymer and epoxy is controlled by curing time constraints between the saturant resin and the rubberized polymer (t_c). The effects of h_p and t_c to the tensile, flexural, and damping properties of CarbonFlex were discussed in the later chapters.

Manufacturing of CarbonFlex

Manufacturing of CarbonFlex can be separated into two cases which are "with" and "without" substrate. In this section, general details of application processes, such as tools and epoxies mixing process, were discussed. Then, the different processes between two cases were explained in details.

Tools. Most of the tools which are used in the manufacturing are typical painting tools. These tools are used for mixing and applying epoxies onto the substrates or fiber fabrics. The list and usage of the tools are shown in table 1.

Table 1

List and Usage of Tools Used in Manufacturing of CarbonFlex

Tool	Usage
Low speed drill	Mixing epoxy
Paint mixing paddle	Mixing epoxy
Measurement cup or scale	Measure required amount of part A and B of epoxy
Buckets	Mixing epoxy
Paint brush and roller	Apply epoxy onto substrate or fabric
Paint tray	Apply epoxy onto substrate or fabric
Staple	Attach fiber fabrics to wood frame
Utility knife	Cut carbon fiber and check CarbonFlex thickness

Epoxy mixing process. Both primer and saturant are composed of two parts (A and B). For both epoxies, mixing ratio (part A to part B) is the same which is 3:1 by volume or 100:30 by weight. There are little different mixing processes between the

primer and saturant. For the primer, after measuring the required amount of part A and B, both parts are mixed together using a low speed drill and a paint mixing paddle for three to five minutes. For the saturant, part A is needed to be pre-mixed for three minutes prior mixing with part B. The good mix will not have streaks or lumps. To reduce the loss of heat from the chemical reaction of the two parts and to increase the pot life (i.e., to control the exothermic reaction time and thus control, the final product cure time), the mixed epoxy should be poured and spread on a paint tray. Occasionally stirring the epoxy will help to increase the pot life too.

CarbonFlex with substrate. This is the case that CarbonFlex is used to wrap around or attach to a substrate. First, a carbon fiber fabric was cut to a desired shape. After preparation of the fabric, the substrate surface was appropriately prepared. Substrate preparation processes are varied depending on the types of substrate materials. For example, rust and painting on a steel substrate must be removed using a grinder. For a concrete substrate, the surface must be dry and clean. If there are small defects such as pores or holes on the surface, the putty (high viscosity epoxy paste) is required to level the defects and provide a smooth surface. After surface preparation, a thin layer (0.003 in.) of primer was applied on the surface. Prior to applying the saturant, the primer must become “tacky.” The tacky state of the primer can be easily indicated by its color. The color will change from clear to amber when the primer is tacky. The time taken to achieve the tacky state is about one hour. Once the primer became tacky, a thin layer (0.022 in.) of the saturant was applied on top of the primer. Then, the prepared carbon fiber fabric was attached to the substrate. In this process, the fabric was stretched to reduce warping and air voids. After the fabric was secured to the substrate, another layer

of the saturant was applied on top of the fabric. In this step, a 3/8 in. “nap” painting roller should be used. The roller must be saturated by the saturant prior the application. Then, the saturated roller was pressed on the fabric to ensure that the saturant penetrated through the fabric. Prior to applying the unique polymer, the saturant was allowed to reach a certain cure state. Cure states of the saturant can be varied by changing the waiting time between mixing the saturant and spraying the polymer. This cure state is a function of time and is referred to as “t_c.” A previous study by Dhiradhamvit et al. 2011 showed that t_c is one of the manufacturing parameters that affected the responses of CarbonFlex. The effects of t_c and other parameters were discussed in subsequent chapters. After an ideal reaction cure time, t_c, was achieved, the polymer was applied to the saturant following a desired thickness, i.e., a desired volumetric fraction of the polymer. The thickness of the polymer is another parameter that can affect behaviors and properties of CarbonFlex. For ease, the thickness (volumetric fraction) of the polymer is herein abbreviated as “$h_{p.}$”

CarbonFlex without substrate. A main intention of these procedures is to produce CarbonFlex sheets for experimental tests. A product from the procedures is a rectangular sheet of CarbonFlex. First, a small wood frame was built as shown in figure 3(a) to be used as a support for the fabric. Then, the fabric was cut to have the same size as the wood frame. After a fabric preparation, the fast curing epoxy (the curing time is five minutes) was applied on a surface of the wood frame. This fast curing epoxy was used to hold the fabric to the wood frame. Then, the fabric was carefully stretched and attached to the wood frame. A construction grade stapler was used to temporary secure the stretched fabric during the curing time of the fast curing epoxy as shown in figure

3(b). Then, the saturant was applied to the fabric using two saturated nap painting rollers. The fabric was squeezed between two rollers to reduce warping and ensure that the saturant penetrated through the fabric. Then, the polymer was sprayed after the desired t_c was achieved. The wood frame can be removed 24 hours after the spraying process.

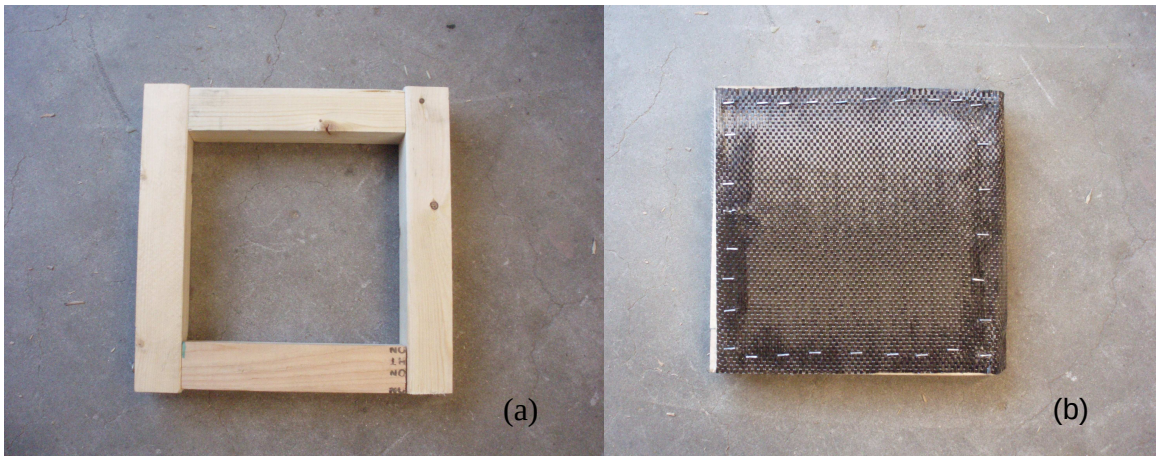

Figure 3. (a) A small wood frame used as a support for the fabric. (b) Carbon fiber fabric was attached to the wood frame using staples.

CHAPTER 3

Previous Research of CarbonFlex

As mentioned in previous chapters, it is strongly believed that the properties of CarbonFlex are functions of two variables. The first variable is a cure-time set parameter (t_c) that affects the mixing of the saturant and the "rubber-like" polymer constituent. Studies have shown that t_c is ideally found such that the saturant is not too "runny" or dry, thus allowing the active molecules to chemically bond the saturant and polymer, resulting in an ideal interfacial cohesion mechanism. A second manufacturing parameter is a thickness term (which can be calculated as the volumetric fraction) of the "rubber-like" polymer, h_p.

To evaluate the mechanical properties of CarbonFlex and to investigate the effects of h_p and t_c, tensile coupon, cyclic loading, and beam free-vibration tests have been conducted. In addition, wood beams wrapped by CarbonFlex were tested using three-point bending method. The results were compared to those of an unwrapped wood beam and a CFRP-wrapped wood beam. Finally, the stress-strain model of a CarbonFlex wrapped wood beam was developed and compared to the experimental results.

Tensile Ductility of CarbonFlex as a Function of Volumetric Fraction of the Polymer Constituent

First, the effects of h_p have been studied via tensile testing according to ASTM D3039/D3039M-08 (ASTM, 2009). The thicknesses of CarbonFlex specimens used in the study are 1/16 and 1/8 inch which correlate to a polymeric constituent volumetric fraction of 60 and 79 percent, respectively. All specimens have the same width and gauge length, which are 9 inches long x 1 inch wide. The results were compared to those of

carbon fiber (CFRP) specimens. Figure 4 indicates that CarbonFlex specimens exhibited greater ductility than CFRP specimens which, expectedly, failed in a brittle-like manner. The CarbonFlex coupon having a volume fraction of 0.79 had an ultimate displacement that was 1.6 times greater than the specimen having a volume fraction of 0.60. In comparison to CFRP, the CarbonFlex ultimate displacements found to be 5.6 and 3.5 times greater for the 1/8 and 1/16 inch thick specimens, respectively. Young's modulus of the 1/8 inch thick specimen (volume fraction of 0.79) was found to be 34,470 ksi which is greater than structural steel (29,000 ksi).

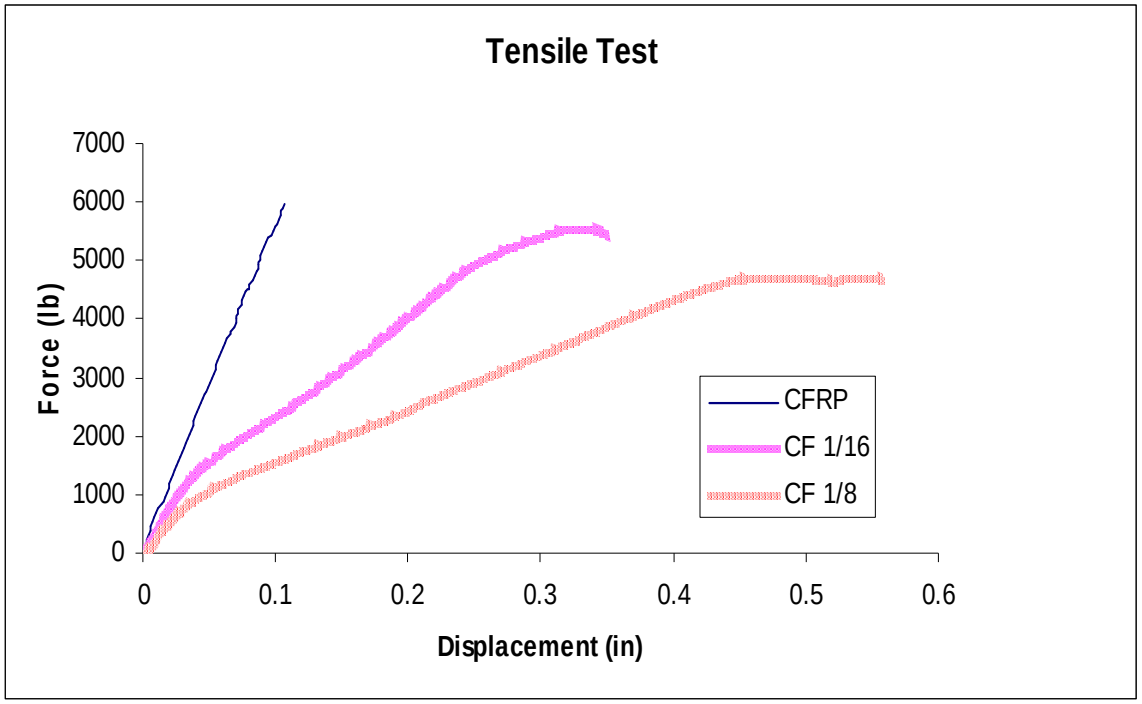

Figure 4. Tensile test result of CarbonFlex specimens.

In order to quantify the ductility of CarbonFlex, six tensile tests (three tests for each specimen type) were conducted. The ductility of each specimen type was calculated using equation 3.1.

$$\mu = \frac{\varepsilon_F}{\varepsilon_Y} \tag{3.1}$$

In this case, μ is ductility, ε_F is the mean of the measured strains at fracture, and ε_Y is the mean of the yield strains. The yield point for each coupon was found using 0.2 percent strain method. The ductility, means and standard deviations of strains at fracture, and at yield strains are summarized in Table 2.

Table 2

Ductility, Strain at Fracture, and Yield Strain of CarbonFlex

Specimen type	1/8 inch thick CarbonFlex	1/16 inch thick CarbonFlex
Strain at fracture	0.0767 ± 0.0054	0.0524 ± 0.0474
Yield strain	0.0099 ± 0.0004	0.0087 ± 0.0023
Ductility	7.676	6.008

Note. Values of strain at fracture and yield strain shown in the table are mean ± standard deviation

The polymer interaction with the epoxy acts as a strongly bonded load transferring path that does not allow energy to be accumulated in the epoxy (which has a much larger stiffness than the polymer) or the fiber, thus localizing damages. As a result, the specimen is able to undergo large post-elastic deformations where the crack growth rate is significantly reduced as large bursts of energy (from fracturing) are quickly dissipated, thus leaving less energy to go towards forming new crack surfaces. This stabilization of the crack growth mechanism allows large cracks to eventually grow stably, thus taking a brittle material and effectively making it behave as a ductile material by simple localizing single damage events. When a volumetric fraction of the polymer was increased, the load transferring paths were also increased. Therefore, the ductility of

CarbonFlex varied directly as a function of at least the volumetric fraction of the polymer.

Figure 5 shows a linear relationship between the volumetric fraction of the polymer and ductility of CarbonFlex. The zero volumetric fraction belongs to the CFRP specimens which have zero ductility. The relationship can be expressed as:

$$\mu = 9.8255 \times V_P \tag{3.2}$$

Where V_P is a volumetric fraction of the polymer.

Stress-Strain Behavior in Tension of CarbonFlex

Experimental results from the specimen having 0.79 polymer's volumetric fraction were used to study the stress-strain behavior in tension of CarbonFlex. The behavior can be separated into elastic and inelastic regions. Within elastic region, Hook's law was assumed. The yield stress was found to be equal to 57.28 ksi. To describe the behavior in inelastic region (yield to maximum stress), A Ramberg-Osgood model which is expressed in equation 3.3 was used.

$$\varepsilon_p = \alpha\left(\frac{\sigma_y}{E}\right)\left(\frac{\sigma}{\sigma_y}\right)^n \tag{3.3}$$

Where ε_p is a plastic strain, σ is stress, σ_y is yield stress, and E is an elastic modulus. α and n parameters were obtained empirically which were found to be 0.15 and 1.82 for α and n, respectively. A comparison between testing and analytical results is illustrated in figure 6 which shows that a stress-strain behavior of CarbonFlex was well predicted by the model.

The model was used with the finite element analysis program “ABAQUS” to predict the force-displacement behaviors of the CarbonFlex. The analysis results well agreed with the experimental results as shown in figure 7.

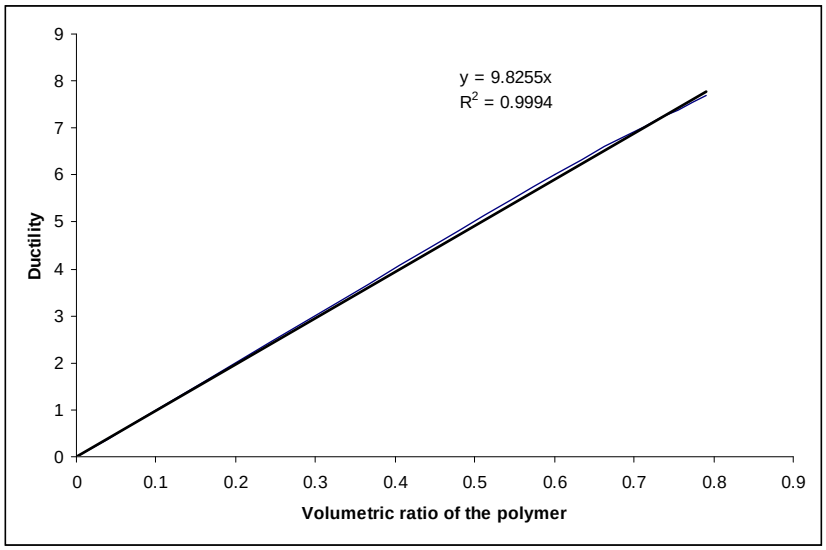

Figure 5. Relationship between volumetric fraction of the polymer and ductility of CarbonFlex.

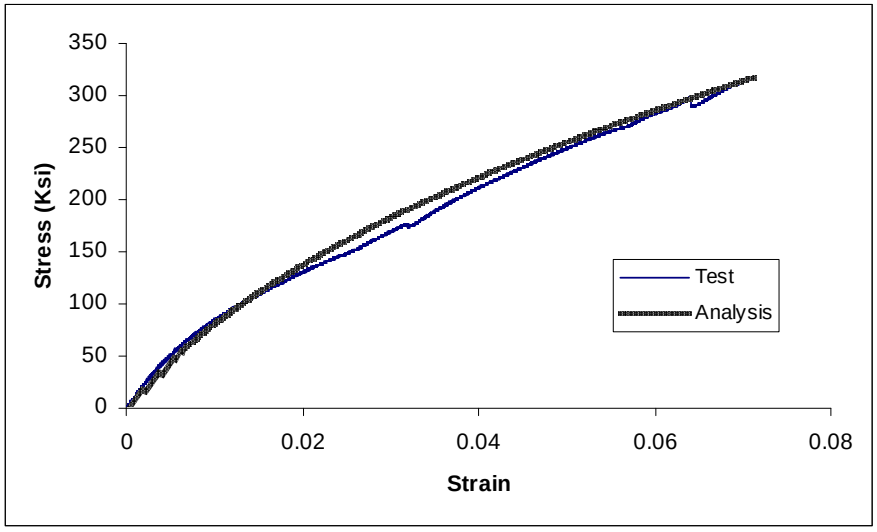

Figure 6. A comparison between testing and analytical results using Ramberg-Osgood model.

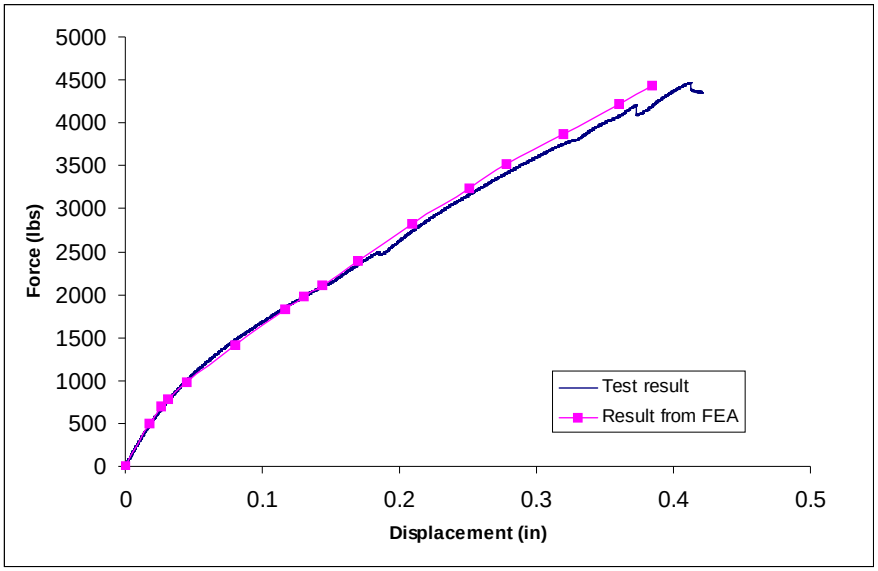

Figure 7. A comparison between testing and finite element analysis results.

Cyclic Loading Test to Study the Viscoelasticity in CarbonFlex

Viscoelasticity is a material behavior phenomenon that exhibits both elastic ("solid-like," or energy-storing) and viscous ("liquid-like," or energy-dissipating) properties. A material that exhibits a constant stress-strain phase difference having a viscosity that is independent of the state of shear conditions is called a Newtonian fluid; Non-Newtonian fluids exhibit viscosity that changes with respect to the state of shear. In purely elastic materials, the phase difference between stress and strain is 0^0, whereas in nearly purely viscous materials, the phase difference approaches 90^0. Viscoelastic materials exhibit a phase difference somewhere in between, and CarbonFlex exhibits an evolutionary phase difference that varies as the deformations in the material and the state of shear change (Weinman & Rajagopal, 2000). Figure 8 shows the experimental stress-strain relationship for CarbonFlex coupons in tension under repeated cycles. The testing

was conducted under a slow rate which is 0.025 inch per minute (0.0005 second^{-1} strain rate).

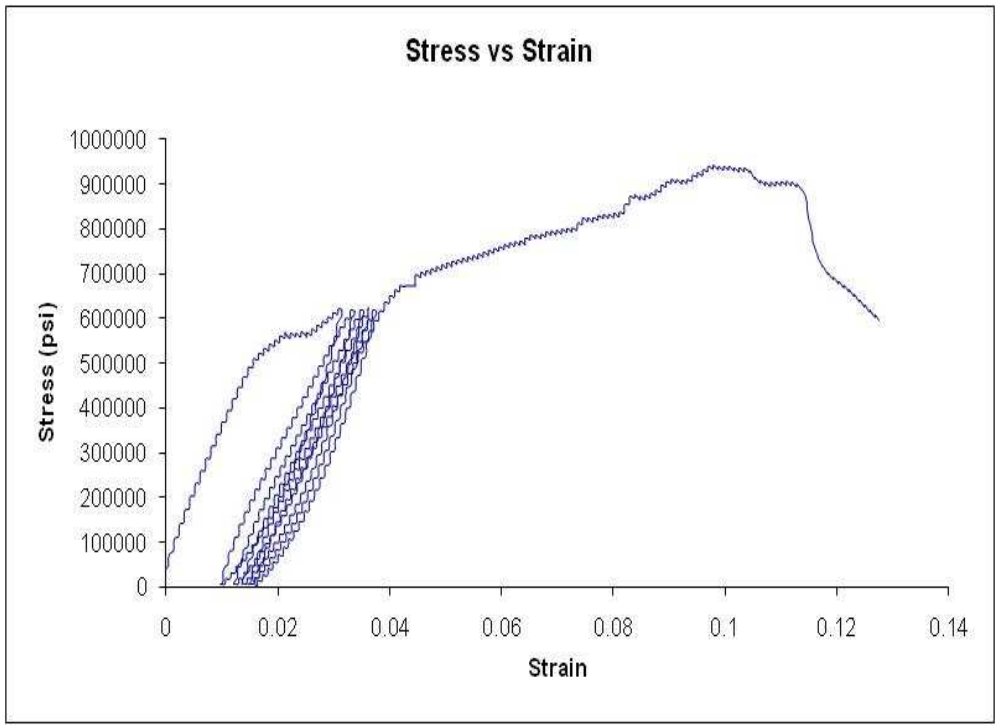

Figure 8. Stress-strain relationship of CarbonFlex coupon under cyclic loads.

The test results were obtained through cyclic loading of coupons (9 in. x 1 in.) loaded at 75 percent of the ultimate post-yield strength of CarbonFlex. The ultimate post-yield strength was calculated from previous tensile test results. The assimilated test results in figure 8 show a transition from elastic to post-yield hardening behavior, where the latter is defined by an evolutionary visco-elastic phenomenon and shows changing anelastic behavior with decreasing backstress per cycle (and thus dislocation pile-up resistance) indicating a changing dissipation of energy in the material so that damage does not accumulate, and finally concluding with a nearly-purely viscous behavior at failure. Figure 9(a-d) illustrates a decreasing backstress for the 1st, 2nd, 4th, and 5th cycles

which shows decreasing anelastic behavior (Shames & Cozzarelli, 1997) and with a same reloading stiffness on each cycle.

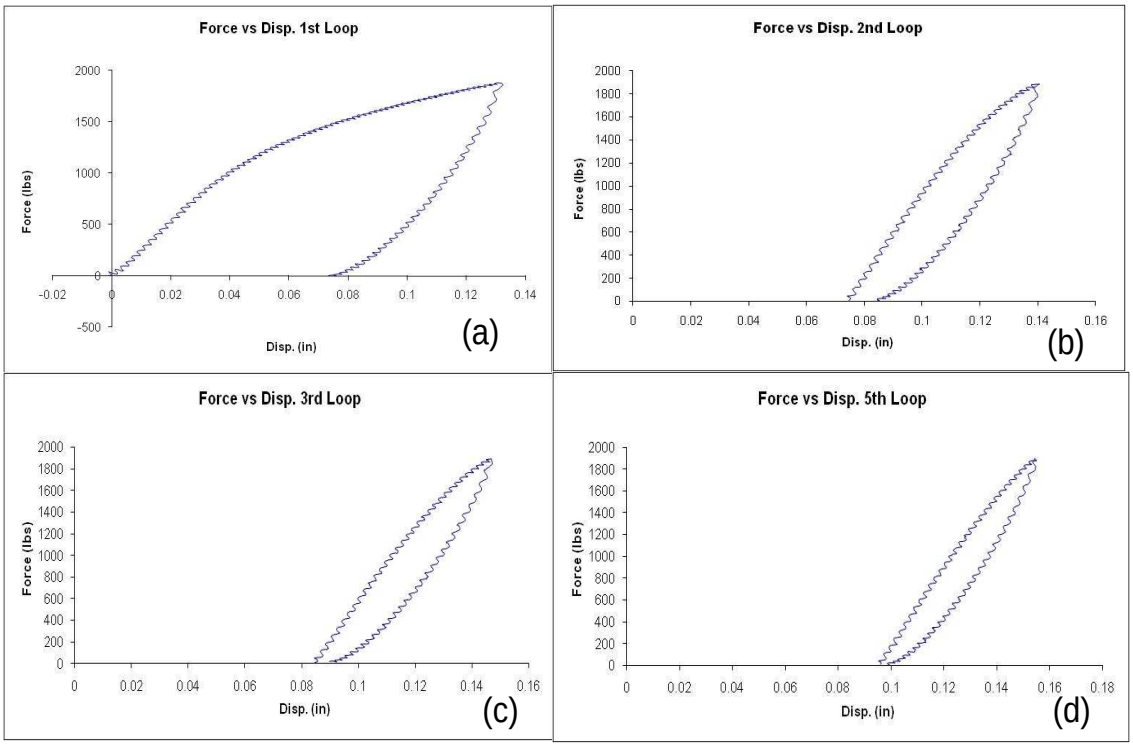

Figure 9. (a, b, c, and d) Test results from the 1st, 2nd, 4th, and 5th cycles, respectively.

High Speed Loading Crush Test to Determine a Flow Rule of CarbonFlex

High speed crush tests of CarbonFlex specimens were conducted at different loading rates which are 2, 3, and 4 m/s. The specimens are 9 in. long foam core specimens having 2 in x 4 in cross-section wrapped by 1/16 in. thick CarbonFlex. The experiments were conducted at Oakridge National Laboratory using the Test Machine for Automotive Crashworthiness (TMAC) which has ability to crush specimens at constant rates up to 8 m/s.

The Kelvin (Voigt) model was used to describe a flow rule of CarbonFlex. The model consists of two components which are linear spring and linear dashpot. The

components are parallel to each other. The linear spring represents a linear behavior of the carbon fiber reinforcements and the dashpot represents a viscoelastic (rate dependent) behavior of the polymeric constituent. Due to the geometry of the specimens, displacements of carbon fibers were assumed to be equal to those of polymeric constituent. In addition, all specimens achieved all most fully geometry recovery after unloading which is one of the important characters of the Kelvin model (Shames & Cozzarelli, 1997). Therefore, the model was selected to be used to derive the flow rule for CarbonFlex. The stress-strain behavior of the model can be described as:

$$\dot{\varepsilon} = \frac{\dot{\sigma}}{E} + \frac{\sigma}{\eta} \tag{3.4}$$

Where $\dot{\varepsilon}$ is strain rate, E is an elastic modulus, σ is stress, and η is a viscous constant. The experimental results showed that stress is also a function of time and can be best described using a quadratic equation which is expressed in equation 3.5.

$$\sigma(t) = C_1 t^2 + C_2 t + C_3 \tag{3.5}$$

The flow rule, which was obtained by substitute equation 3.5 into 3.4 and integrate the equation 3.4, can be expressed as:

$$\varepsilon(t) = \exp\left(-\frac{E}{\eta}t\right) \times \left[I_1 + I_2 + I_3\right] \tag{3.6}$$

$$I_1 = \frac{C_1}{\eta}\left(\frac{t^2}{E/\eta} - \frac{2t}{(E/\eta)^2} + \frac{2}{(E/\eta)^3}\right) \times \exp\left(\frac{E}{\eta}t\right) \tag{3.7}$$

$$I_2 = \frac{C_2}{\eta}\left(\frac{t}{E/\eta} - \frac{1}{(E/\eta)^2}\right) \times \exp\left(\frac{E}{\eta}t\right) \tag{3.8}$$

$$I_3 = \frac{C_3}{E}\left(\exp\frac{E}{\eta}t\right) \tag{3.9}$$

Figure 10 (a), (b), and (c) show comparisons between testing and analytical results from the test at 2, 3, and 4 m/s loading rates, respectively. The analytical results were obtained using equation 3.6. The comparisons show good agreement between analytical and experimental results.

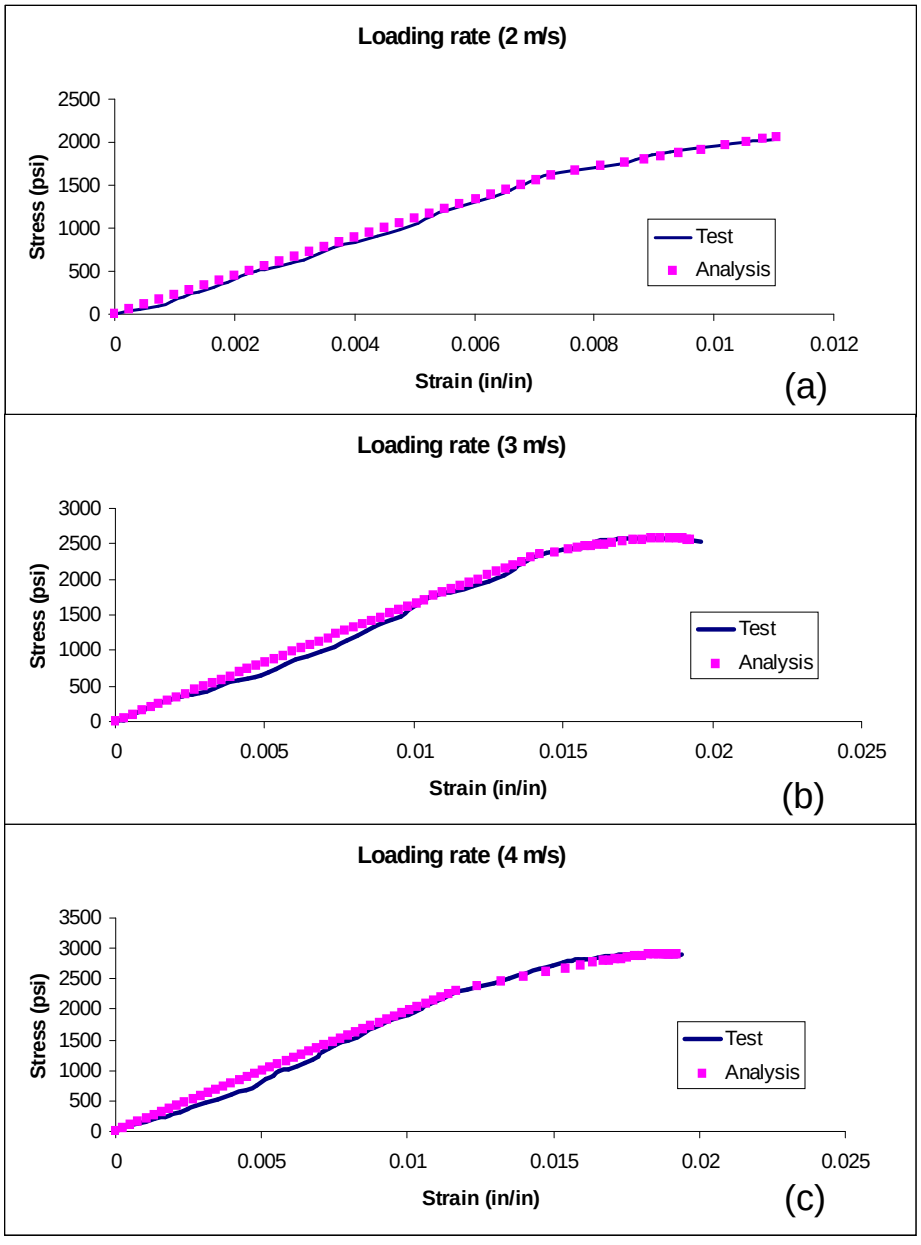

Figure 10. Comparisons between testing and analytical results from the test at (a) 2 m/s, (b) 3 m/s, and (c) 4 m/s loading rates.

Beam Free Vibration Test Results Used to Study Effects of h_p and t_c to Damping of CarbonFlex

In order to evaluate the seismic properties (damping ratio and natural frequency) of CarbonFlex, free vibration tests were conducted using a small high-frequency shake table. Three types of materials - steel, CFRP, and CarbonFlex - were tested using the shake table. The specimens are thin-beams having the same width and span length (1 in. x 9 in.). The testing apparatus is shown in figure 11. Both ends of specimens were mechanically fixed to the table by screws. Four accelerometers were used. Two of them measured the accelerations of the table to ensure that the shake table did not tilt during loading. The other accelerometers monitored each specimen's responses at the mid-span and at the quarter-span). In addition, a laser vibrometer was mounted to the rigid frame to measure the velocity of each specimen at mid-span. In a series of free-vibration tests, impact forces were introduced to each specimen.

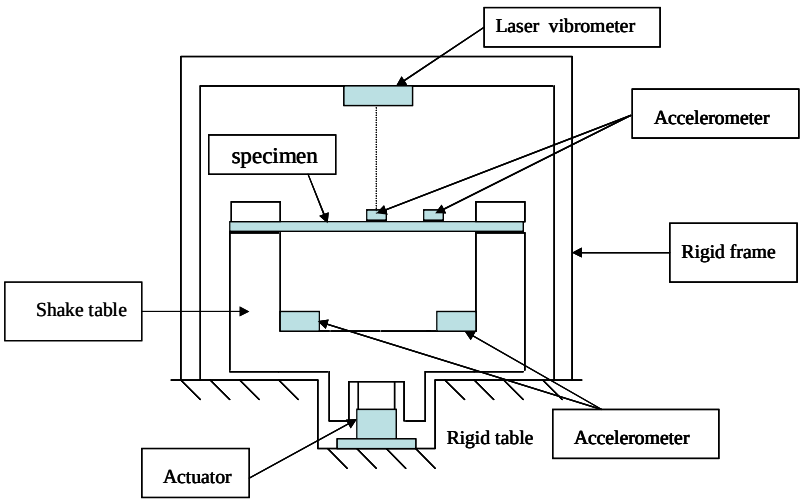

Figure 11. Free vibration test apparatus for CarbonFlex specimens.

The velocity time-histories at the mid-span of each material were measured and shown in figure 12. Although the CarbonFlex specimen having a thickness of 1/8 inch and a curing reaction parameter, t_c, of two was subjected to the greatest impact force that produced an initial velocity of about 0.2 mm/sec while CFRP and steel had initial velocities of about 0.05 and 0.08 mm/sec, the velocity of CarbonFlex specimen decreased in the least amount of time (0.16 sec.) as compared to 0.5 sec and 1.5 sec of CRFP and steel, respectively. The damping ratio of each material was then calculated using a logarithmic decrement method (Singiresu, 2003). Although CarbonFlex is a Non-Newtonian material, which has varying damping properties, the tests were conducted in the linear range of the material, therefore enabling the logarithmic decrement method to be a valid method for evaluating the damping properties. For CarbonFlex, the damping ratio was found to be 4.64 percent which is 2.4 and 14 times greater than the damping ratios of CFRP and steel, respectively.

The free-vibration tests of specimens having various h_p and t_c manufacturing parameters were carried out to study the effects of h_p and t_c against the seismic performance of the specimens. Damping ratios of two different h_p (1/8 and 1/16 inch) specimens with the same t_c (3) were compared in figure 13(a). The damping ratio increased by about 60 percent following a 31.7 percent increase in the volumetric fraction of the overlying polymeric constituent, which equated to doubling the thickness of the polymeric constituent. This indicates that the polymeric constituent itself is a damping agent that can provide increased energy dissipation.

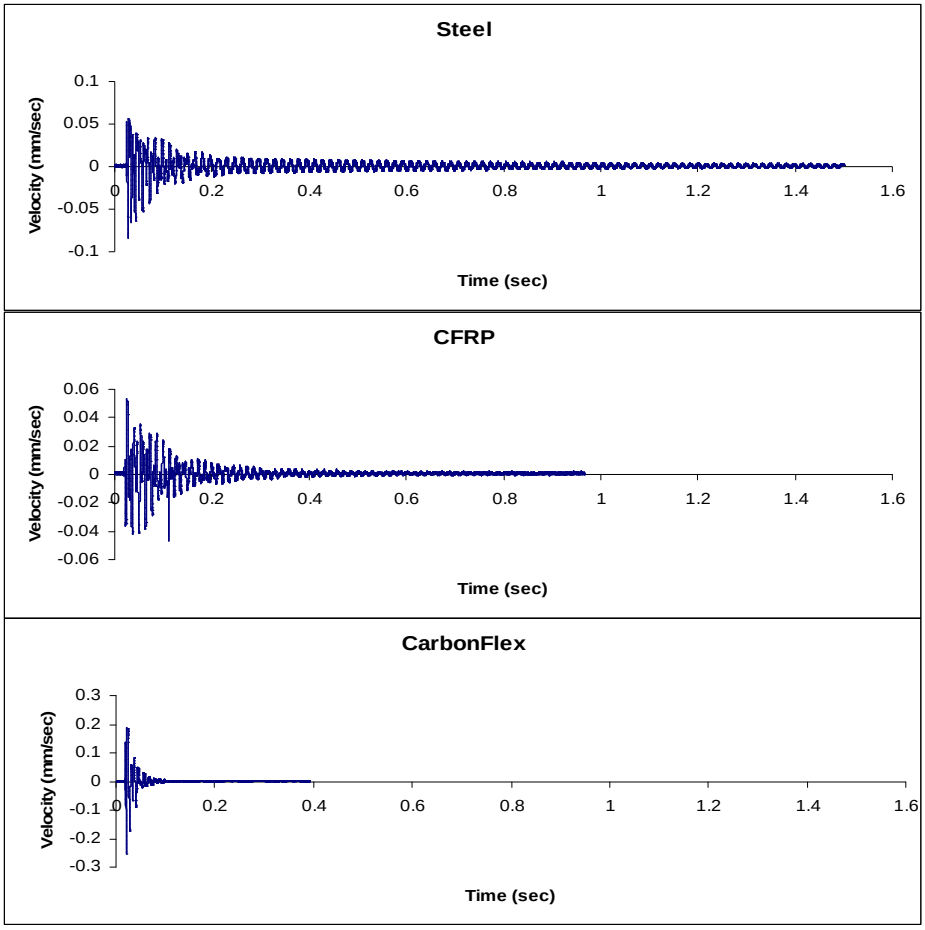

Figure 12. Free vibration testing results from various specimen types.

Three of the 1/8 inch thick CarbonFlex coupons having t_c equal to two, three, and five were also tested. The damping ratios of these specimens are shown in figure 13(b) and show that the shorter that t_c is in its cure set time, the more chemically reactive the saturant and polymer are which affects the molecular bond properties between the carbon fiber's epoxy and the polymer. Thus, a lower cure time appears to indicate higher damping. One possibility for this is that the "infused" polymer/ epoxy interfacial cohesive region represents the dynamic nature of the bond strengths in terms of enabling molecular mobility (and relaxation, thus more friction-type damping) or enabling bond translations and rotations (thus more viscous-type damping), see (Evans & Ritchie,

1997). In addition, the reaction between the polymer and epoxy phases and the resultant residual stress field may, in some manner, affect the properties and behaviors of the fiber/ matrix interface, thus alleviating the onset of typical failure modes in many fiber-reinforced composites, including matrix cracking, fiber-matrix debonding, fiber breakage, and fiber pullout (which is defined as the separation of the fiber from the matrix, following breakage in continuous fibrous composites, such as CFRP); there is also inter-lamina delamination, but this is for multiple lamina, and the present study concentrates only on single-ply laminates. Thus, a larger greater t_c parameter results less damping ratio, where the damping ratio seems to decrease more prominently once t_c exceeds three hours although this chemical interaction will be investigated in future research. This, however, is the first scientific evidence that shows the effects of t_c on the properties of CarbonFlex.

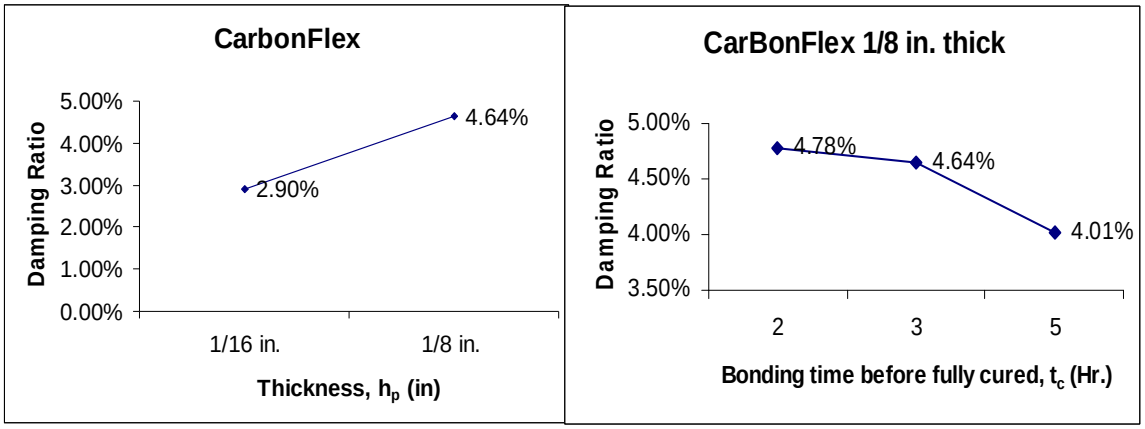

Figure 13. (a) Effect of h_p to damping ratio of CarbonFlex. (b) Effect of t_c to damping ratio of CarbonFlex.

Flexural Test of CarbonFlex Wrapped Wood Beams

Three point-bending tests of wood beams were conducted according to ASTM D143-09 (ASTM, 2009). The 2 in. x 4 in. wood beams had a span length of 28 inches and

were simply supported. The beams include 1) unwrapped beam (W), 2) carbon fiber wrapped beam (CFRP), 3) 1/16 inch thick CarbonFlex wrapped beam (1CF), and 4) 1/8 inch thick CarbonFlex wrapped beam (2CF). The test results (force-deflection) are shown in figure 14. The experimental test results indicated that the unwrapped beam suddenly failed after the peak load had been reached while the CFRP-wrapped beam provided virtually no ductility to the beam, especially in comparison to the 1CF and 2CF beams which showed 1.58 and 2.5 times greater ultimate displacements, respectively. Moreover, the stiffness of the 2CF beam became less negative during increasing inelastic displacements following the peak load. This implies the region of sustainable negative stiffness and stabilized crack growth. Interestingly, after the most significant load drop, which occurred at 3.5 in. displacement, the 2CF beam showed a positive slope in the stiffness as the strength increased and external energy was dissipated by CarbonFlex resulting in increasing ultimate displacements.

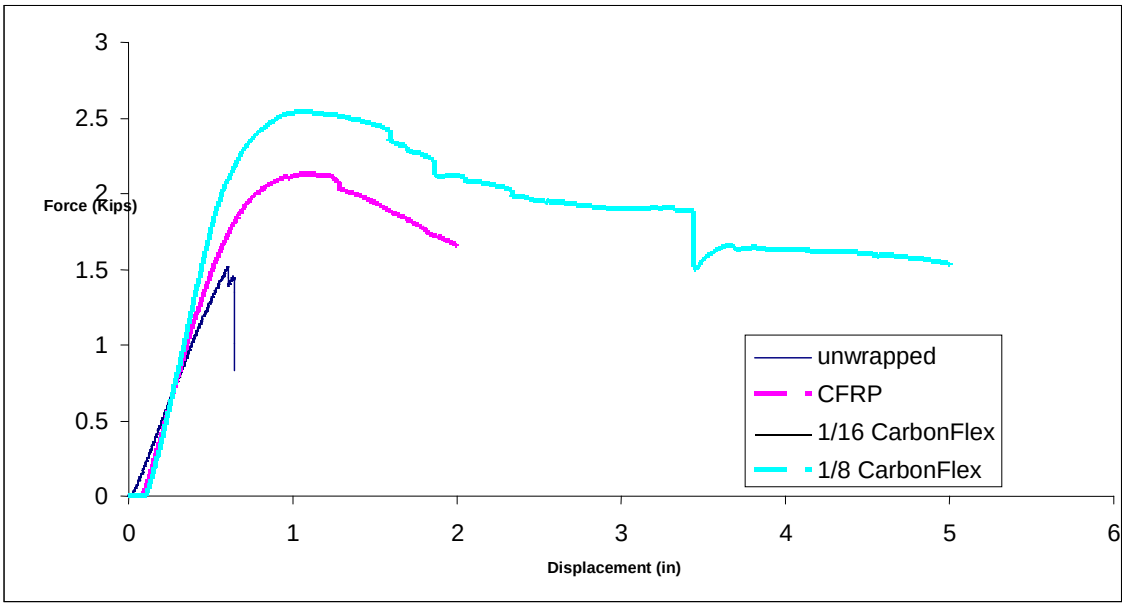

Figure 14. Force-displacement from three-point bending test.

The Stress-Strain Model for CarbonFlex Wrapped Wood Beam

A stress-strain model of the CarbonFlex wrapped wood beam has been developed and compared to the test results of the 2CF beam. The model can be separated into three regions which are the elastic region, the region between the post yield strength and the point of peak strength, and finally the region between the maximum strength and the ultimate points. In order to compare the results with the force-deflection experimental test results, the post-yield moment at each cross-section along the length of the beam was calculated, found by integrating the stress-strain models of the aforementioned regions which are shown in equation 3.10, 3.11, and 3.12. Within the elastic range, Hooke's law was assumed, where the modulus of elasticity of the CarbonFlex-wrapped wood beam was calculated from experimental results of the 1/8 thick CarbonFlex-wrapped wood (2CF) beam shown in Figure 14. Equation 3.10 describes the distribution of the elastic stress along the depth of the beam's cross-section.

$$\sigma_x = \frac{y}{e}\sigma_{yield} \text{ for } \frac{\varepsilon_x}{\varepsilon_{yield}} \le 1 \tag{3.10}$$

Stress and strain at some distance y (vertical direction) away from the neutral axis of the beam cross-section are defined as σ_x and ε_x; e is a distance from neutral axis to the beam's fiber that starts to yield, as shown in figure 15. The yield point of the material is defined by $(\sigma_{yield}, \varepsilon_{yield})$.

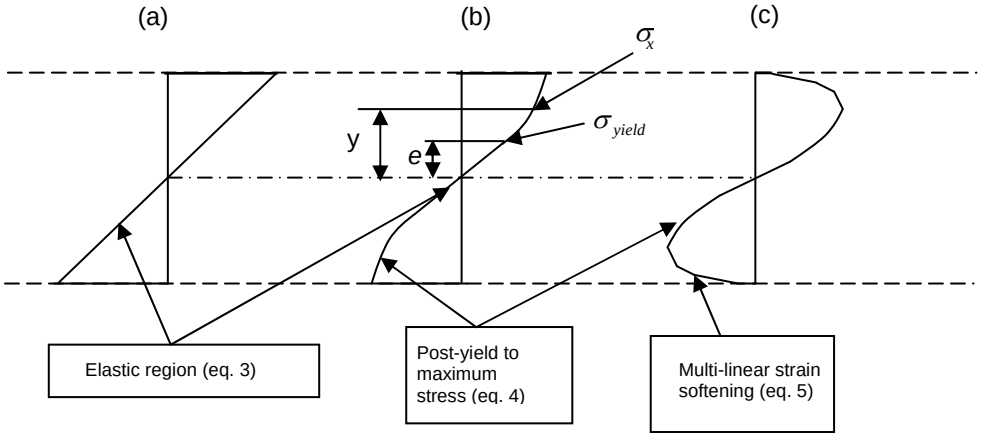

Figure 15. The stress distribution of each stress stage at the beam cross-section.

The stress-strain relationship of the region initiating with the occurrence of the post-yield strength up until the point of maximum strength has been developed using a constitutive relationship formulated on continuum mechanics theory that was previously developed by Attard (2005) and later applied by Attard and Mignolet in (2008). It is repeated here as equation 3.11 for convenience.

$$\frac{\sigma_x}{\sigma_{yield}} = 1 + 2\alpha_h\left(\frac{\varepsilon_x}{\varepsilon_{yield}} - 1\right) - \frac{\alpha_h}{\Delta_\varepsilon}\left(\frac{\varepsilon_x}{\varepsilon_{yield}} - 1\right)^2 \quad for \quad \begin{cases} 1 \le \dfrac{\varepsilon_x}{\varepsilon_{yield}} \le \Delta_\varepsilon + 1 \\ and \quad \dot{\varepsilon} \begin{cases} > 0 \quad if \quad \varepsilon_{yield} > 0 \\ < 0 \quad if \quad \varepsilon_{yield} < 0 \end{cases} \end{cases} \tag{3.11}$$

In equation 3.11, parameters α_h and Δ_ε are found experimentally; α_h defines the average modulus degradation (in term of initial elastic modulus; and E is the modulus of elasticity. Δ_ε is defined as a constant such that the post-yield strains are calculated as $\Delta_\varepsilon \varepsilon_{yield}$ and the strain at maximum stress, ε_m, is equal to $(\Delta_\varepsilon + 1)\varepsilon_{yield}$.

The results of the experimental tests revealed that the CarbonFlex-wrapped beam did not fail when the stiffness of the beam became zero, but following the peak load,

material softening was observed which did coincide with the sustainable negative stiffness which became less negative, as shown in figure 16. It is believed that the stiffness became less negative because CarbonFlex stabilized crack growth in the damaged substrates thus allowing any single crack that formed to become protected by dissipating incoming energy and thus not allowing the formation of new crack surfaces. The energy dissipation occurs via the polymer-epoxy cohesion interaction.

Many researchers have used power-law equations to describe the stress field in strain-softened regions (Chung & Mai, 1988; Miyauchi & Murata, 2007). However, the CarbonFlex-wrapped beam exhibited not only strain-softened behavior but also a region of significant sustainable negative stiffness which makes the system very unique. Therefore, the proposed model below was developed in the "sustainable" softened region as a function of strain using a multi-linear equation shown in equation 3.12, which appears to match well with experimental test data.

$$\sigma_x = \sum_{i=\Delta_\varepsilon+1}^{\Delta_\varepsilon+n+1}\left(\sigma_m + \alpha_i E\left(\varepsilon_{i+1} - \varepsilon_i\right)\right) \text{ for } \Delta_\varepsilon + 1 \le \frac{\varepsilon_x}{\varepsilon_{yield}} \tag{3.12}$$

Where σ_m and ε_m are stress and strain at maximum strength. *n* is a number of linear interpolation steps after maximum stress occurred which can be found using equation 3.13.

$$n = i \quad \text{when } i - 1 < \frac{\varepsilon_{\max} - \varepsilon_m}{\varepsilon_{yield}} \le i + 1 \text{ and } i = 1,2,3\ldots \tag{3.13}$$

n must be a positive integer and greater or equal to 1; $\varepsilon_{\max}$ is the strain at the extreme fiber of the cross-section; and the parameter α_i defines the slope of each linear interpolation step so that the slope is equal to $\alpha_i E$. Figure 15 shows the stress distribution

of each stress stage at the beam cross-section. After obtaining stress-strain relationships, the moment at any cross-section can be found by integrating equation 3.10, 3.11, and 3.12. Then, the force can be calculated as $F = \frac{4M}{L}$ (three-point bending simply supported beam).

Displacement calculation. For a general simply supported beam with a span length L and a concentrated load at the mid-span, the (maximum) post-yield displacement, Δ_p, at the mid-span is given by:

$$\Delta_p = \frac{L}{2}\int_0^{\phi_p} f(\Delta\phi)d(\Delta\phi) - \frac{1}{2}\int_0^{\phi_p} f^2(\Delta\phi)d(\Delta\phi) \tag{3.14}$$

The portion of the beam that has at least just yielded is defined as a post-yield length (PYL). In equation 3.14 and 3.15, PYL is defined as $f(\Delta\phi)$ which is a function of the post-yield curvature, $\Delta\phi$. The PYL can be also calculated as a function of the moment as described by Attard (2005):

$$PYL = \frac{L}{2M_E}\left(M_E - M_{yield}\right) \tag{3.15}$$

Where, M_E is a moment at mid-span for a simple supported beam. M_{yield} is a yielding moment calculated from yield stress. Although the force and deflection of the beam are separately calculated, the plot of force-deflection curve can be accomplished by pairing the force and deflection associated with the same strain. The comparison between experimental and numerical force-deflection curves is shown in figure 16. The computed stress-strain of the CarbonFlex wrapped beam was also shown in figure 17.

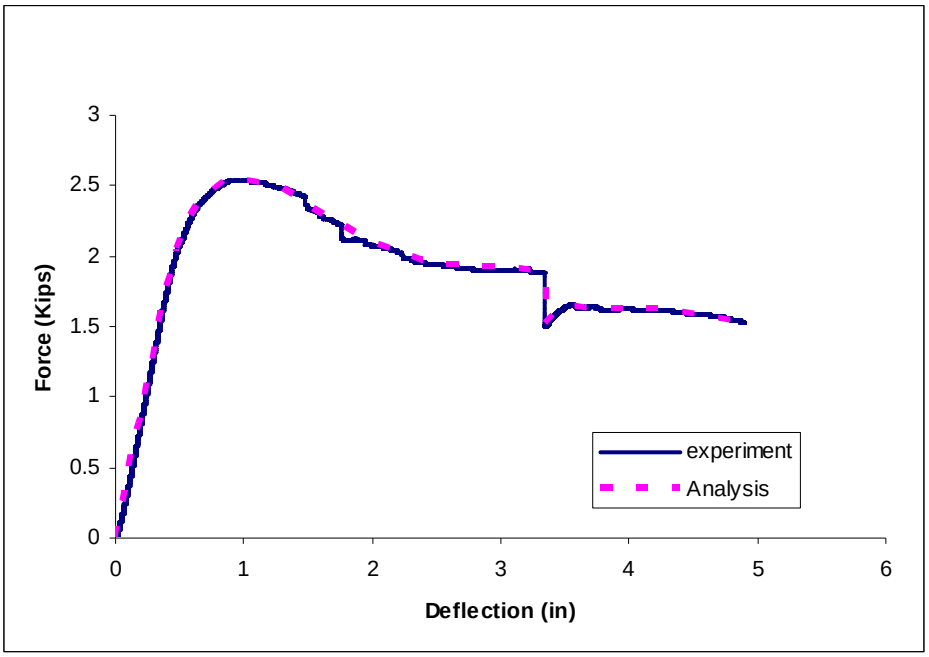

Figure 16. Comparison between experimental and numerical results.

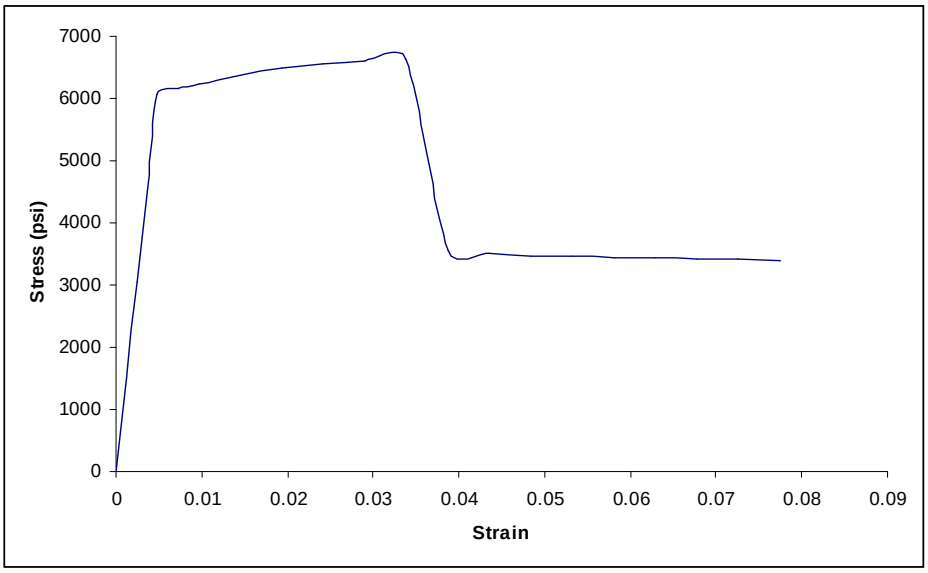

Figure 17. Stress-strain of the CarbonFlex wrapped beam.

CHAPTER 4

CarbonFlex Shear Wall: Specimen Details

To evaluate the potentials of CarbonFlex as an optional material used in seismic protection for wood structures, 16 walls and two single-story structures were tested. Wall specimens can be separated into two types which are perpendicular walls (PPW) and parallel walls (PLW).

PPWs are walls subjected to the loads that are perpendicular to the wall's plane. The objective of testing PPW is to find the suitable CarbonFlex wrapping schematic that should be used for this wall type. Six PPW specimens were constructed and tested. Five specimens were wrapped by CarbonFlex with different schematics and the other was sheathed by plywood panels.

PLWs are walls subjected to the loads that are parallel to the wall's plane (shear wall). This wall type is the main key used to evaluate seismic performance of CarbonFlex shear walls and to find the proper wrapping method. Ten PLW specimens were constructed to have identical size. Three PLW walls were sheathed by plywood panels and seven walls were wrapped by CarbonFlex.

In addition, two identical size single-story structures were constructed. The first structure was sheathed by conventional plywood. The other was tightly wrapped by CarbonFlex. The wrapping ideas, purposes, and details of each specimen were discussed in this chapter.

The experiment was separated into three phases. The objectives of phase one are finding the suitable CarbonFlex wrapping method and testing the capability of the testing system. In this phase, all PPW and six PLW specimens were tested. Phase two is

composed of four PLW specimens. The purpose of this phase is to ascertain the performance of CarbonFlex shear walls under the seismic loads. Finally, two single-story structures were tested in phase three to evaluate the benefits of using CarbonFlex as a seismic protection system for low-rise wood structures. The testing phase, type, sheathing schematic, and sheating material of each specimen were summarized in table 3.

Specimen Details: Phase 1

Six PPW and six PLW walls were tested in this phase. Details of each specimen were discussed in this section. CarbonFlex specimens tested in this phase have the same h_p and t_c which are 2 mm and 2.5 hours, respectively. Instead of using nails, CarbonFlex was attached to walls using epoxies (primer and saturant). First, a thin layer of the primer was applied on the substrates at the attaching location. One hour after applying the primer, a thin layer (about 0.02 inch) of the saturant was applied on top of the primer. Then, the carbon fiber strips (pre-cut to desired sizes) were attached on top of the saturant. Construction grade staplers were used to temporarily hold the carbon fiber strips while the bonding between CarbonFlex strips and substrates were not fully developed. One more layer of the saturant was applied on the strips using painting rollers to press the strips in order to make sure that the saturant penetrated through carbon fiber.

Walls subjected to the load perpendicular to the wall (PPW). All PPW specimens have the same dimensions which are 8 ft tall and 5 ft wide. One of them was sheathed by plywood panels; another was fully wrapped by CarbonFlex, and other four specimens were “joint wrapped” by CarbonFlex strips having different development lengths (varied from 1 ft to 4 ft). The connections at the top (studs to a top plate) and bottom (studs to a sill plate) of these “joint wrapped” walls were wrapped by CarbonFlex.

Each joint was wrapped by a 1.5 inch wide strip of CarbonFlex from the front side of the wall to underneath the sill plate (or over the top plate) and from underneath the sill plate to the back side of the wall as shown in figure 18.

Table 3.

Summarize of Testing Specimens' Details.

Testing phase	Specimen type	Sheathing schematic	Sheathing material
1	PPW	1 ft CF joint wrap	CF (h_p = 2 mm, t_c = 2.5 hrs)
1	PPW	2 ft CF joint wrap	CF (h_p = 2 mm, t_c = 2.5 hrs)
1	PPW	3 ft CF joint wrap	CF (h_p = 2 mm, t_c = 2.5 hrs)
1	PPW	4 ft CF joint wrap	CF (h_p = 2 mm, t_c = 2.5 hrs)
1	PPW	Fully sheathing	CF (h_p = 2 mm, t_c = 2.5 hrs)
1	PPW	Fully sheathing	7/16 inch thick Plywood
1	PLW (dummy wall)	Fully sheathing	3/8 inch thick Plywood
1	PLW	Fully sheathing	7/16 inch thick Plywood
1	PLW	Fully sheathing	7/16 inch thick Plywood
1	PLW	Fully sheathing	CF (h_p = 2 mm, t_c = 2.5 hrs)
1	PLW	CF strip bracing	CF (h_p = 2 mm, t_c = 2.5 hrs)
1	PLW	CF strip bracing with plywood	CF (h_p = 2 mm, t_c = 2.5 hrs) and 7/16 inch thick plywood
2	PLW	Fully sheathing	CF (h_p = 4 mm, t_c = 2.5 hrs)
2	PLW	Fully sheathing	CF (h_p = 4 mm, t_c = 3.5 hrs)
2	PLW	CF Fully sheathing with plywood	CF (h_p = 4 mm, t_c = 3.5 hrs) and 1/4 inch thick plywood
2	PLW	Fully sheathing with a window	CF (h_p = 4 mm, t_c = 2.5 hrs)
3	Single-story wood structure	Plywood fully sheathing with a window and a door	7/16 inch thick Plywood
3	Single-story CF structure	CF fully sheathing with a window and a door	CF (hp = 4 mm, tc = 2.5 hrs)

Note. CF = CarbonFlex, mm= millimeter, hrs = hours, h_p = thickness of the polymeric constituent, and t_c = time duration between mixing the saturant and spraying the polymeric constituent.

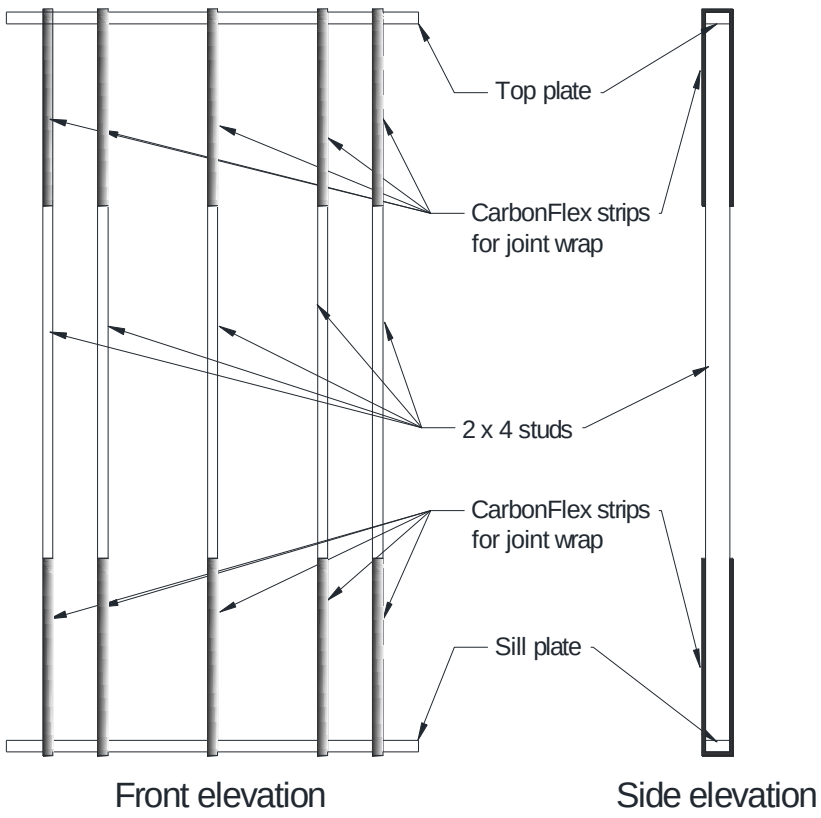

Figure 18. Front and side elevation views of a joint wrapped wall.

The first PPW specimen was the wall sheathed with 7/16 inch plywood. The plywood was attached to 2 in. x 4 in. wood studs using 6d common nails spacing at 6 in. on center (OC). This wall is used as a baseline to compare with other walls wrapped by CarbonFlex.

Joints of the PPW walls (joints between studs and sill or top plates) are not rigid due to nature of nail connections. Therefore, when the walls were subjected to the loads perpendicular to the walls' plane, walls moved in the rocking motion causing the opening gaps between studs and the top (or sill) plate. In addition, for PPW walls, the highest

moment and stress concentration (which were absorbed by nails) occurred at the joints resulting in the possibility of excessive nail deformation and joint damages. Thus, the idea of using CarbonFlex to wrap the joints was emerged. CarbonFlex provided additional energy dissipation and acted as a stud hold-down for the joints. Some of energy that otherwise concentrated at joints' fasteners was dissipated via CarbonFlex strips resulting in reduction of stress concentration and damages at the joints' fasteners. In this study, four PPW walls were wrapped by CarbonFlex at the joints. Each wall was wrapped with different length of CarbonFlex varied from 1 ft to 4 ft as shown in figure 19. The direction of reinforcing carbon fiber in CarbonFlex was aligned with the longitudinal axis of the studs.

The last PPW specimen was fully wrapped by CarbonFlex as shown in figure 20. The reinforcing fiber was aligned with the longitudinal axis of the wall which is the direction that the maximum tension occurred.

Walls subjected to the load parallel to the wall (PLW). Six PLW specimens have the same dimensions which are 8 ft tall and 8 ft wide. Three specimens were sheathed by plywood panels. Other two walls were sheathed by CarbonFlex. The last wall was sheathed by CarbonFlex strip bracing and two plywood panels.

The first wall is the dummy wall. The purpose of testing this wall is to calibrate the feedback control parameters used to control the actuator to simulate earthquake records. The wall was sheathed by two sheets of 4 ft x 8 ft x 3/8 in. plywood. Each sheet was placed so that the longer side was parallel to the ground. 6d common nails were used as the fasteners. Nail spacing was 12 in. OC at boundary edges of the sheets and at the connections between plywood sheets and interior studs.

Figure 19. (a) 1 ft joint wrapped wall. (b) 2 ft joint wrapped wall. (c) 3 ft joint wrapped wall. (d) 4 ft joint wrapped wall.

Figure 20. The CarbonFlex fully wrapped PPW wall.

All three feedback parameters were calibrated by running tests with various wave records which are sine waves, the Northridge and the Imperial Valley earthquake records having small amplitudes (0.5 and 1 in.). The feedback error was minimized after the tests.

The second wall is the plywood shear wall number one (PW1). This shear wall was sheathed by four panels of 4 ft x 4 ft x 7/16 in. plywood as shown in figure17. 8d common nails were used as the fasteners. Nail spacing was 6 in. OC at boundary edges and interior studs. Two Simpson tension strong ties (HTT5) were installed at the bottom corners of the wall. Both hold downs were anchored to the base plate (sill) using 1/2 in. x 3 in. lag screws.

The third wall is the plywood shear wall number two (PW2). The wall was sheathed by two panels of 4 ft x 8 ft x 7/16 in. plywood as shown in figure 21. Each sheet was placed so that the longer side was parallel to the ground. The 8d common nails were used with the spacing of 6 in. OC at boundary edges and interior studs. The hold downs

were anchored to the base plate using 5/8 in. bolts instead of lag screws as in the plywood shear wall number one. The bolts were embedded in rapid set® concrete poured on top of the sill plate. The concrete blocks were anchored to the sill plate using six of 1/2 in. lag screws.

Figure 21. The plywood shear wall number one.

The forth wall is the CarbonFlex strip bracing wall (CFSBW). Instead of plywood, ten pieces of 3 in. wide CarbonFlex (2 mm thick (h_p), 2.5 hours t_c) strips were used as sheathing material. Five strips were attached diagonally in each direction as shown in figure 22. First, the wall was tested without hold down. After tested, end studs were pulled out from sill plate. Therefore, the wall was retrofitted by replacing the sill plate and two Simpson tension strong ties (HTT5) were installed. Instead of using

concrete blocks as in the plywood shear wall number two, the pressure treated lumber was used to strengthen the sill plate at the hold down location. 5/8 in. bolts were fastened through the bottom of the sill plate to anchor hold downs.

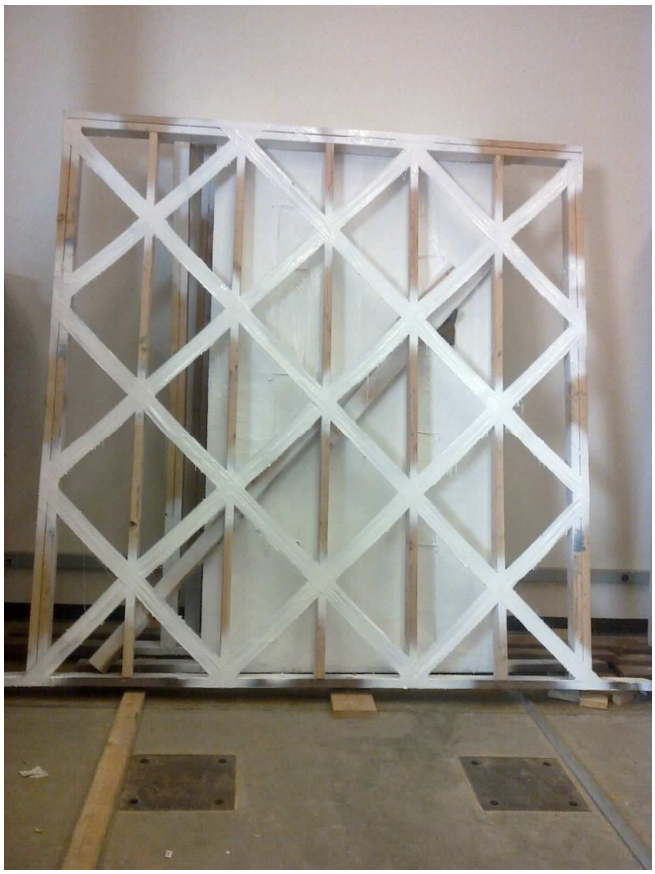

Figure 22. The CarbonFlex strip bracing wall.

The fifth wall is the CarbonFlex strip bracing with plywood wall (CFSPW). This wall was constructed in the same manner as the CarbonFlex strip bracing wall. In addition, two panels of 4 ft x 8 ft plywood were attached to the wall (on top of the CarbonFlex strips) using 8d common nails spacing at 6 in. OC at boundary edges and interior studs. Two Simpson tension strong ties (HTT5) were installed the same way as in the strip bracing wall (the forth wall).

The sixth wall is the CarbonFlex fully wrapped wall number one (CFFW1). This wall was sheathed by 2 mm thick (h_p), 2.5 hours t_c, CarbonFlex. The direction of the reinforcing carbon fibers in CarbonFlex is parallel to the ground as shown in figure 23. Two Simpson HTT5 hold downs were installed in the same way as the strip bracing wall (the forth wall).

Figure 23. The CarbonFlex fully wrapped wall number one.

Specimen Details: Phase 2

This phase composes of four PLW walls. The objectives of the tests are: 1) to study the effects of h_p and t_c to lateral resistance of CarbonFlex shear walls, 2) to evaluate the performance of CarbonFlex hold downs (U-wrap) compared to typical hold downs, 3) to investigate effects of having additional plywood in a CarbonFlex fully wrapped wall,

and 4) to evaluate the performance of CarbonFlex-wrapped wall with opening (a window).

Figure 24 shows the CarbonFlex fully wrapped wall number two (CFFW2). This wall was wrapped by 5/32 in. (4 mm) thick (h_p), 3.5 hours t_c, CarbonFlex. Two Simpson tension strong ties (HTT5) were installed at both end studs. In addition, 4 in. x 9 in. CarbonFlex strips were placed at bottom of the panel in between studs to form an "L-wrap". The purpose of these strips is to increase shear capacity at the bottom of the panel.

Figure 24. The CarbonFlex fully wrapped wall number two.

The second wall in this phase is CarbonFlex fully wrapped wall number three (CFFW3). This wall was sheathed by 5/32 in. (4 mm) thick (h_p), 2.5 hours t_c, CarbonFlex. In addition, two pieces of 5 in. x 11.5 ft CarbonFlex strips were attached diagonally to form cross-bracings. From previous tests in phase one, one of the failure modes in

CarbonFlex PLW walls is studs pulled out from the sill plate. Therefore, both end studs were wrapped by two CarbonFlex strips to form a “U-wrap”. Additional two strips of CarbonFlex were placed at the sides of end studs (one strip per side) to form an “L-wrap” as shown in figure 25. In addition, a 1.5 in. wide CarbonFlex strip was wrapped at each interior stud to form a “U-wrap”. For the load transfer system, a steel C-channel was used as a foundation of the wall. The sill plate was anchored to the C-channel. The C-channel was anchored to the strong ground by three of 1-1/4 in. bolts. The Simpson hold down was not used in this specimen.

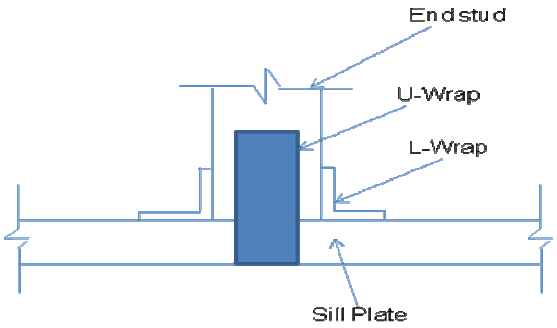

Figure 25. U-wrap and L-wrap at the end studs.

The third wall is the CarbonFlex fully wrapped plywood shear wall (CFPW). First, two panels of 4 ft x 8 ft x 1/4 in. plywood were attached to the studs using 8d common nails at 6 in. OC Then, the wall was wrapped by 5/32 in. (4 mm) thick (h_p), 2.5 hours t_c, CarbonFlex in the same manner as the fully wrapped wall number three. Testing results from this wall were compared to those of the fully wrapped wall number two to study effects of having additional plywood panels in a CarbonFlex fully wrapped wall.

The last wall in this phase is the CarbonFlex-wrapped wall with opening (CFOW). This wall was wrapped by 5/32 in. (4 mm) thick (h_p), 2.5 hours t_c, CarbonFlex in the same manner as the fully wrapped wall number three. In addition, there is a 2 ft x 4

ft opening located at 12 in. from the edge as shown in figure 26. Testing results from this wall were compared to those of the fully wrapped wall number two.

Figure 26. The CarbonFlex-wrapped wall with opening.

Specimen Details: Phase 3

In this phase, two-8 ft tall, 9.5 ft x 8 ft structures were built and tested. One of the structures was sheathed by plywood panels. The structure is illustrated in figure 27 (wood house). The other was fully wrapped by CarbonFlex which is shown in figure 28 (CarbonFlex house). Both structures have two opening. One opening is the 6 ft x 3 ft door located on one of the walls that is perpendicular to the load. The other is 2 ft x 4 ft window located on one of the walls that is parallel to the load.

The wood house consists of two shear walls. One wall is fully sheathed. The other wall has a window opening. Both shear walls were sheathed with 4 ft x 8 ft x 7/16 in. plywood panels. 8d common nails were used as the fasteners. Nail spacing was 6 in. OC

at boundary edges and at connections between plywood sheets and interior studs. The plywood sheets were installed so that the longer side of the sheets was parallel to the ground. At the middle of the wall, the blockings were installed parallel to the ground to support the boundary edges of plywood sheets. Four Simpson tension strong ties (HTT5) were installed at the corners of the house.

Figure 27. The single-story wood structure.

The CarbonFlex structure was wrapped by 5/32 in. (4 mm) thick, 2.5 hours t_c, CarbonFlex. In addition, 4 in. x 9 in. CarbonFlex strips were placed at bottom of the walls between studs to form an “L-wrap”. Four Simpson tension strong ties (HTT5) were installed at the corners of the house. Figure 28 shows the house with both openings.

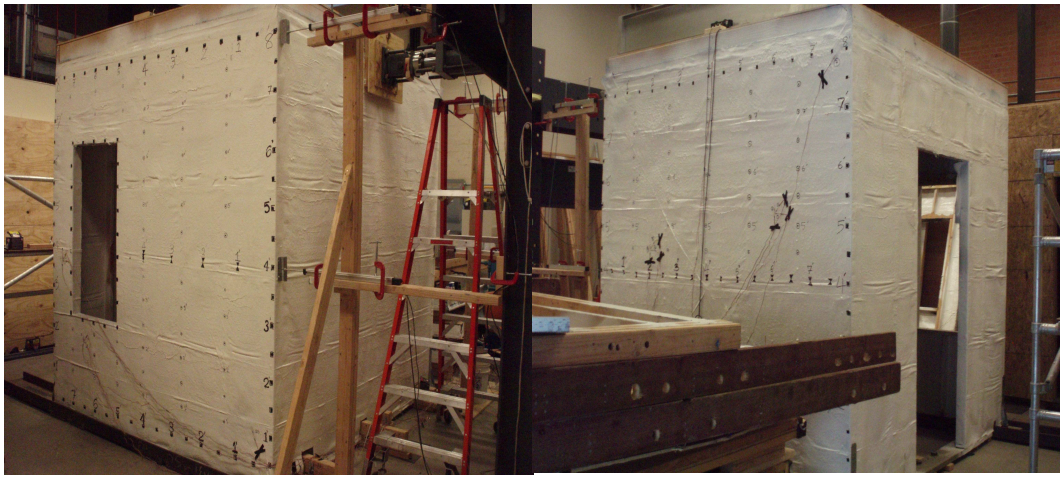

Figure 28. The single-story CarbonFlex-wrapped structure.

Testing results from the CarbonFlex house were compared to those of the wood house. The comparisons showed that CarbonFlex can sustain the structure integrity of the single-story structure while a lot of damages were observed from the wood house. Discussions and comparisons of testing results from every specimen were provided in the next chapter.

CHAPTER 5

CarbonFlex Shear Wall: Experimental Results

Results from seismic tests of wood-framed specimens sheathed with conventional plywood and CarbonFlex were reported and discussed in this chapter. The discussions began with experimental results from walls subjected to loads perpendicular to the wall (PPW) following by results from walls subjected to parallel loads (PLW). Finally, experimental results from the single-storey plywood structure were compared to those of the CarbonFlex structure.

Phase 1: Walls Subjected to Load Perpendicular to the Wall (PPW)

The actuator was connected to the top of specimens using a steel connector. The actuator's position was adjusted so that its axis was perpendicular to the wall's plane. Each specimen was tested using an increasing amplitude sine wave having three cycles. Each cycle has different amplitude which are two, three, and four inches, respectively. The sine wave is shown in figure 29.

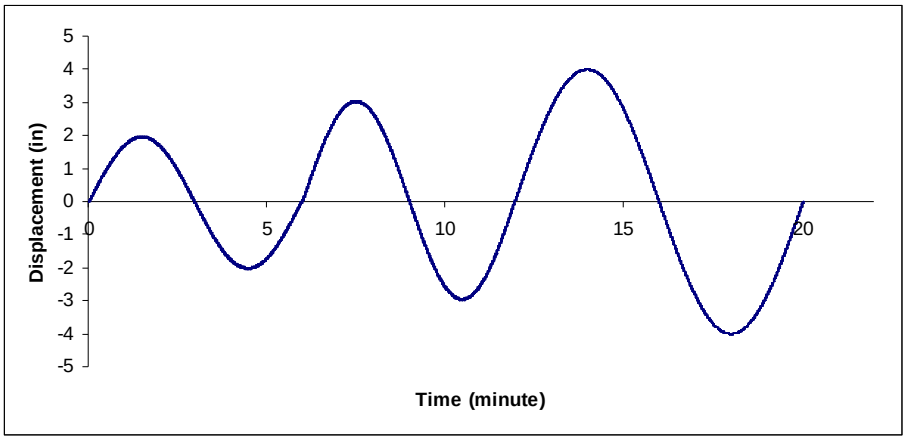

Figure 29. An increasing amplitude sine wave used in PPW tests.

Both CarbonFlex and plywood specimens exhibited highly nonlinear behavior. Figure 30 illustrates a comparison of testing results between the plywood sheathed PPW and the CarbonFlex fully wrapped PPW. With the same areal amount of sheathing material, the CarbonFlex PPW has greater stiffness and maximum load than the plywood PPW. This might be because CarbonFlex has higher stiffness than plywood in tension. In addition, the plywood PPW may rely on the nails connecting studs to sill and top plates as its stiffness and energy dissipation providers. To support this assumption, a cantilever wood beam test was conducted.

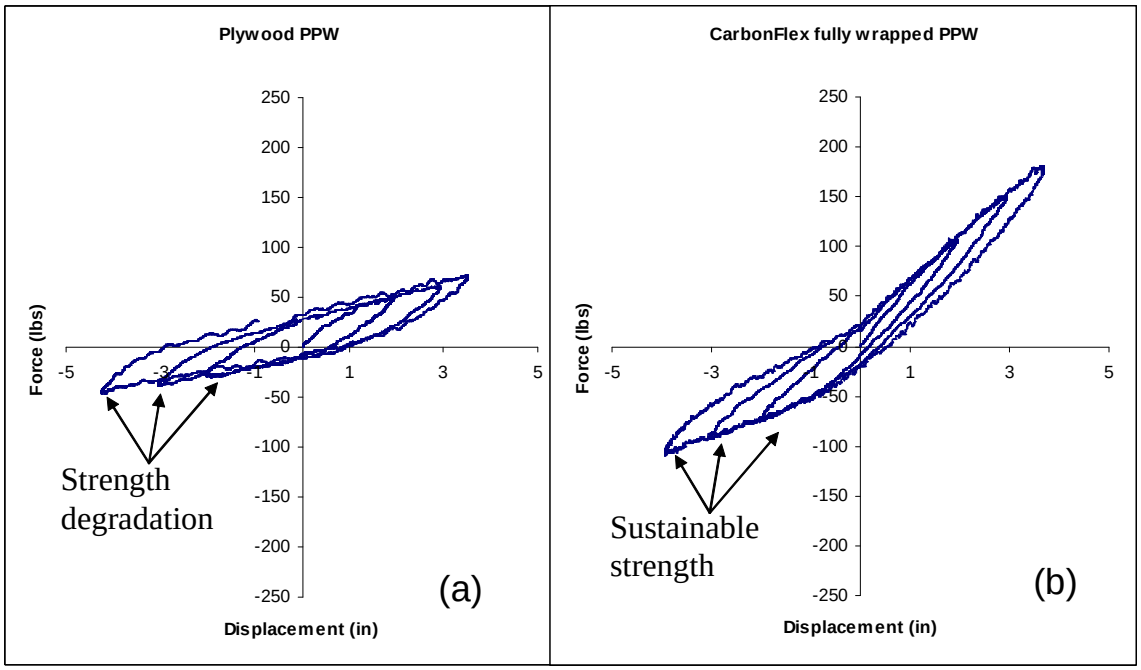

Figure 30. Sine wave testing results of (a) the plywood sheathed PPW and (b) a CarbonFlex fully wrapped PPW.

The purpose of the cantilever wood beam test is to find a relationship between fixed-end moments and rotations of the beam. Figure 31 shows a cantilever wood beam

test set-up. The beam is a 2 in x 4 in lumber having a seven inches span length. The beam was connected to the wood frame using two nails.

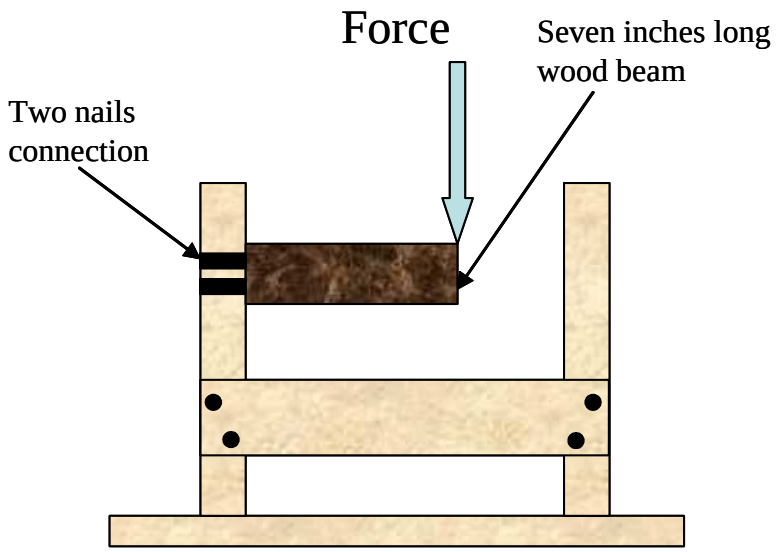

Figure 31. A cantilever wood beam testing apparatus.

The moments and rotations can be calculated from forces and displacements obtained from the testing machine using equation 5.1 and 5.2.

$$M = FL \tag{5.1}$$

$$\theta = ARCTAN\left(\frac{\Delta}{L}\right) \tag{5.2}$$

Where M is fixed-end moments, F is forces, θ is rotations, Δ is displacements, and L is a span length. The fixed-end moment and rotations were compared to those obtained from results (linear part) of the plywood PPW specimen. However, the equation used to calculate fixed-end moments for plywood PPW is different because it is not a cantilever beam. Therefore, equation 5.3 was used to calculate the moments for plywood PPW.

$$M = \frac{FL}{2} \tag{5.3}$$

In addition, the plywood PPW composed of seven studs. To have a fair comparison, the forces obtained from plywood PPW test were divided by seven before calculating the moments.

Figure 32 shows a comparison of testing results from a cantilever beam and the plywood PPW specimen. The relationship between moments and joint rotation of the plywood PPW is almost the same as that of the cantilever beam. This implies that the nails connecting the joints mainly provided moment-resistance and stiffness to the plywood PPW. Furthermore, the CarbonFlex fully wrapped PPW has a higher stiffness which implies that the forces were resisted not only by the joints' nails, but also by CarbonFlex. Therefore, there was less stress concentration at the nails which are critical components of the wall making the CarbonFlex fully wrapped PPW stronger and more durable than the plywood PPW.

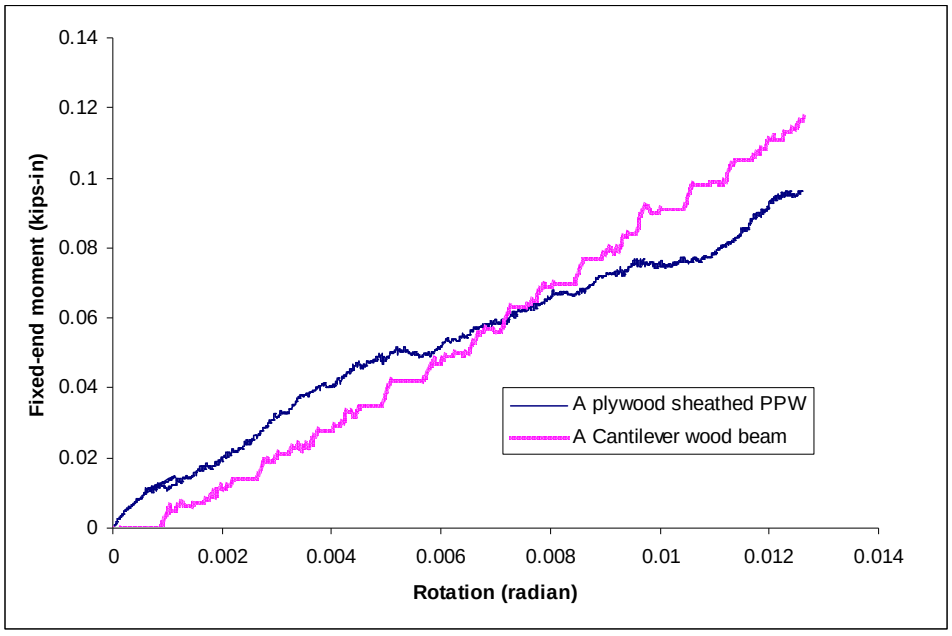

Figure 32. Testing results from a cantilever beam and a plywood PPW specimen.

A CarbonFlex panel did not only increase stiffness but also help sustain structural integrity of PPW. As can be seen from figure 30(a), strength and stiffness of the plywood PPW degraded every cycle. Li, Foschi, and Lam (2012) created a numerical model that can predict behaviors of a wood-nailed connection and a wood shear wall. The model can also capture the degradation of the shear wall's strength and stiffness. They described that when the nail moved back and forth horizontally, the wood medium around the nail's shank was crushed and compressed creating a gap as shown in figure 33 and a degradation of stiffness of the wood-nailed connection varies directly to the size of the gap.

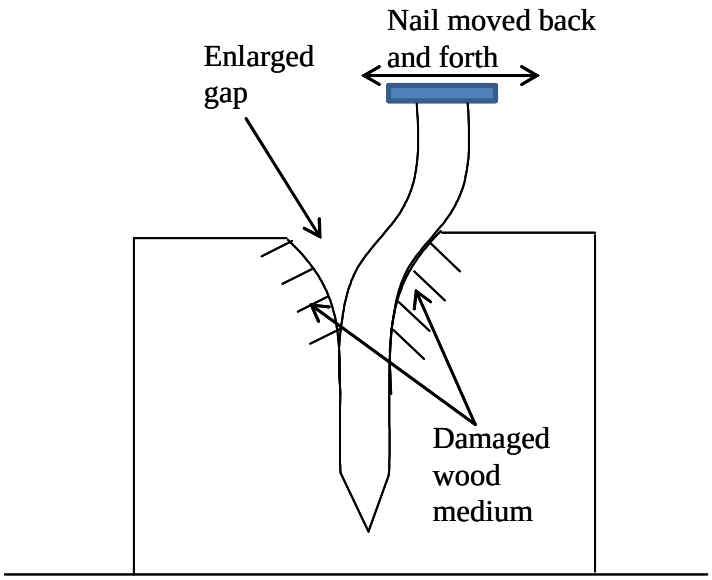

Figure 33. Wood damages around a nail's shank created a gap which deteriorated a stiffness of the wood and nail connection.

Although stiffness of the CarbonFlex fully wrapped and the joint wrapped PPW specimens also degraded, the strength of CarbonFlex specimens were sustained even though they were subjected to higher loads as shown in figure 30(b). This confirmed that CarbonFlex absorbed energy and reduced the forces which would be dissipated through

the nail. Consequently, damages at the wood medium around the nails' shank were reduced resulting in the sustainable strength of the CarbonFlex-wrapped PPW specimens.

After the tests, no severe damage could be observed from all specimens. However, studs of the wall sheathed by plywood were pulled out a little bit from both top and sill plates as shown in figure 34.

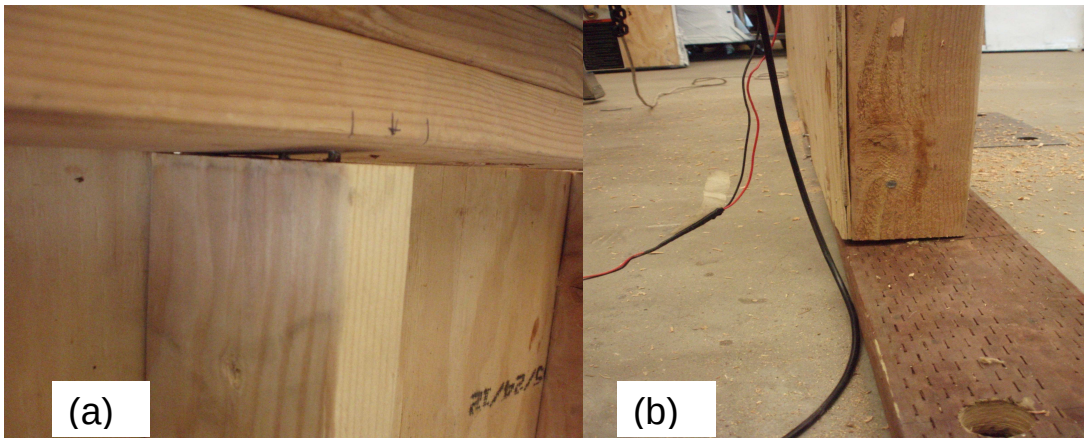

Figure 34. (a) Studs were pulled out from the top plate. (b) Studs were pulled out from the sill plate of the wall sheathed with plywood.

The objective of testing PPW is to find a suitable CarbonFlex wrapping schematic that should be used for PPW walls in the CarbonFlex house specimen. Therefore, stiffness and damping ratio are interested quantities used to select the best wrapping schematic. However, the test results indicated that stiffness of PPW is very low compared to that of the shear wall (PLW). Therefore, only damping ratio was used in wrapping method selection.

To find the damping ratio, two free vibration tests were conducted for each wall. Each CarbonFlex-wrapped PPW was pushed to have a small initial displacement and released. The displacements were recorded. The logarithmic decrement method was used to calculate damping ratios. To have a fair comparison, an average damping ratio of each

wall was divided by the amount (area) of CarbonFlex used in each wall to obtain damping ratio per square inch (DSI) of CarbonFlex. Table 4 shows an average damping ratio and DSI of each wall. The one ft CarbonFlex joint wrapped PPW provided the maximum DSI. Therefore, the one ft joint wrap was selected to be used for the walls subjected to the perpendicular loads in the CarbonFlex structure specimen tested in phase 3.

Table 4

Average Damping Ratios per Square Inch of CarbonFlex PPW

Wall Type	Average damping ratio	DSI ($1/in^2$) x 10^{-5}
1 ft CarbonFlex joint wrapped wall	0.296	53.6
2 ft CarbonFlex joint wrapped wall	0.317	28.7
3 ft CarbonFlex joint wrapped wall	0.377	20.4
4 ft CarbonFlex joint wrapped wall	0.374	17
CarbonFlex fully wrapped wall	0.406	7.06

Note. DSI = average damping ratio per square in of CarbonFlex. in^2 = square inch.

In addition, the relationship between damping ratio and lengths of CarbonFlex strips in joint wrapped PPWs was determined. Figure 35 shows a parabolic relationship between average damping ratios and the lengths of CarbonFlex strips. The parabolic relationship can be expressed by equation 5.4.

$$ADR = 0.0042L_{CF}^2 + 0.0048L_{CF} + 0.288 \quad (5.4)$$

Where *ADR* is an average damping ratio and L_{CF} is a length of CarbonFlex.

Phase 1: Walls Subjected to Load Parallel to the Wall (PLW)

Three modified 1994 Northridge earthquake records were used to test PLW specimens. The records can be categorized using their peak displacement levels which are low (LPD), moderate (MPD), and high (HPD) peak displacement. For the LPD test,

the record was modified so that the maximum displacement of the record is 0.15 inch. The purpose of this test is to quantify an initial effective stiffness and energy dissipation of undamaged specimens.

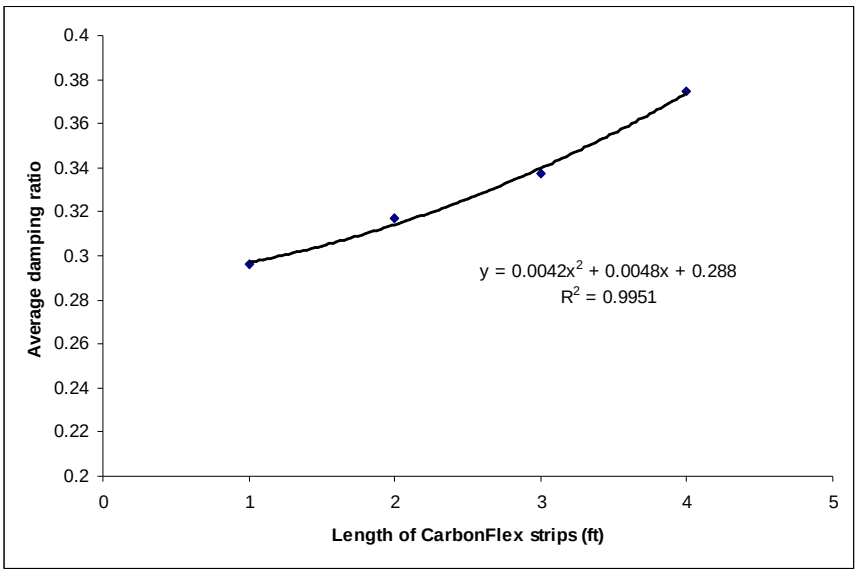

Figure 35. The relationship between average damping ratios and lengths of CarbonFlex.

Because the actuator used to generate the earthquake has a maximum stroke up to eight inches, the earthquake record was modified so that the specimens can be tested by the highest level of displacement without exceeding the actuator's capacity. Therefore, two experimental cases can be conducted. The first case is the Moderate Peak Displacement (MPD) test having displacements within the range of negative four to positive four inches. In the second case, the High Peak Displacement (HPD), the earthquake record was modified so that its minimum and maximum displacements fell within the range of zero to eight inches.

After tested by the LPD record, PLW specimens were tested using the MPD record which is shown in figure 36. The maximum and minimum displacements of the MPD record are +3.78 and -3.5 inches, respectively.

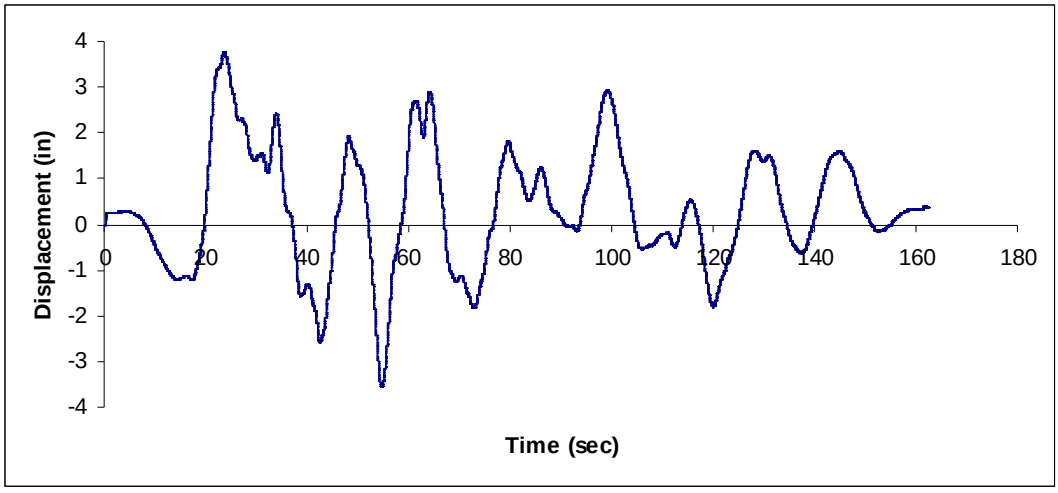

Figure 36. The Moderate Peak Displacement record (MPD).

If the specimens survived the MPD record (still able to be tested), the specimens would be tested using the HPD record which is a modified version of the MPD record. The HPD record begins with a ramp function until the displacement reaches four inches. After that, the MPD record is superimposed to the ramp function. The minimum and maximum displacements of the record are 0 and +7.85 inches, respectively. The HPD record is shown in figure 37.

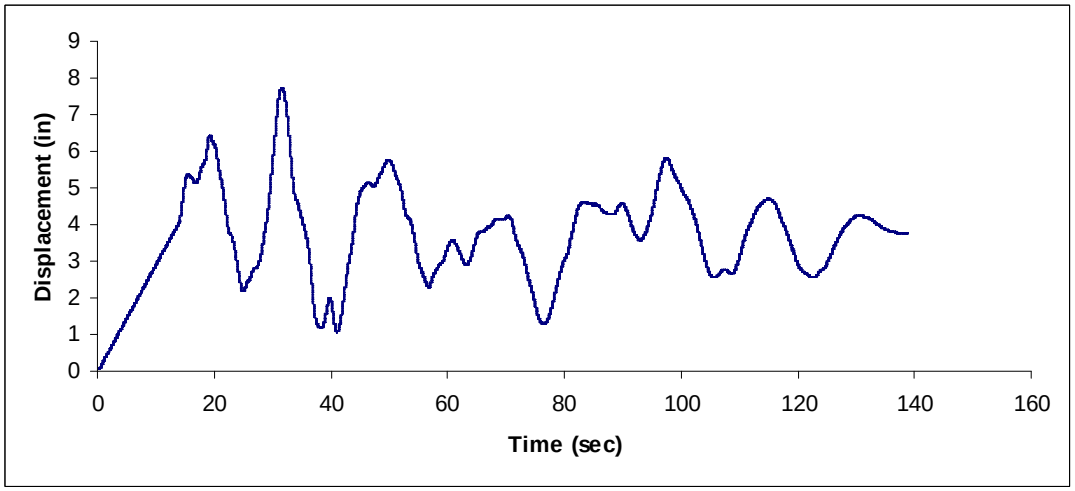

Figure 37. The High Peak Displacement record (HPD).

Plywood shear walls. Effects of several conditions, such as aspect (height to width) ratio, length and opening dimensions, hold-down positions, and sheathing materials, to the performance of wood frame shear walls were studied widely by many researchers (Lebeda, Gupta, Rosowsky, & Dolan, 2005; Patton-Mallory, Soltis, Wolfe, & Gutkowski, 1985; Salenikovich & Dolan, 2003; Sinha & Gupta, 2009).

A few researchers studied the influences of small-size sheeting panels to the performances of wood-framed shear walls. For example, (Martin, Skaggs, & Keith, 2005) tested four shear walls having 4.5 ft x 8.5 ft dimensions. Two specimens were sheathed with a full size plywood panel and two-6 in x 96 in plywood panels. The other two specimens were sheathed by three panels of which the smallest dimension is not less than 24 inches. The test results indicted that the differences between specimens having 24-inch panels and six-inch panels are negligible and the use of six inches narrow panels did not affect the stiffness and strength of the wall.

Specimens tested in the study have 2:1 height-to-width ratio which is a maximum aspect ratio (without strength reduction penalty) allowed in the 2008 Wind and Seismic, Special Design Provisions for Wind and Seismic (American Wood Council, 2008) which is referred by the 2009 International Building Code (International Code Council, 2009a). However, most of conventional shear walls have low aspect ratio and a wall having high aspect ratio might act more like a cantilever beam of which deformations are dominated by bending of studs not by shear deformations of the wall. Therefore, experimental tests of a specimen (PW1) which has 1:1 aspect ratio and sheathed with four-4 ft x 4 ft plywood panels were conducted. The results were compared with those of the plywood

shear wall number two (PW2) having 1:1 aspect ratio and sheathed with two-full size plywood panels.

Figure 38 shows a comparison of a force-displacement curve between PW1 and PW2 from the tests with LPD record. It can be seen that PW1 has a lower stiffness than PW2. This might be because PW1 acted as two-4 ft x 8 ft walls connected together while the PW2 acted as an 8 ft x 8 ft wall as shown in figure 39(a) and (b).

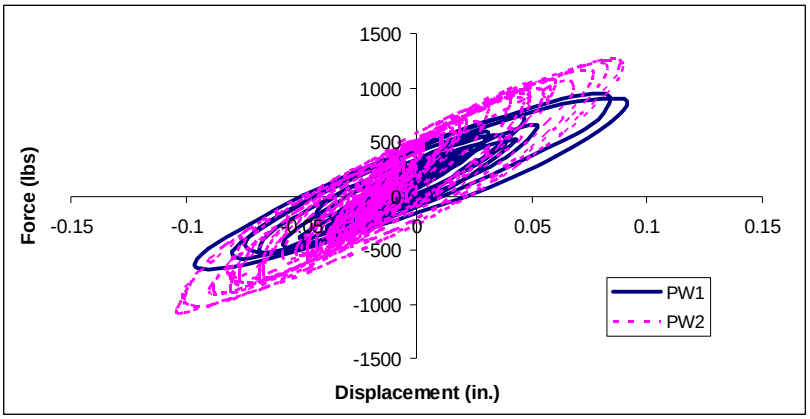

Figure 38. Force-displacement curves of PW1 and PW2 tested by LPD record.

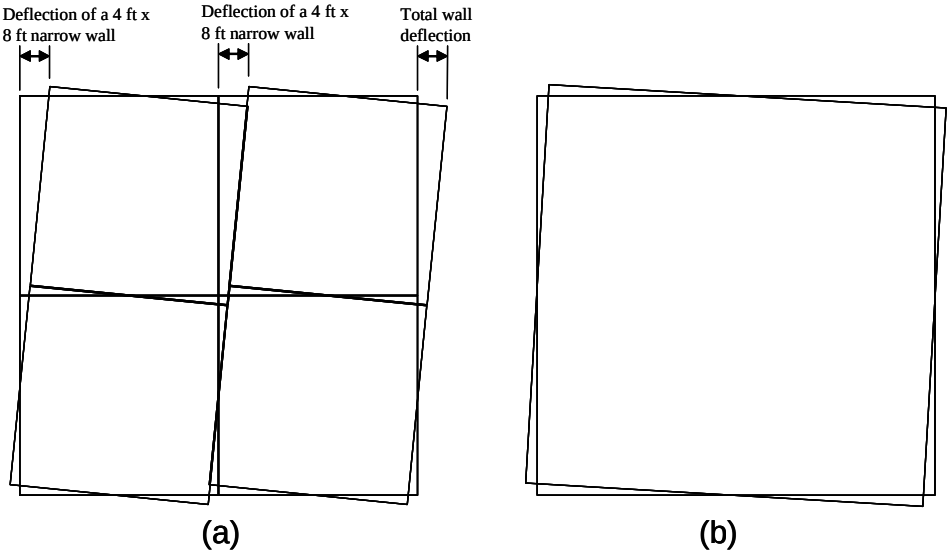

Figure 39. (a) PW1 acted as two-4 ft x 8 ft walls connected together. (b) PW2 acted as a 8 ft x 8 ft wall.

The 2009 International Building Code provides equation 23-2 by which a shear wall's displacement can be calculated. For convenience, it is shown here:

$$\Delta_{pw} = \frac{8vh^3}{EAb} + \frac{vh}{Gt} + 0.75he_n + \frac{hd_a}{b} \quad (5.5)$$

Where Δ_{pw} is a shear wall's deflection, v is a shear force at the top of the wall, h is a height of the wall, E is elastic modulus of studs, A is a cross-section area of boundary elements (end-studs), b is a width of the wall, Gt is a panel rigidity through the thickness, e_n is a nail slip, and d_a is a hold-down slip. Diaphragms and Shear Walls Design/Construction Guide (APA – The Engineered Wood Association, 2001) described that deflections of framing members (Δ_{bend}), through thickness shear deformations of sheathing panels (Δ_{shear}), deformations due to nails' slip (Δ_{nail}), and deformations due to slip of hold-down ($\Delta_{holddown}$) are represented by the frist, second, third, and forth terms on the right-hand side of equation 5.5, respectively.

The maximum force and displacement from the LPD test were very low. Therefore, the Δ_{nail} and $\Delta_{holddown}$ could be neglected. Δ_{shear} depends on shear modulus and thickness of the sheathing panels (Gt) and the shear force (v). Because PW1 and PW2 used the same panel type (same Gt) and the shear force was assumed to be distributed equally along the length of the walls (same v), both walls should have the same Δ_{shear}. Therefore, the only factor that affected the deflection of the walls when subjected to the LPD record is Δ_{bend}.

Considering the PW1 as two-narrow shear walls as shown in figure 39(a), the deflection of each narrow wall should be equal to the total deflection of the wall. Assuming that shear force was distributed equally along the wall's length, thus each

narrow wall took half of the total shear force (v/2). The width of the narrow wall is equal to four feet which is half of the width of PW2 (b/2). For the PW2, both end-studs were built from double-2 in. x 4 in. lumbers. Thus, the cross-sectional area of end-stud is 21 in^2 (2 x 3.5 x 3). For the narrow wall in PW1, one of its end-studs is a double-2 in x 4 in of which the cross-section area is 10.5 in^2. Another end-stud is a stud at the middle of the wall which is a single 2 in x 4 in lumber. However, this stud was shared by two-narrow walls. Therefore, the total end-stud cross-sectional area of PW2 is 13.125 in^2 {10.5 + (3.5 x 1.5/2)} which is 62.5 percent of that of PW1 (0.625A). Therefore, bending deflection of PW1 and PW2 can be calculated using equation 5.6 and 5.7, respectively.

$$\Delta_{bPW1} = \frac{8(v/2)h^3}{E(0.625A)(b/2)} \tag{5.6}$$

$$\Delta_{bPW2} = \frac{8vh^3}{EAb} \tag{5.7}$$

By rearranging equation 5.6 and 5.7, the stiffness of PW1 (k_{pw1}) and PW2 (k_{pw2}) can be expressed as:

$$k_{pw1} = \frac{v}{\Delta_{bPW1}} = 0.625 \times \frac{EAb}{8h^3} \tag{5.8}$$

$$k_{pw2} = \frac{v}{\Delta_{bPW2}} = \frac{EAb}{8h^3} \tag{5.9}$$

By comparing equation 5.8 and 5.9, an effective stiffness of PW1 is 37.5 percents less than that of the typical wall (PW2).

Because both specimens were not damaged prior the test and the maximum displacement of LPD is very small, the stiffness computed from the test results reflects an initial stiffness of each wall. However, the walls exhibited highly nonlinear behavior.

Thus, an effective stiffness (K_{eff}) was computed and used as one of the performance indicators. An effective stiffness is defined as a slope of a straight line passing point A and B on the force-displacement curve as shown in figure 40.

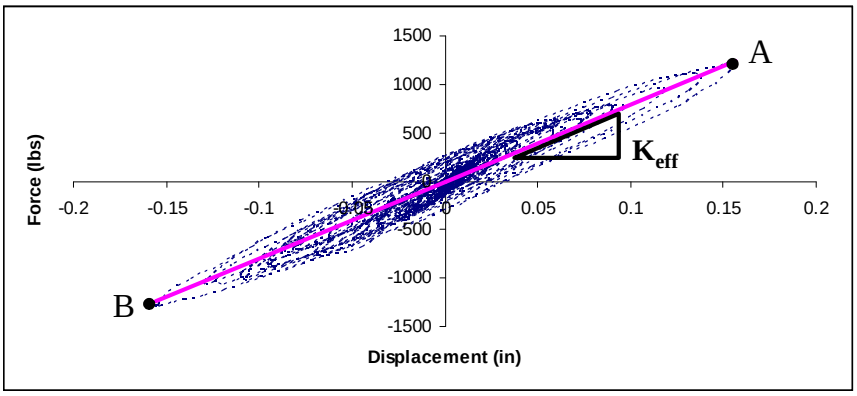

Figure 40. Definition of an effective stiffness (K_{eff}).

Point A is the point of the force associated with the maximum displacement while point B is the point of the force associated with the minimum displacement. The K_{eff}s are 8141.84 and 12316.76 lbs/in. for PW1 and PW2, respectively. The K_{eff} of PW1 is 34 percent less than that of PW2 which is close to the calculation from equation 5.8.

To evaluate performances of the shear wall sheathed by smaller size plywood panels (PW1), a load at allowable inter-story displacement was compared to that of the PW2 and to the designed shear capacity. Both PW1 and PW2 walls were constructed using the same sheathing material and nail schedule. Therefore, their allowable shear capacity should be the same. According to the 2009 International Building Code, table 2306.2.1 (1) (International Code Council, 2009a), the allowable (designed) shear capacity of the walls is 2040 pounds (255 pound per foot of the wall's width). The allowable inter-story drift for seismic design is given in table12.12-1, ASCE 7-10. For residence building (design category II), the allowable story drift is 0.025h, where, h is a story's height in

inch. The height of PW1 and PW2 is 96 inches (8 feet). Therefore, the allowable drift is 2.4 inches.

The loads at allowable displacement of PW1 and PW2, which were obtained from MPD test, are 5742.19 and 6876.95 pounds, respectively. The load of PW1 is 16.5 percent less than that of PW2 implying that the stiffness of PW1 is less than that of PW2 too. The reduction of the stiffness is not consistent to the calculation from equation 5.8 because the specimens' behaviors were highly nonlinear when they were subjected to the MPD record while equation 5.8 assumed that the walls have an elastic behavior.

To compare the loads with the designed shear capacity, the loads must be divided by an overstrength factor specified in ASCE 7-10, table 12.2-1 (American Society of Civil Engineers, 2010), before they can be compared to the allowable capacity. An overstrength factor for wood-framed shear wall is 2.5. After divided by an overstength factor, the loads from both walls are greater than the designed shear capacity.

In conclusion, the dimension of sheathing panels can affect stiffness of a shear wall. The small width panel might discretize the width of a full-size wall which can increase the wall's aspect ratio resulting in reduction of the wall's stiffness. However, the wall sheathed by 4 ft x 4 ft panels had an acceptable performance (it has a higher load capacity than a designed shear capacity at the allowable displacement). In the future, a thorough study of panel's dimension effects should be conducted.

Selecting a wrapping configuration for CarbonFlex shear walls. Two wrapping configurations, which are CarbonFlex strip bracing and CarbonFlex fully wrapping were implemented in two specimens which are a strip bracing (CFSBW) and a

fully wrapped (CFFW1) walls. Construction details of the specimens were discussed in the previous chapter.

An idea behind a wrapping scheme of the strip bracing wall (CFSBW) came from experimental results of steel plate shear wall (SPSW) tests. A SPSW consists of boundary members (columns and beams) and an infill thin steel plate (Qu, Bruneau, Lin, & Tsai, 2008). Astanesh-Asl (2000) described behaviors of the SPSW that the system acts as a vertical plate girder in which columns act as flanges, the plate acts as a web, and the beams act as stiffeners. When the SPSW was subjected to horizontal in plane loads, inclined tension and buckling strips occurred on the steel plate (Timler & Kulak, 1983; Elgaaly, 1998). Thorburn, Kulak, and Montgomery (1983) found that the bucking zones have a minimal contribution to the ultimate strength of the system. They also proposed the first numerical model to predict behaviors of SPSW which has been widely accepted by many researchers and engineers (Shishkin, Driver, & Grondin, 2009). In the model, the steel plate was considered as many inclined tension "strips" resisting the horizontal movement of the SPSW.

Because a CarbonFlex panel (in fully wrapped wall) is a thin plate, tension and buckling strips were expected to occur on it. Therefore, to save materials, CarbonFlex strips were used in lieu of the fully sheathing panel. The strips represented the tension zones and the voids (gaps) between the strips represented the buckling zones.

Many parameters, namely effective stiffness (K_{eff}), maximum load (P_M), load at maximum displacement (P_{MD}), and maximum hysteretic energy dissipation (D_{HM}) were obtained from experimental results and used as performance indicators. All indicators were quantified and summarized in table 5. The hysteretic energy dissipation per cycle,

which reflects the hysteretic damping ratio of the wall, is defined as an area under the force-displacement curve of each full cycle. The maximum hysteretic energy dissipation (D_{HM}) was found in the cycle that the maximum load occurred.

An effective stiffness of each wall was calculated from the LPD test as mentioned before. K_{eff} of CFSBW is 41 percent less than that of CFFW1. Although CFFW1 has the lower maximum load than CFSBW, its D_{HM} and P_{MD} are higher. These were results of two sudden droppings of the load in CFSBW when its strips were broken. After reaching the peak load, the sill plate of the CFFW1 was broken due to the high over turning moment that was transferred to the sill plate by the hold-down. However, CFFW1 still be able to sustain the load resulting in gradually decreasing of the post-peak loads**.** For CFSBW, after the peak load, one of the strips was broken resulting in the first "sudden" dropping of the load which implies that the CFSBW has less ductility than CFFW1. One more strip was also broken when the wall was pulled (subjected to the negative displacement) resulting in another sudden dropping of the load as shown in figure 41.

Table 5

Summary of Performance Parameters of CFFW1 and CFSBW

Parameter	CFFW1	CFSBW
Effective stiffness (K_{eff}) (pound/inch)	7965.11	4675.44
Maximum load (P_M) (pound)	5192.58	5947.27
Load at maximum displacement (P_{MD}) (pound)	3516.41	1093.75
Maximum hysteretic energy dissipation (D_{HM}) (pound-inch)	17420.17	14245.05

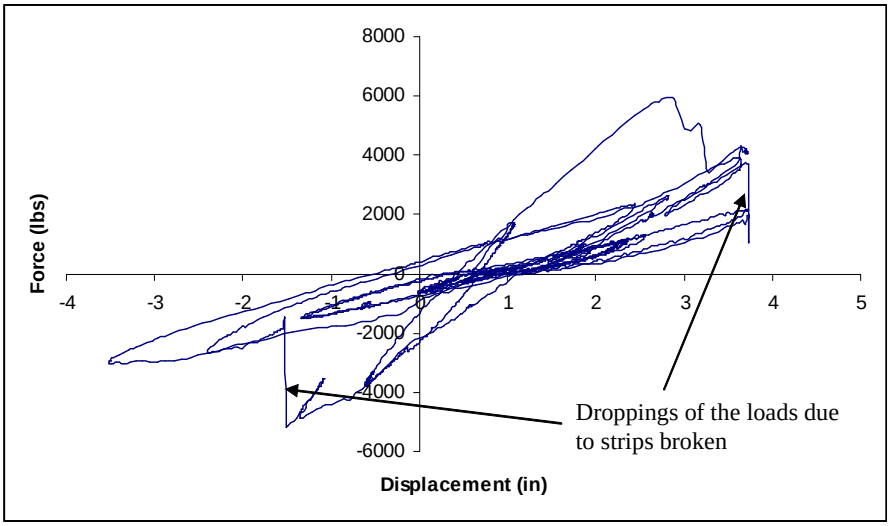

Figure 41. Dropping of the loads due to strips broken in CFSBW.

In conclusion, the CFSBW had a higher maximum load but its K_{eff}, P_{MD}, and D_{HM} were less than those of the CFFW1. In addition, the sudden dropping of the loads is an undesirable behavior. However, one may argue that these worsening performances might be a result of not having enough bracing strips but adding more strips consumes more construction times. Man-hour spent in order to construct the CFSBW, which has ten bracing strips, is 7.6 man-hours while man-hour spent to construct the CFFW1 is 5 man-hours. Therefore, increasing numbers of bracing strips is tedious and impractical. Thus, the fully wrapping scheme is a suitable wrapping method for CarbonFlex shear walls.

Phase 2

Previous experimental results showed that the fully wrapping scheme is a suitable wrapping method because it has better performances and is practical to construct. Therefore, four-CarbonFlex-wrapped wood-framed shear walls were constructed using a fully wrapping scheme in this phase. The four walls consist of CarbonFlex fully wrapped wall number 2 and 3, CarbonFlex fully wrapped with plywood, and CarbonFlex fully

wrapped with opening. For convenience, the descriptions of each wall were summarized in table 6.

Table 6

Descriptions of Testing Walls in Phase 2

Name of the wall	Name abbreviation	h_p (in)	t_c (hrs)	Special Configuration
CarbonFlex fully wrapped wall number 2	CFFW2	5/32	3.5	The wall was used as a baseline.
CarbonFlex fully wrapped wall number 3	CFFW3	5/32	2.5	Both end studs were held by CarbonFlex U- and L-wraps instead of HTT5 hold-downs.
CarbonFlex fully wrapped wall with plywood	CFPW	5/32	2.5	The wall was sheathed by plywood panels before wrapped by CarbonFlex.
CarbonFlex fully wrapped wall with opening	CFOW	5/32	2.5	The wall has a 2 ft x 4 ft window located 16 in. from the edge near the actuator side.

Note. in = inch, hrs = hours

In addition, physical observations from tests in phase 1 (see Appendix A) indicated that a better method to transfer the load to the strong ground was needed. Therefore, steel C-channels were used as a foundation for the specimens in phase 2 and 3. The specimens were anchored to the C-channels by 5/8 inch bolts at 1 ft spacing. The C-channels were anchored to the strong ground by three 1-1/4 inches bolts. The Simpson HTT5 hold-downs were anchored to the C-channels. Therefore, the loads were transferred to the C-channel instead of the sill plate, and the sill plates of specimens were protected from breaking.

CarbonFlex fully wrapped wall number 2 (CFFW2). The main purpose of this section is to study and describe behaviors of CarbonFlex fully wrapped wall. Therefore,

performances of the wall were not compared with those of other walls in this section. Instead, the behaviors of the wall were discussed in this section and the comparisons were carried out in the discussions of other walls.

When CFFW2 was subjected to the LPD record, the wall exhibited a high nonlinearity behavior. The stiffness of the wall was not deteriorated as can be seen that all of cycles were parallel to one another as shown in figure 42. The K_{eff} of 5,700 lbs/in. was calculated from the test results.

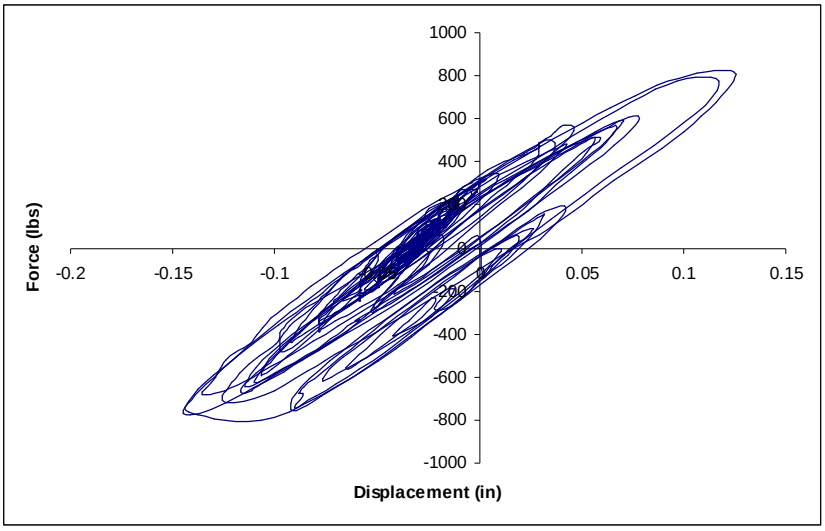

Figure 42. Force-displacement curve of CFFW2 tested with the LPD record.

From the MPD record test, inclined wrinkles of tension and buckling strips (TBS) were observed on the wall's panel as shown in figure 43. The upper point of each TBS pointed to the same direction as the movement of the wall (pointed away from the actuator when the wall was pushed and pointed to the actuator when the wall was pulled). TBS occurred in between studs which acted as boundaries for each panel's section.

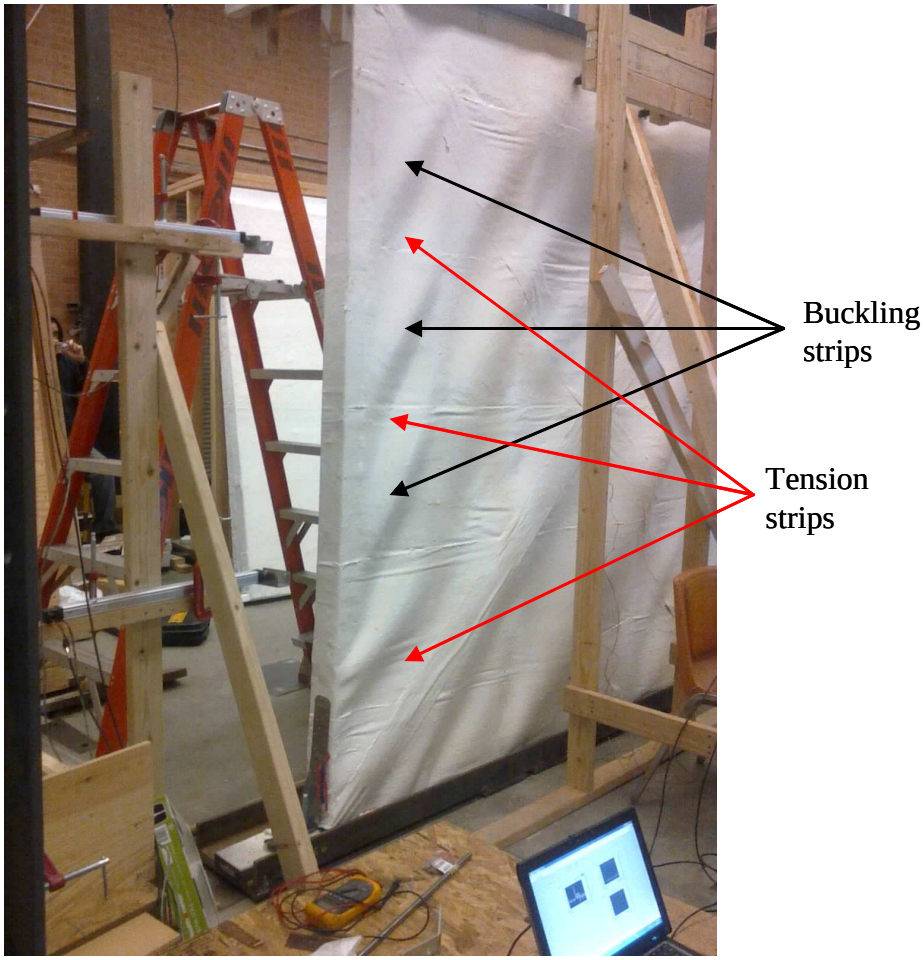

Figure 43. Tension and buckling strips (TBS) occurred on the panel of CFFW2.

In SPSW, it is well-known that the incline angle of TBS is a function of properties of the wall's boundaries (moment of inertia, spacing, and cross-sectional area of columns and beams) (Berman, 2004). The incline angles of TBS in CarbonFlex walls were also affected by the boundaries. Unfortunately, it cannot be clearly seen from the CFFW2 because the studs were spaced equally and their cross-sectional properties were the same. This boundary effect could be easily observed from the test of the wall with opening and was discussed in that section. The TBS did not occurred permanently if the panel and the boundaries still be intact. CFFW2 was not severe damaged in the MPD test. Therefore,

TBS were not observed after the test. However, in HPD test, the panel edge at the top corner of the wall was torn and some permanent TBS were observed.

Pinching was also observed from the force-displacement curve as shown in figure 44. However, unlike plywood shear walls, pinching in CFFW2 did not occur due to the damages at the wood level and bending of fasteners. In contrast, appearance of pinching was due to buckling of the sheathing panel which occurred shortly prior to the initiation of TBS. Therefore, it is called herein as "Buckling Induced Pinching (BIP)."

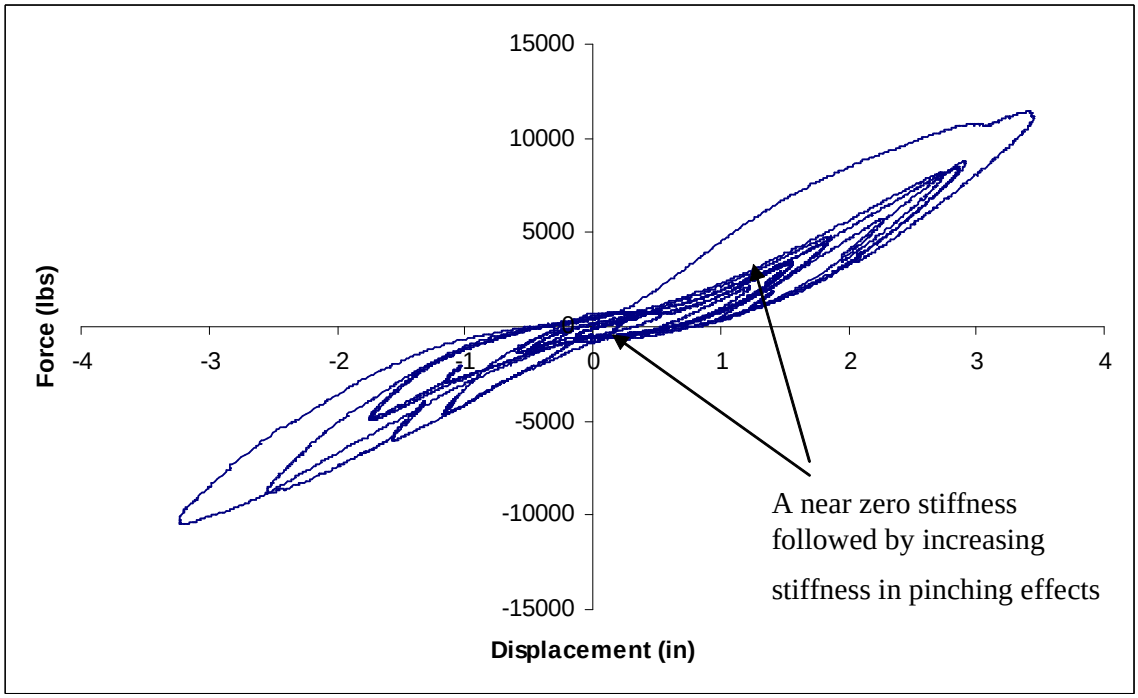

Figure 44. Pinching effects were observed from the force-displacement curve of CFFW2 tested with the MPD record.

BIP can be described by considering the CFFW2 as a wall having several "rectangular sections" on the wall's panel. The width and height of each rectangular section are equivalent to a space between studs and a height of an inclined tension strip, respectively. Therefore, each rectangular section contains one tension strip. A step-by-

step explanation of BIP phenomenon associated with the first hysteretic cycle obtained from the MPD test is shown in figure 45 and described here as:

Step 1: The wall was subjected to the compressive loads (pushing or positive) causing each rectangular section to deform.

Step 2: The area inside the rectangular sections started to buckle resulting in “zero stiffness” (perfectly plastic) portion in BIP.

Step 3: The hysteretic movement was changing direction. The wall was subjected to tensile loads (pulling or negative) resulting in an unloading path of the hysteretic cycle.

Step 4: At this stage, the rectangular sections deformed to another direction. Therefore, the rectangular sections looked like a “mirror reflection” of those in step 1.

Step 5: Buckling occurred again at the area inside the rectangular sections causing another “zero stiffness” portion.

Step 6: The tension strip initiation point was reached. A tension strip started to occur diagonally on each rectangular section. Then, the rectangular section acted more like a truss with a cross-bracing. Therefore, the stiffness of the wall increased.

Figure 46 (a)-(h) show hysteretic cycles, number 1 to 8, respectively. All hysteretic cycles exhibited small perfectly plastic portions before increasing of the stiffness. The plastic displacements from buckling starting point to the point of increasing stiffness (tension strip initiation point) of both loading direction from each hysteretic cycle were quantified. The average and standard deviation of the plastic displacements are 0.204 and 0.018 inch, respectively. The plastic displacements were almost not changed from cycle to cycle regardless of the hysteretic total displacements (damage levels) that the wall had experienced. This embraced the idea stating that the pinching in

CarbonFlex shear wall was not a result of damages in the wood level but it occurred according to the buckling induced pinching concepts.

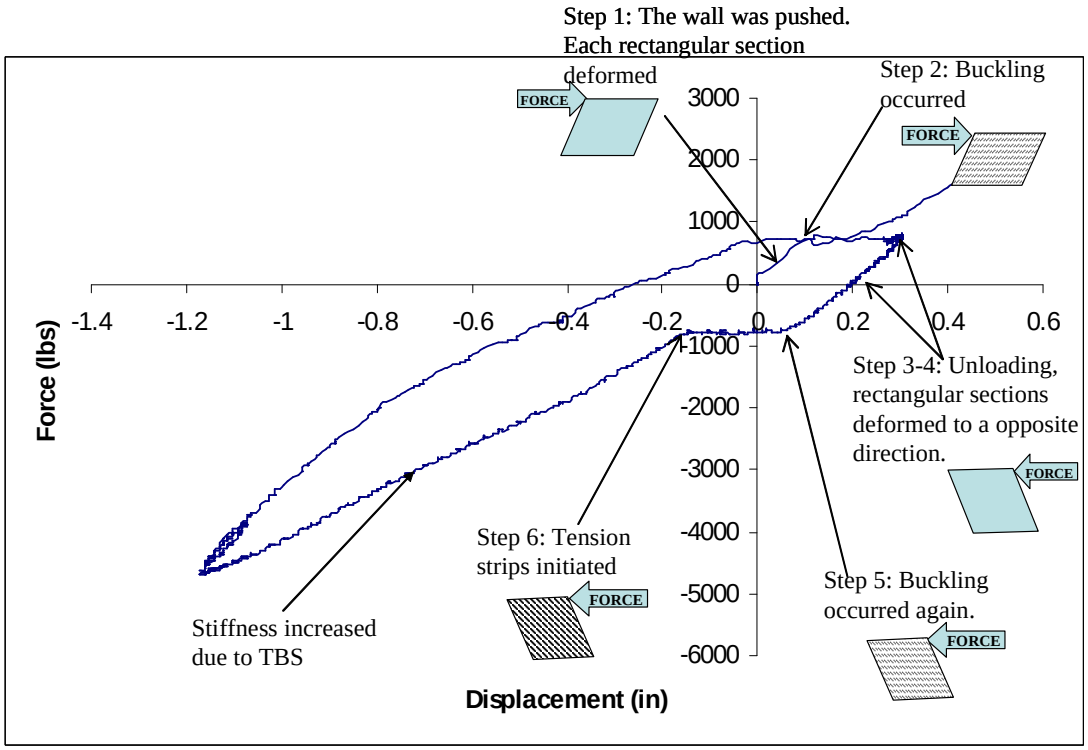

Figure 45. A step-by-step explanation of BIP phenomenon.

Although the loads at buckling points in compressive loading were slightly higher than those in tension loading, they were nearly constant in each loading direction. The average and standard deviation of the loads at buckling in compressive loading are 732.58 and 26.56 lbs, respectively. For tension loading, the average and standard deviation of the loads are -587.76 and 83.92 lbs, respectively. The different in the buckling load levels indicated that the buckling might depend on the loading direction.

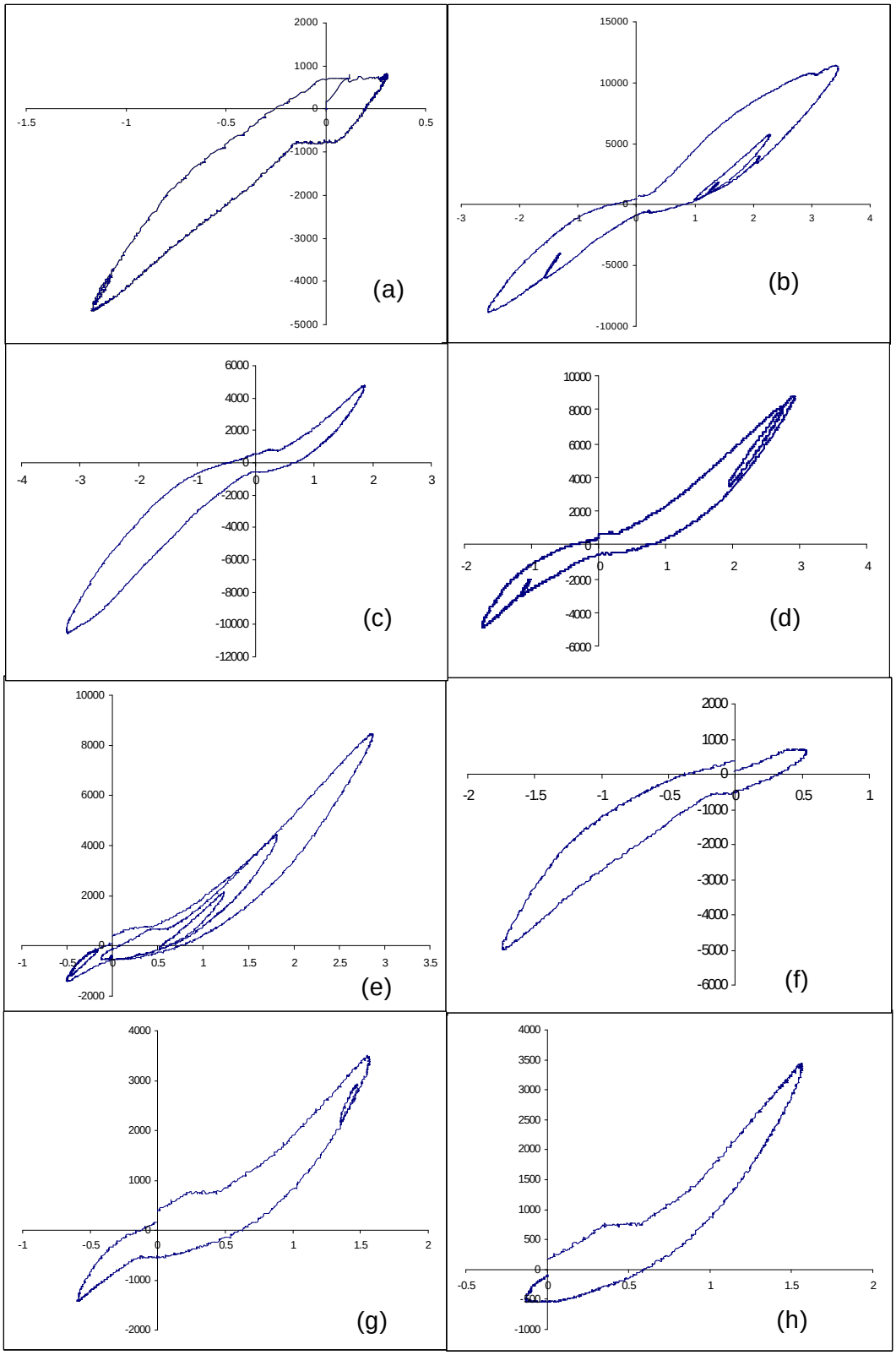

Figure 46. (a-h) Hysteretic cycles of CFFW2 number 1 to 8, respectively.

In every hysteretic cycle, after tension strip's initiation point was reached, stiffness of the wall increased. For example, considering an increasing stiffness portion of a hysteretic cycle (taken from cycle number 3) in tension loading direction (negative force), figure 46(c), the increasing stiffness portion began at the TBS initiation point and ended at unloading point. From reviews, the curve could be discretized to be four linear sections having different stiffness. The stiffness increased from 1324 lbs/in. in the first linear section to 2746.2 and 3695.7 lbs/in. in the second and third sections, respectively. In the last section, the stiffness decreased to 2302.08 lbs/in. The average velocity at each linear section was also calculated which are 0.98, 1.29, 1.36, and 1.03 in/sec, for section 1, 2, 3, and 4, respectively. As can be seen, the stiffness is not only a proportion to the displacement but also a proportion to the velocity. The velocity increased in section 1 to 3 and decreased at section 4 as the wall's movement approached the unload point. The stiffness also increased in section 1 to 3 and decreased in the last section. This indicated that the viscoelastic property of CarbonFlex played a significant role in the unique behavior of CarbonFlex shear walls.

Figure 44 shows that the wall was subjected to the highest load and maximum displacement in the second cycle. After that, the wall was able to sustain the high stiffness in another loading direction. In the following cycles, stiffness of the wall was softened resulting in 44 percent reduction of stiffness. This might be the result of "Mullins Effect."

Mullins effect typically occurs in filled and non-filled rubber-like materials (Diani, Fayolle, & Gilormini, 2009). Bever (1992) explained the Mullins effect that "When new samples of (filled) rubber vulcanizates are stretched to a point P and then

allowed to retract, subsequent extensions to the same strain require a lower force." Therefore, a material having Mullins effect will be "soften" when it is stretched again. Usually, in softening region, the stiffness of the material having Mullins effect will increase and the maximum stress will be recovered when the strain reached the maximum strain of the previous cycle. This correlated to the hysteretic behavior of CFFW2. After the softening occurred in the third cycle, the stiffness increased. In addition, the peak loads of each cycle tended to reach the maximum load in the second cycle but the maximum load could not be reached because the maximum displacements of following cycles were less than the maximum displacement occurred in the second cycle.

Unloading paths also had a unique trend which is having a short linear portion at the beginning following by a strain-hardening behavior. Furthermore, in both loading directions, unloading paths tended to meet at the same load path prior approaching to the buckling points resulting in sustained load level and stable hysteresis.

After the MPD test, damages could not be observed. No permanent TBS appeared on the wall's panel. After that, CFFW2 was tested with the HPD record. Due to the ability of actuator's controller, the wall must be loaded with the linear ramp function until the actuator stroke reached four inches. Then, the cyclic load was initiated to create the maximum displacement of 7.44 in. Figure 47 compares results from the HPD test with those from the MPD test. The comparison shows a superior performance of CFFW2 which is the ability to recover the high stiffness even it was subjected to the MPD record. In addition, the wall was able to sustain the stiffness resulting in further increasing loads.

Also, the comparison is good evidence supporting that Mullins effect played an important role in behaviors of CFFW2. If a line (dashed line in figure 47), which has a

slope equal to the stiffness of the wall when the softening occurred in the MPD test, was drawn from the curve from the MPD test (point A). It will reach the curve from the HPD test at a higher load (point B) than the maximum load occurred in the MPD test. This coincided with the recovery of the maximum stress in Mullins effect. In other words, in the third cycle of the MPD test, if the wall experienced larger displacements than the maximum displacement in the second cycle, the maximum load and stiffness would be recovered.

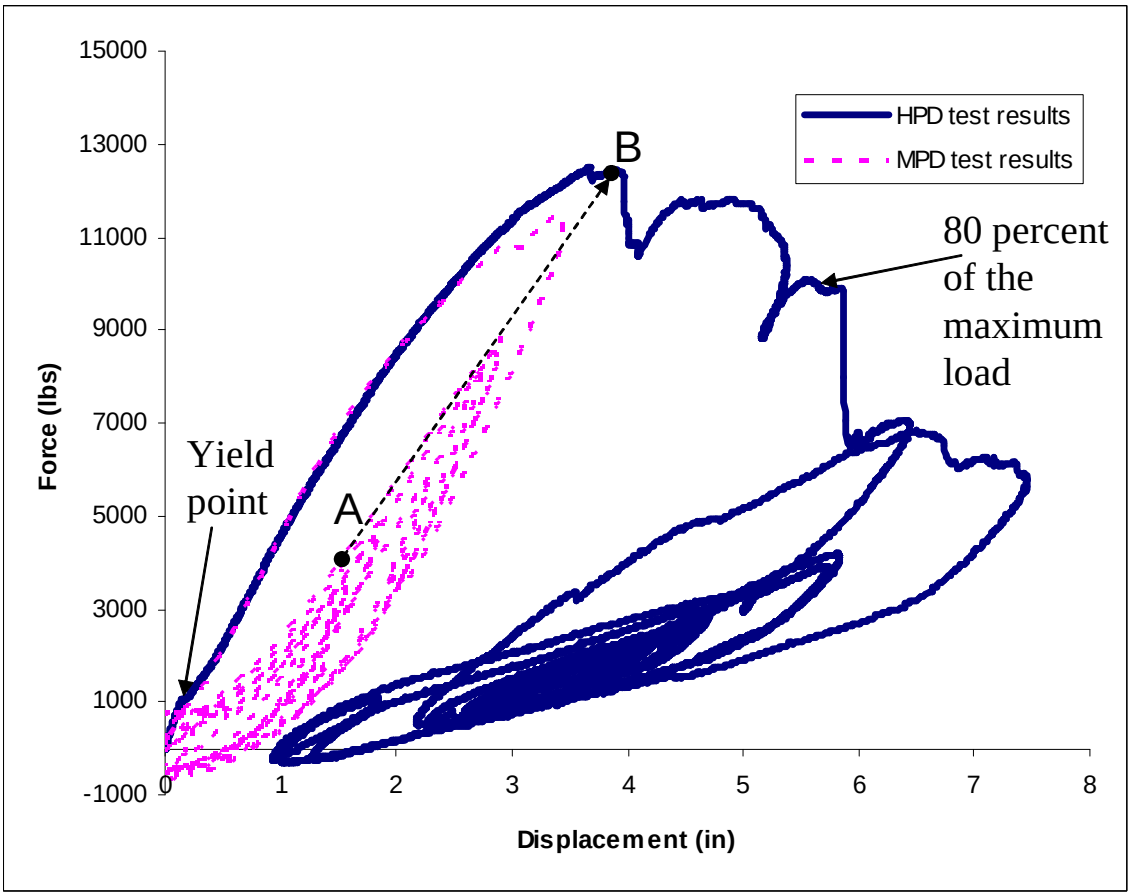

Figure 47. Experimental results from the MPD and HPD tests of CFFW2.

The physical sign of yielding can be seen from figure 47. The physical sign of yielding occurred at the displacement of 0.2 in. with associated load of 870.56 lbs which

is close to the buckling loads in the compression direction observed in the MPD test. The maximum load capacity of 12501 lbs was reached at the wall's displacement of 3.68 in. Many researchers (Salenikovich, Dolan, & Easterling, 1999; Salenikovich & Dolan, 2003; White, Miller, & Gupta, 2009) defined the failure displacement of shear walls as the displacement that the post-maximum load drops to 80 percent of the maximum load. With this condition, the failure displacement is 5.56 in. Therefore, the ductility ratio, which is a ratio of failure displacement to yield displacement, is 27.8.

In conclusion, CFFW2 has a unique hysteretic behavior which is a result from a combination of TBS, BIP, viscoelasticity, and Mullin effect. With these phenomena, the wall's high strength and stiffness could be recovered. Consequently, the wall has a very high maximum load capacity and ductility.

Response modification factor (R-factor) for CarbonFlex shear walls. According to ASCE7-10, table 12.14-1 (Design Coefficients and Factors for Seismic Force-Resisting System for Simplified Design Procedure), the light-frame walls sheathed with wood structural panels rated for shear resistance (wood shear wall system) shall use R-factor is 7.

Typically, R-factor can be calculated using two methods which are 1) equal maximum displacement and 2) equal energy (work done). The equal maximum displacement method assumes that the "assumed" elastic response of structure has the same maximum displacement as "tested" plastic response of structure as shown in figure 48.

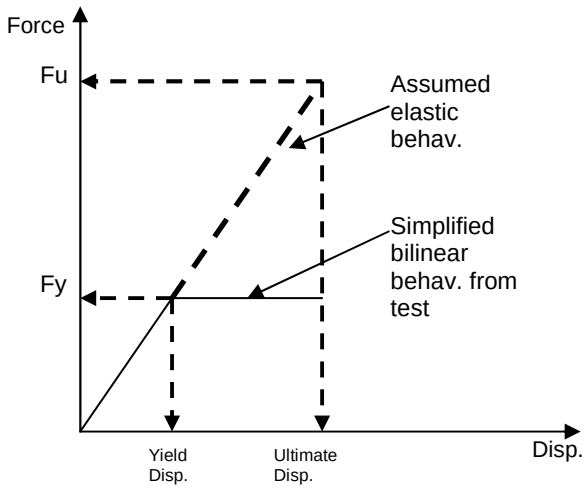

Figure 48. Assumption of equal maximum displacement method.

After, calculating "Fu" from the assumed elastic response, R-factor can be calculated as:

$$R = \frac{F_U}{F_y} \tag{5.10}$$

However, the equal maximum displacement method might not be conservative. Therefore, the equal energy method was used to calculate R-factor for carbonFlex-wood home.

The equal energy method assumes that the energy in "assumed" elastic response of structure (area under the linear curve in figure 48) is equal to the energy of plastic response (area under the simplified bilinear). By knowing the yield point from the test results and setting area under linear curve equal to area under bilinear curve, the F_u is an only unknown. After calculating Fu, the R-factor can be calculated using equation 5.10.

The R-factor of two CarbonFlex walls which are CFFW1 and CFFW2 was calculated using the equal energy method. An example of the calculation was provided in Appendix C. The average R-factor is 8.18. Compared to the R-factor of wood shear wall structures (7), the R-factor can be improved by 16.86 percent by using CarbonFlex.

CarbonFlex fully wrapped wall number 3 (CFFW3). The U- and L-wraps, which were previously described, were used to hold both end-studs instead of HTT5 hold-downs. The wall was tested with the LPD record. The wall could sustain its stiffness resulting in expansion of hysteretic cycles associated with increasing displacements. Although the wall has a different type of hold-downs, the K_{eff} of the wall is 5212.71 lbs/in. which is very close to that of CFFW2. In addition, the force-displacement curves of both walls are just slightly different. Therefore, Types of hold-down have minimal effects to the walls' behavior when they were subjected to small displacements.

The wall was also tested using the MPD record. Although the wall did not experience severe damages, lifting up at both end-studs due to over-turning moment was observed. Figure 49 compares results from CFFW2 and CFFW3 when they were subjected to the MPD record. CFFW3 had about 50 percent lower stiffness than that of CFFW2 resulting in having low strength capacity and energy dissipation. CFFW3 was not as strong as CFFW2 because the U- and L- wraps were not as stiff as HTT5 hold-downs. Therefore, CFFW3 was allowed to rotate more than CFFW2. When it had more rotation, the shear strength, which was provided by the shear deformations (tension and buckling strips) of the CarbonFlex panel, was reduced. The tension and buckling strips are the major energy dissipation mechanisms of CarbonFlex shear wall. Thus, CFFW3 also dissipated less energy per cycle than CFFW2. In addition, A little bit detaching of the panel from framing was also observed. However, U- and L- wraps could hold both end-studs and the wall had small damages.

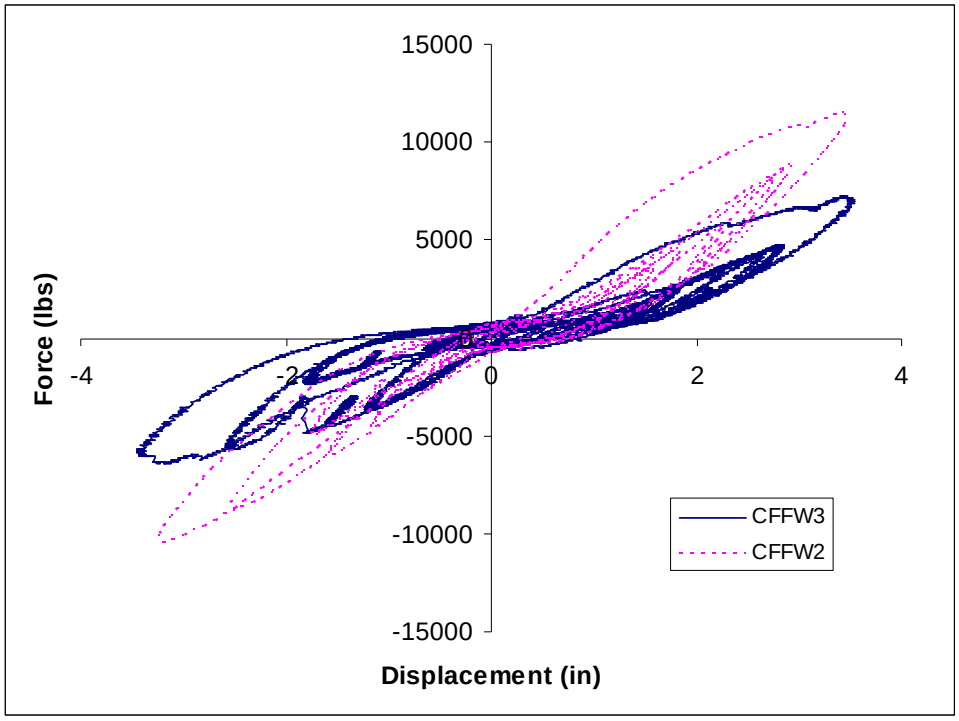

Figure 49. A comparison of experimental results from the MPD test between CFFW2 and CFFW3.

CFFW3 survived the test with MPD record. Therefore, the test with HPD record was conducted. Comparing the results from HPD to MPD test, the stiffness of CFFW3 decreased slightly. Furthermore, the maximum force observed in the MPD test was reached at about the same displacement as shown in figure 50. This implied that CFFW3 experienced minimal damages during the MPD test. Interestingly, CFFW3 could sustain its stiffness resulting in increasing maximum shear capacity. The ultimate force of 7660.5 lbs was reached at the displacement of 3.94 in. After that, the U- and L- wraps at the end-stud near the actuator were broken and the end-stud was pulled out from the sill plate causing the crack initiation at the bottom corner of CarbonFlex panel. After the wraps were broken, there was nothing to resist the over-turning moment. Therefore, the wall

was rotated resulting in more “Mode I” crack propagation at the bottom of the wall and dramatic loss of shear capacity.

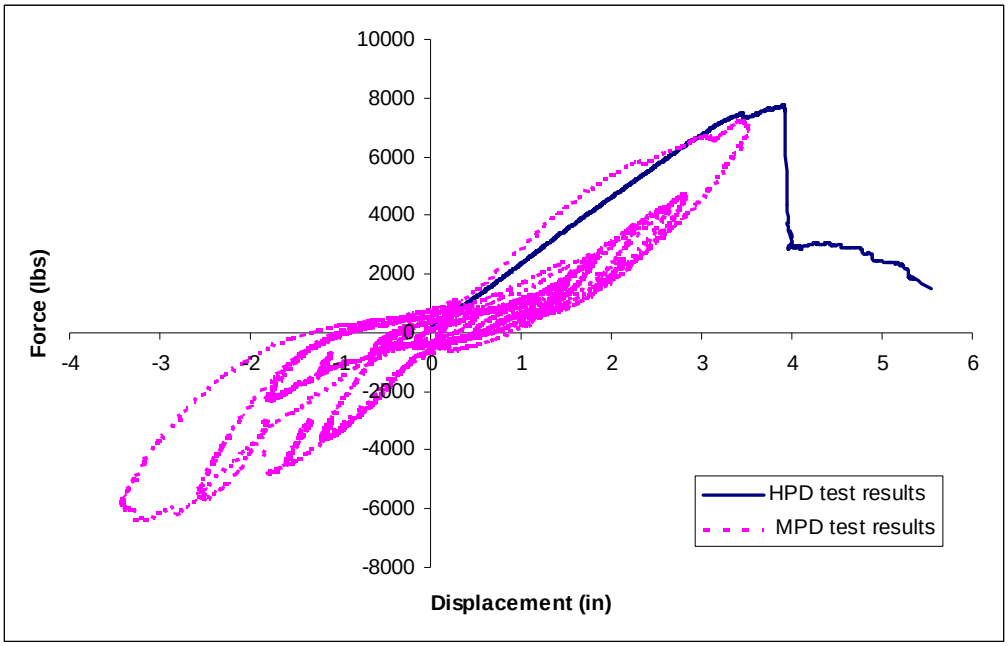

Figure 50. Experimental results from the MPD and HPD tests of CFFW3.

Learning from failure of CFFW3 helped improve the wrapping schematic of the CarbonFlex-wrapped structure tested in phase 3. To prevent Mode I crack propagation, 3 in. x 9 in. CarbonFlex strips were attached to the top and bottom edges of the structure at 16 in. spacing.

CarbonFlex fully wrapped with plywood wall (CFPW). The sheathing material for this wall is a plywood panels strengthened by CarbonFlex. It is believed that this sheathing material is more rigid than conventional plywood used in PW1 and PW2 because it was strengthened by CarbonFlex, and CarbonFlex connected two-4 ft x 8 ft plywood panels to act as one unit (as one-8 ft x 8 ft panel). Therefore, results from this test are good examples of problems associated with having “too rigid” sheathing material. The wall exhibited high nonlinearity even though it was subjected to small displacements

of LPD records. After the wall experienced displacement demands that were greater than 0.1 inch, the wall's stiffness decreased as shown in figure 51. The small displacements of the LPD records created more damages (indicated by the stiffness degradation) to CFPW compared to other walls equipped with less rigid sheathing materials, this is a result of having a "too rigid" sheathing panel which cannot dissipate enough energy. Therefore, most of the energy must be released through nails' bending and damages in wood medium.

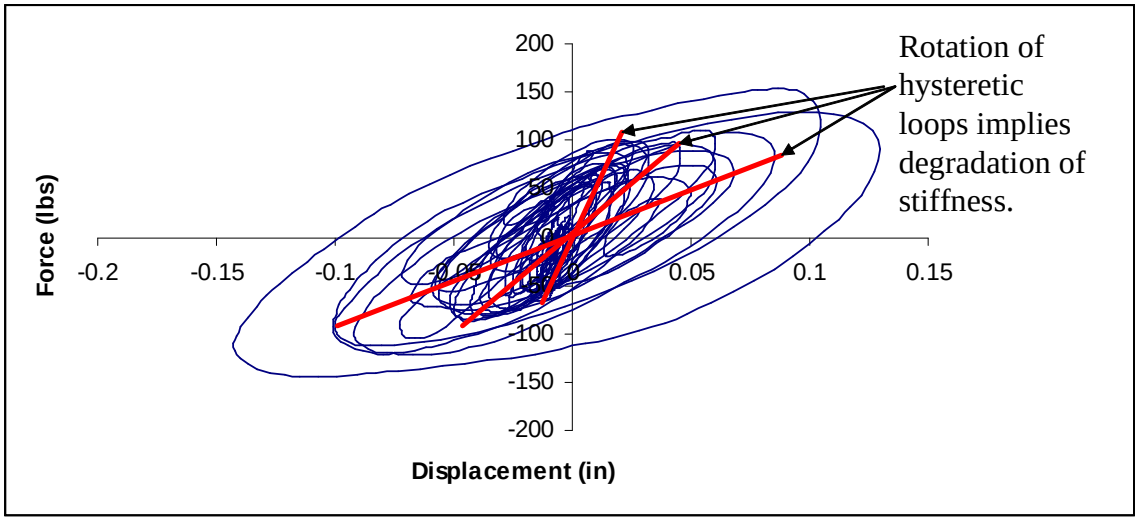

Figure 51. Force-displacement curve of CFPW tested with the LPD record.

The wall was tested with the MPD record. Pinching effects can be seen from the test as shown in figure 52. Pinching behaviors indicated accumulate damages at the wood level (studs). Chui and Ni (1997), which was referred in Caassidy (2002), clearly described the pinching effects that: "On the first loading the wood fibers around the fastener are compressed and crushed. Upon displacement reversal (unloading), the fastener is initially still in contact with the wood. This accounts for the high value of initial stiffness. After a certain distance of travel, the fastener leaves the compressed

wood behind and moves almost freely in the reversed direction until it contacts wood again on the opposite side. This behavior explains the low unloading stiffness and near-zero load intercept of the cycles. The loading segment is the reverse phenomenon. After a certain distance of free travel in the loading direction, the fastener bears on the wood again on the opposite side, which accounts for the sharp increase in stiffness." Not only damages in the wood medium that affected wall's stiffness and pinching phenomenon, but stiffness degradation of nails also influenced the behaviors.

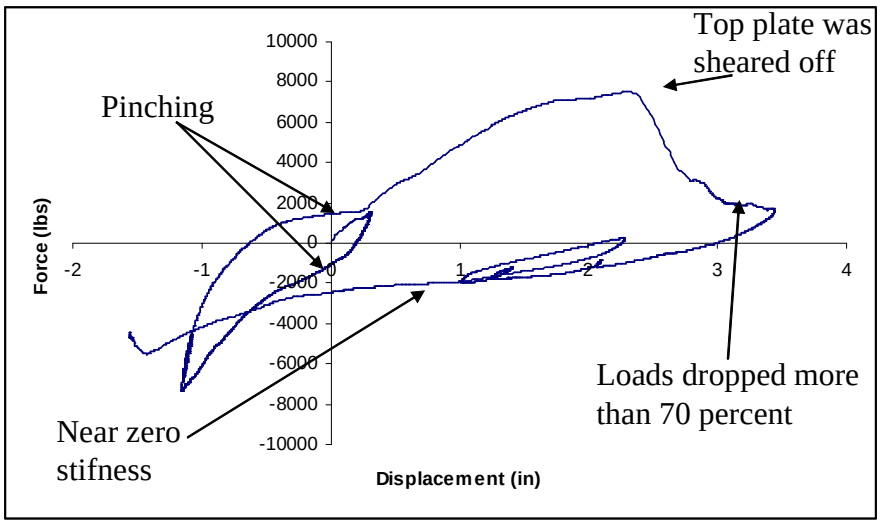

Figure 52. Pinching effects and damages occurred during the MPD test of CFPW.

In addition, while the wall was pushed (positive displacements) at about 2.4 inches, the top plate was sheared off. After losing the top plate, the load of the wall dropped more than 70 percent following by near zero stiffness in a subsequent unloading path. This unusual failure occurred because the nails connecting the panel to studs were not allowed to have enough slip. Typically, when a wood-framed shear wall is subjected to the lateral loads, theirs sheathing panels will be deformed allowing studs to rotate. Fasteners connecting sheathing panels to studs will also slip, which provides hysteretic

damping to release energy. However, with too rigid panel, studs in CFPW were not allowed to have adequate movements. Therefore, most of energy accumulated at the top plate, which was connected directly to the actuator. Then, energy was transferred to the nails connecting the panel to the studs along the top edge of the wall (the energy was not distributed to all nails as it supposed to be). Therefore, the nails at the top plate were subjected to the energy exceeding their capacity causing the shear off of the top plate and disconnecting of the load transferring path of the wall. Then, the wall failed.

CarbonFlex fully wrapped with opening wall (CFOW). Currently, two widely accepted approaches to design and construct a wood-framed shear wall with opening are a segmented and a perforated shear wall. These two methods are slightly different. The segmented shear wall considers the shear wall as multiple "fully sheathed" segments combining together. The total shear resistance of the wall is the summation of a lateral resistance of each fully sheathed segment and do not count the resistance from small sheathed areas under and over the openings. To construct a shear wall using this approach, hold-downs are needed to be installed at both ends of each fully segment as shown in figure 53(a).

Perforated shear wall approach count on the shear resistance contributed from all sheathed areas. The method considers the shear wall as a unit. To construct a shear wall, two hold-downs are required to be installed at both ends of the wall (not at every segment) as shown in figure 53(b). In 1981, Hideo Sugiyama proposed an empirical equation to predict the shear strength of a perforate shear wall (Line & Douglas, 1996). The equation was adopted by many building codes, such as Standard Building Code 1996 Revised Edition and the Wood Frame Construction Manual for One- and Two- Family

Dwelling – 1995High Wind Edition, as a basis of their equations to calculate allowable shear strength (Dolan & Johnson, 1997).

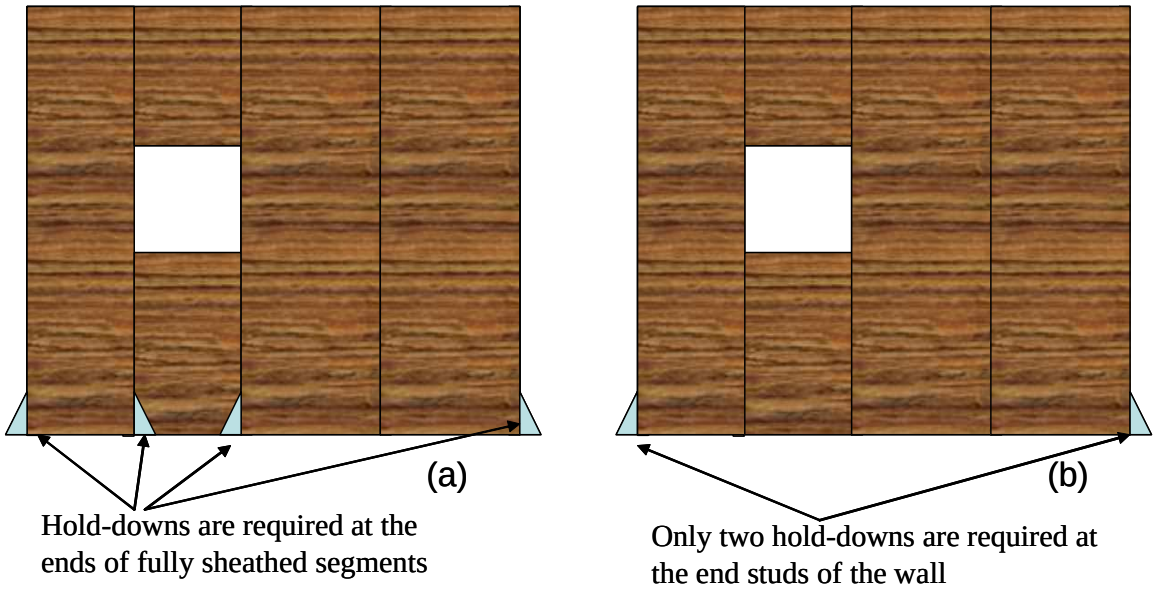

Figure 53. (a) A segmented shear wall. (b) A perforated shear wall.

The CFOW specimen was constructed using the perforated shear wall approach. The purpose of the test is to provide a pioneer study of the perforated CarbonFlex shear wall. According to Sugiyama's approach, the shear capacity (or stiffness) of a perforated shear wall can be calculated by multiplying the shear capacity (or stiffness) of a typical fully sheathed shear wall having the same length with the shear capacity ratio (F_s) which is described in equation 5.11 (Dolan & Johnson, 1997).

$$F_s = \frac{r}{(3 - 2 \times r)} \tag{5.11}$$

r is a sheathed area ratio counting on effects of opening size. The sheathed area ration can be determined by using equation 5.12.

$$r = \frac{1}{(1+\frac{\alpha}{\beta})} \tag{5.12}$$

Where, α is a ratio of opening area to the total wall area and β is a ratio of the summation of lengths of fully sheathed segments to the total length of the wall. The shear capacity ratio was determined using dimensions of CFOW. The calculated shear capacity ratio is equal to 0.667.

The 2008 Wind and Seismic, Special Design Provisions for Wind and Seismic (SDPWS) (American Wood Council, 2008) provides a shear capacity adjustment factor (C_0) which can be calculated from modified Sugiyama's empirical equation as shown in equation 5.13.

$$C_0 = \left(\frac{r}{3-2r}\right)\frac{L_{tot}}{\sum L_i} \tag{5.13}$$

$$r = \frac{1}{1+\frac{A_0}{h\sum L_i}} \tag{5.14}$$

Where, A_0 is area of openings, h is the height of the wall, $\sum L_i$ is a summation of lengths of fully sheathed segments, and L_{tot} is a total length of the wall. From calculation, C_0 of CFOW is one. However, the code also provides C_0 in its table 4.3.3.5. To select the C_0 from the table, $\sum L_i$, L_{tot}, h, and the maximum opening height are required. From the table, a selected C_0 of CFOW is 0.84.

During the MPD test of CFOW, a technical problem occurred so that only the loads in tension loading direction could be recorded. Therefore, only forces and displacements in tension loading from CFFW2 were used to compare with those of CFOW. Prior comparisons, the forces obtained from CFFW2 were factored by a shear

capacity ratio (F) calculated from Sugiyama's equation and a selected shear capacity adjustment factor (C_0). Figure 54(a) shows a comparison between a force-displacement curve of CFFW2 factored by Sugiyama's shear capacity ratio and that of CFOW. Sugiyama's shear capacity ratio provided good estimations for forces and stiffness when the wall's displacements did not exceed two inches. When the wall was subjected to higher displacement demands, the shear capacity ratio underestimated forces and stiffness resulting in a conservative estimation of the shear capacity. The results from CFFW2 factored by C_0 were compared to those of CFOW in figure 54(b) which indicates that forces and stiffness were overestimated using C_0.

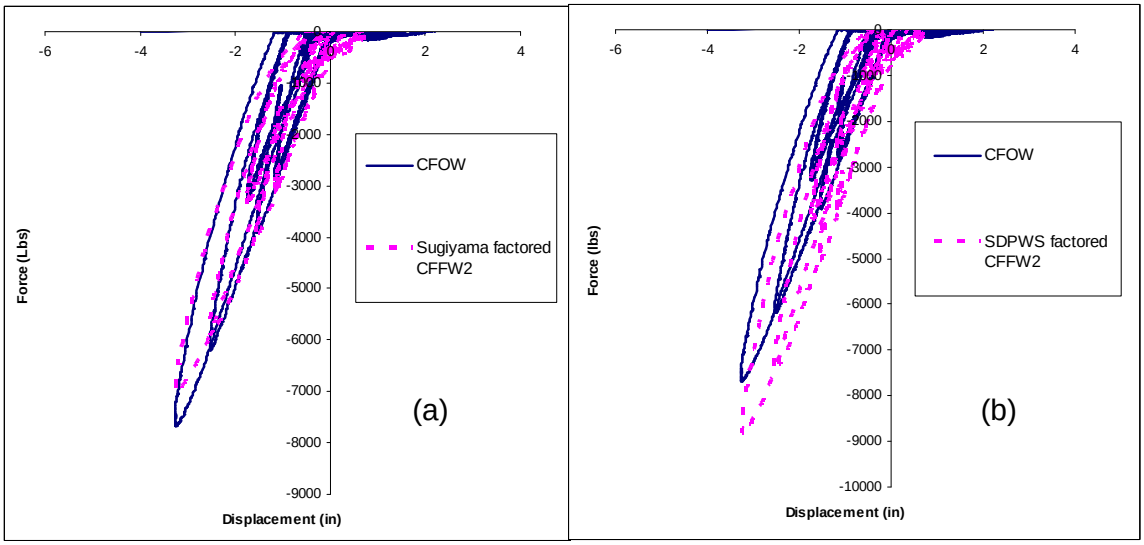

Figure 54. Comparisons of force-displacement curves between CFOW and (a) CFFW2 factored by Sugiyama's shear capacity ratio, (b) CFFW2 factored by a shear capacity adjustment factor.

Until having more information, the Sugiyama's equation might be a suitable choice for predicting the shear capacity of perforated CarbonFlex shear walls although it gave a conservative results. In the future, thorough studies of perforated CarbonFlex

shear walls should be conducted. Several walls with different opening sizes and positions should be tested. In order to establish an empirical equation to estimate the shear capacity of the wall, experimental tests of fully wrapped CarbonFlex shear walls having the same sizes should also be conducted.

Tension and buckling strips (TBS) also occurred on the panel of CFOW. The strips also appeared on small areas above and below the opening as shown in figure 55. This supports the idea of the perforated shear wall approach that count on the shear capacities of these small areas toward the total shear capacity of the wall. As mentioned before in the discussion of CFFW2, spaces between boundaries (studs) affected the incline angles of TBS in CarbonFlex walls. This can be clearly seen from figure 55. The spacing between the end-stud to the window of CFOW is 6 in. while the spacing between studs under the opening is 11.25 in. The incline angle at the space between the end-stud to the window is larger than that occurred at the wider space. In other words, the incline angle varied inversely to the spacing between studs.

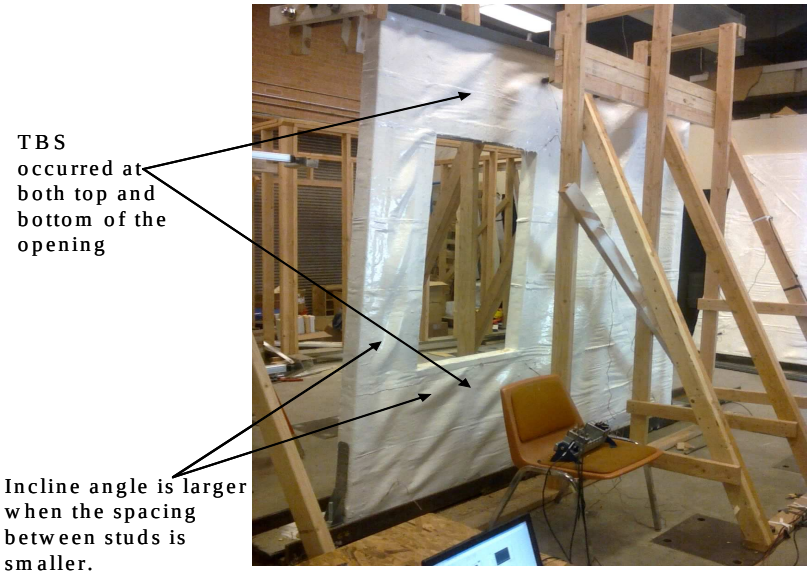

Figure 55. TBS occurred on the panel of CFOW.

Phase 3

Two-8 ft x 8 ft x 9.5 ft wood-framed structures were tested in this phase. The first one is the "Plywood" house which was equipped with two conventional plywood shear walls (a 8 ft x 8 ft fully sheathed shear wall and a 8 ft x 8 ft shear wall with opening). The other structure also had two shear walls. However, this structure was fully wrapped by CarbonFlex.

The main purpose of the experiments in this phase is comparing performances of the conventional wood sheathed and CarbonFlex-wrapped structures. Performances of The plywood house were investigated using the LPD, MPD, and HPD records. However, the CarbonFlex house could be tested using only the LPD and MPD records because strength of the structure exceeded the actuator's limit and could not be tested using the HPD record. Therefore, the behaviors and performances in LPD and MPD tests of the structures were compared side-by-side. Finally, the results from the HPD test of the plywood house were compared to those of the CFFW2 and CFFW3.

For abbreviation, the word "side-wall" refers to the wall of the house that parallel to the load and does not have opening. In addition, the word "window-wall" refers to the wall parallel to the load having a 2 ft x 4 ft opening.

Results from the LPD test. Figure 56(a) and (b) show the results from the plywood and CarbonFlex houses, respectively. No damage could be physically observed during and after the test from both structures which agreed with experimental results showing that stiffness of both structures was not deteriorated as can be seen from figure 56 that all hysteretic loops were parallel to one another.

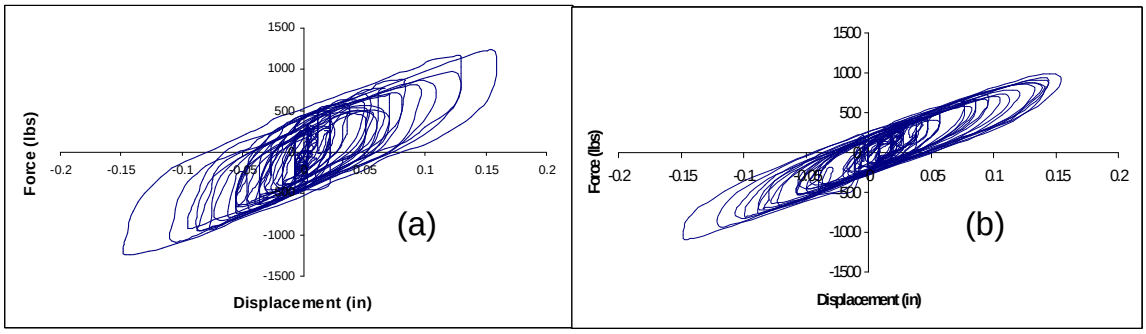

Figure 56. Force-displacement curve from the LPD test of (a) the plywood house. (b) the CarbonFlex house.

Although the maximum displacement of the test is small and no sign of damage was observed, both plywood and CarbonFlex houses had highly nonlinear behaviors. The nonlinearity of the plywood house is a result of hysteretic damping of the nails which is the main energy dissipation of the structure. For the CarbonFlex house, the viscoelasticity of the material might play a significant role in the structure's nonlinearity and be an important mechanism to dissipate energy of CarbonFlex house.

The K_{eff} of both structures were measured at 6083.2 lbs/in. and 6302.53 lbs/in. for the plywood and CarbonFlex houses, respectively. The D_{HM} of each structure was obtained from the hysteretic cycle having the largest area. The D_{HM} of both structures are 271.25 lbs-in. and 149.46 lbs-in. for the plywood and CarbonFlex houses, respectively. The plywood house had a greater D_{HM} (for a very small displacement level) implying that the initial hysteretic damping of the plywood house was greater than that of the CarbonFlex house. These results showed that a conventional plywood shear wall had a good hysteretic damping when it was not damaged. However, its ability to dissipate energy might be decreased when it experienced greater displacements which created more damages.

Quasi-static test of CarbonFlex house. Due to the high load capacity of CarbonFlex-wrapped house, initially, it could not be tested with the MPD record (the load exceeded the capability of the actuator. The stiffness of the house was too high and the load reached the capacity of the actuator (24000 pounds) at displacement about three inches.

To decrease stiffness so that the house could be tested, the quasi-static test was conducted. The load protocol used in the test is a sine wave having different amplitudes, which are 2.74, 3, 3.5, 3.6, 3.69, 3.71, 3.75, 3.78, and 3.89 inches. The amplitude of the sine wave was increased depending on the stiffness of the house in the previous cycle. For example, the test started with the sine wave having the maximum amplitude of 2.74 inches. After the structure had been tested for five cycles, the reduction of the peak load and a little bit of stiffness degradation (rotation of the hysteretic loops) could be observed. Therefore, the maximum amplitude of the sine wave was increased to be three inches for the next five cycles (cycle number 6 to 10). The maximum amplitude had been increased until the maximum displacement of the structure reached 3.89 inches, which is the maximum capacity of the actuator, in the last three cycles. Figure 57 illustrates force-displacement curves from the quasi-static test. Although the house was subjected to 36 cycles of high-load level (the maximum load of each cycle was greater than 20000 pounds and the maximum load was 23686.3 pounds), the house still be very strong and could sustain a very high strength. From physically observation, debonding, detaching, and damage of CarbonFlex panel could not be observed.

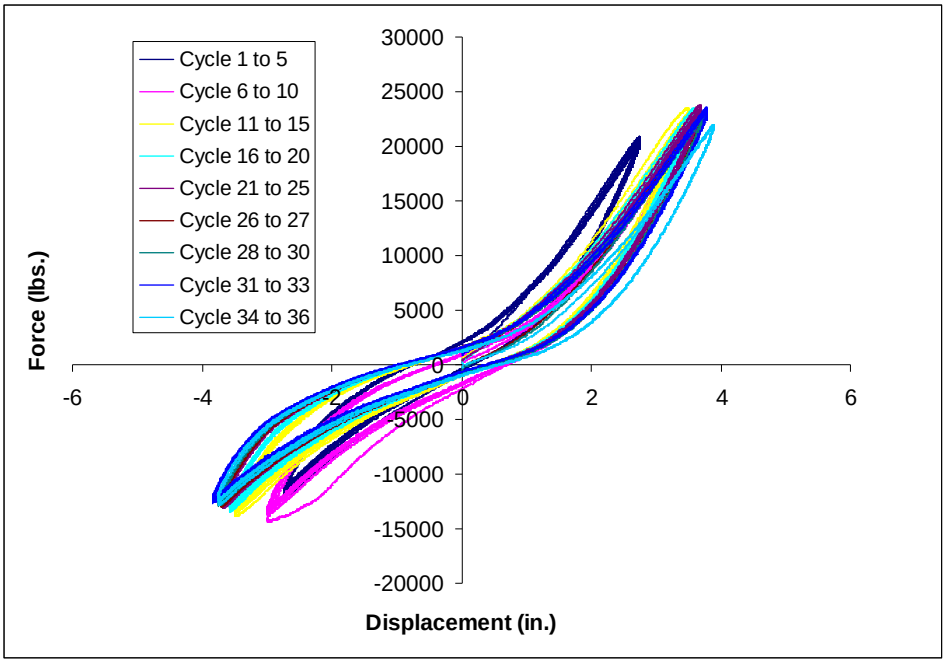

Figure 57. Force-displacement curve from quasi-static test of the CarbonFlex house.

Results from the MPD test. Nails pulled out, which created gaps between plywood sheets and studs, could be seen at the edges of plywood panels at both side- and window-walls of the plywood house while no damage could be observed from the CarbonFlex house. Figure 58(a) and (b) show the force-displacement curves of the plywood and CarbonFlex houses, respectively. Although, from the LPD test, the initial stiffness of the CarbonFlex house was not so different from that of the plywood house, the CarbonFlex house was a lot stiffer than the plywood house when they were subjected to larger displacement demands from the MPD record. Consequently, the CarbonFlex house had more than twice greater load capacity than the plywood house. This is a result from having stronger panel's fastening method (epoxy) in the CarbonFlex house. In addition, larger displacement demands from the MPD record had a better ability to induce TBS than smaller displacements in the LPD record resulting in a rapidly increased and

sustainable stiffness of the CarbonFlex house while the stiffness of the plywood house highly relied on the nail connections which were damaged as the displacements increased. In addition, because stiffness of plywood panels was a lot higher than that of the nails, the panels acted as a “rigid” bridge connecting weaker nails together. Therefore, their “high” stiffness was minimally contributed to the stiffness of the structure. In contrast, CarbonFlex is more flexible than plywood and the bonding between CarbonFlex panels and wood studs are stronger than nail connections. This combination allowed most of a high stiffness of CarbonFlex to participate in the stiffness of the structure.

As examples, figure 59(a) and (b) show comparisons of the hysteretic cycle number three and six, respectively. Pinching effects could be seen from both structures. However, pinching in the plywood house occurred due to damages as mentioned before. Therefore, stiffness of the plywood house had a slower increasing rate than that of the CarbonFlex house of which stiffness rapidly increased due to TBS. As a result, the CarbonFlex house had a higher load at the same displacement level.

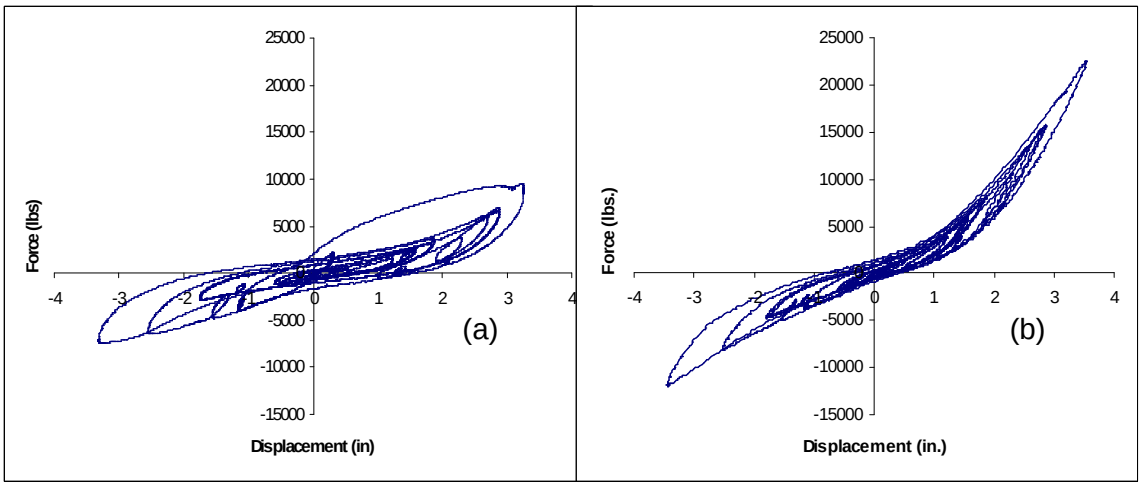

Figure 58. Force-displacement curves from the MPD test of (a) the plywood house. (b) the CarbonFlex house.

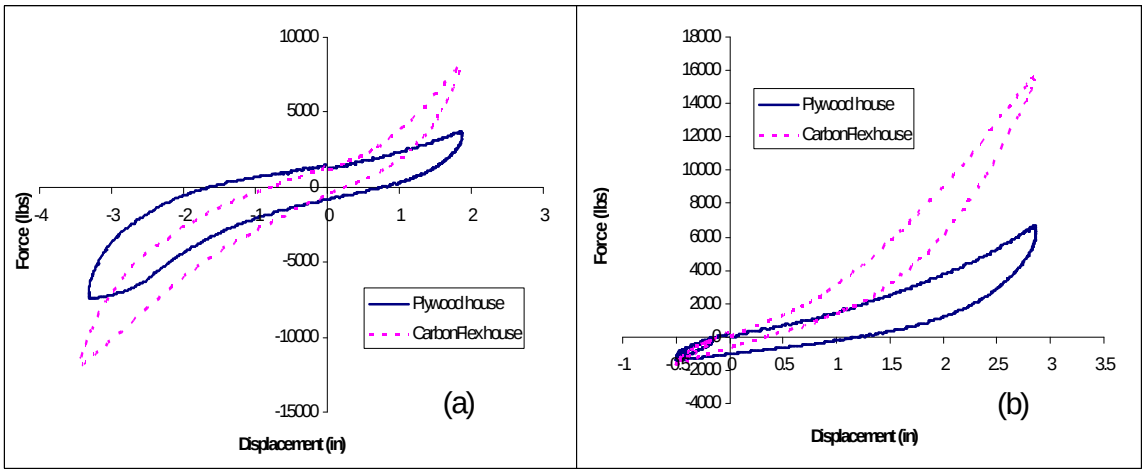

Figure 59. Rapidly increasing stiffness of the CarbonFlex house compared to a slowly increasing stiffness of the plywood house obtained from hysteretic cycle number (a) three and (b) six.

Results from the HPD test. The CarbonFlex house could not be tested with the HPD record due to its high stiffness. Therefore, the results from CFFW2 were used to compare with those of the plywood house. Figure 60 shows the results from the HPD and MPD tests of the plywood house. Due to the permanent damages occurred in the MPD test, the high "undamaged" stiffness of the structure could not be recovered. Instead, the beginning stiffness in the HPD test matched to the "damaged" stiffness in MPD test. Unlike the results of CFFW2 and CFFW3 shown in figure 47 and 50, respectively, the stiffness of the walls could be recovered. As a result, the CFFW2 dissipated more energy (area under force-displacement curve) than the plywood house even after it was subjected to the MPD record.

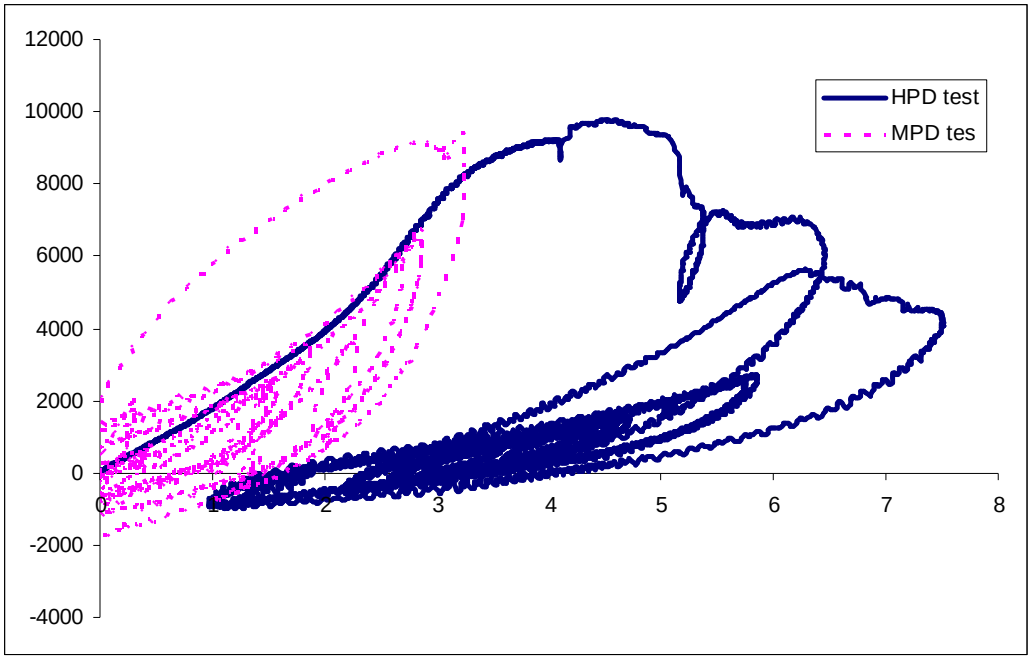

Figure 60. Experimental results from the MPD and HPD tests of the plywood house.

The ability to recover stiffness of CarbonFlex shear walls might be able to protect the structures from aftershocks and mainshock-aftershocks. According to Huang, Qian, and Fu (2012), in 2008, the magnitude 8, Wenchuan earthquake created damages to many buildings. After that, 86403 aftershocks (eight aftershocks have magnitude greater than 6 and 40 aftershocks have magnitude more than 5) struck the damaged structures creating more severe damages and collapses. Therefore, the ability to recover high stiffness of the CarbonFlex shear walls can provide a better protection to structures than the conventional plywood shear walls.

CHAPTER 6

Debris Impact Testing for CarbonFlex-Storm Shelter

Tornadoes

American Meteorological Society (Glickman & American Meteorological Society, 2000) defined a tornado as "a violently rotating column of air, pendent from a cumuliform cloud or underneath a cumuliform cloud, and often (but not always) visible as a funnel cloud." Currently, full understanding of a tornado's formation is under investigation by scientists. However, most of tornadoes occurred from a huge thunderstorm called a "supercell." Two key ingredients creating a supercell thunderstorm are "wind-shear" and "updraft." Grazulis (2001) described that several wind-shears flow in different speeds and directions create a horizontal rotating air tube. That said, warmer air near the ground which has a lower density than the cooler air tends to move upward creating the vertical moving air called "updraft." Updraft tilts a rotating air tube to a vertical position creating a supercell thunderstorm. With proper conditions, a tornado spawns in a supercell.

In 1971, Tetsuya T Fujita introduced a Fujita scale (F scale) to classify the intensity of a tornado using damage levels that it created. However, the construction qualities and methods of structures damaged by tornadoes were not considered in the F scale, resulting in overestimated wind speeds required to damage structures (McDonald, 2001). In 2004, the modified F scale, which is called the Enhanced Fujita scale (EF scale), was proposed. The EF scale related wind speeds to damage levels (degrees of damage) of various types of buildings, structures and trees (damage indicators). The EF scale (McDonald & Mehta, 2004) classified tornadoes into six classes from EF0 to EF5.

Associated wind speeds and damages of each EF class are shown in table 7. Recently, the EF scale started being used by the National Oceanic and Atmospheric Administration (NOAA) instead of the F scale (Federal Emergency Management Agency, 2008).

Table 7

Wind Speeds and Damages in the Enhanced Fujita Scale (EF Scale)

EF classes	Wind Speeds (mph)	Damages
EF0	65-85	Chimneys are damaged, tree branches are broken, shallow-rooted trees are toppled.
EF1	86-110	Roof surfaces are peeled off, window are broken, some tree trunks are snapped, unanchored mobile homes are overturned, and attached garages may be destroyed.
EF2	111-135	Roof structures are damaged, mobile homes are destroyed, debris becomes airborne (missiles are generated), large trees are snapped or uprooted.
EF3	136-165	Roofs and some walls are torn from structures, some small buildings are destroyed, non-reinforced masonry buildings are destroyed, most trees in forest are uprooted.
EF4	166-200	Well-constructed houses are destroyed, some structures are lifted from foundations and blown some distance, car are blown some distance, large debris becomes airborne.
EF5	>200	Strong frame houses are lifted from foundations, reinforced concrete structures are damaged, automobile-size missiles become airborne, trees are completely debarked.

Note. mph = miles per hour, damages descriptions were obtained from FEMA 320 Taking Shelter From the Storm: Building a Safe Room for Your Home or Small Business (Federal Emergency Management Agency, 2008).

Wind Induced Damage and Damage Chain

During strong winds, components of buildings, such as roofs, windows, doors, and walls, could be damaged. For example, Uematsu and his coworkers (as cited in Tamura, 2009) described the failure processes of the roof as the suction pressure that occurred at the eaves, creating eaves' damages. After the eaves failed, the internal

pressure and lifting force were increased. Consequently, roofing materials were blown off. The blown-off materials could then consequently become wind-borne missiles and create additional damage to the downstream structures. This damage phenomenon is called a “damage chain” (Tamura, 2009).

Wind-Borne Debris (WBD)

Beside high velocity winds that create harsh pressure, Wind-Borne Debris (WBD) is categorically one of the lethal weapons of fatal storms. WBD can originate from loosened structural materials or objects lying on the ground. Wills, Lee, and Wyatt (2002) categorized WBD to be three types using the difference of debris’s dimensions. The first type is debris for which all three dimensions are similar (“cubic-like”), such as rocks and a small piece of wood. The second type consists of debris that one of its dimensions is longer than the other two dimensions (“rod-like”), for example, a bamboo stick, or a 2 x 4 piece of lumber. The last type is “sheet-like” debris such as roofing materials, plywood panels, and gypsum boards.

Many researchers (Tachikawa, 1983; Lin, Holmes, & Letchford, 2007; Lin & Vanmarck, 2009) have studied behaviors of WBDs. In 1983, Tachikawa (1983) introduced a dimensionless parameter “K” which is a proportional factor relating wind force to gravity force. Later, Holmes, Baker, & Tamura (2005) proposed the name “Tachikawa Number (T_a)” as an official name of the K parameter. For convenience, an equation describing T_a is presented in equation 6.1.

$$T_a = \frac{\rho_a U^2 A_d}{2mg} \tag{6.1}$$

where, ρ_a is air density; U is a wind speed; A_d is a plane area of the debris; m is mass; and g is gravity (Tachikawa, 1983). T_a could be used to determine trajectories of all types of WBDs (Holmes et al., 2005). Lin and Vanmarcke (2008) developed an equation to calculate the horizontal velocity of debris (u) as a function of T_a, debris's shape, the shape coefficient (C) which equals to 0.911, 0.809, and 0.801 for plate, cube, and rod-liked debris, respectively, and the horizontal traveling displacement of the debris (x). This is expressed in equation 6.2.

$$\frac{u}{U} = 1 - e\wedge(-\sqrt{2CT_a x^*}) \tag{6.2}$$

where $x^* = \frac{gx}{U^2}$ (6.3)

Equation 6.1 implies that larger and lighter weight debris has a greater value of T_a and equation 6.2 indicates that the greater value of T_a, then the higher debris's velocity will be; therefore, debris that has larger plane area and lighter weight tends to fly longer and faster than a smaller or heavier one.

Storm Shelter Used in the Wood Home Constructions

In August 2008, the Federal Emergency Management Agency (FEMA) issued the third edition of "Taking Shelter From the Storm: Building a Safe Room for Your Home or Small Business" (FEMA P-320) in which a guideline that helps home owners or business owners to assess their risk from storms is provided (FEMA 2008). The guideline categorizes 'risk' into three classes: low, moderate, and high. Two maps along with a table containing degrees of risk are provided. The first map gives frequencies of tornado events that occurred within 2,470 square miles. The second map provides wind speed zones. After obtaining the frequency of tornado events and the wind speed zone for their

structures, the owners can obtain a risk degree from the table. For low risk area, the need of safe room is an owner's preference. For moderate risk area, owners should consider having a safe room for their protection; in high risk areas, a safe room is needed.

Owners are able to purchase safe rooms from certified manufacturers or they may choose to build it themselves. If the latter decision is preferred, FEMA P-320 also provides several construction plans and cost estimations for various types of safe rooms. These plans were proved that they met or exceeded the requirements in the ICC/NSSA Standard for the Design and Construction of Storm Shelters (ICC-500) which provides a standard for design and construction of storm shelters. Beside the requirements of fire safety, occupancy, accessibility, and other limitations, ICC-500 required that the safe room must pass both pressure and debris impact testing. The "pressure testing" represents the tremendous wind pressures that a storm shelter might be subjected to during storms. The debris impact test is used to qualify whether a storm shelter can withstand the impact from WBD.

As mentioned before, impact loads from debris are sources of tornado damages. To resist impact loads, both structural design and material selection are important. According to preliminary tests (see chapter 3), CarbonFlex has high strength and damping which motivated the concept of utilizing CarbonFlex in the design of storm shelters, and, consequently, a study was developed as pilot research to provide primary knowledge that might be used to navigate future development of the CarbonFlex-storm shelter to withstand tornadoes (as well as earthquakes forces). Thus, debris impact tests of CarbonFlex-wrapped wall panels and door assemblies were conducted. The experiments were performed at the facility of Wind Science and Engineering center

(WiSE) at Texas Tech University in Lubbock, Texas. The study was motivated by funding from the Department of Homeland Security (DHS).

Debris Impact Test

The ICC-500 (International Code Council) requires that all storm shelters be designed to withstand impacts of WBDs. It also provides impact testing criteria for both tornado and hurricane shelters. For example, the debris impact missile for tornado shelters shall be a 15-pound, 12 ft long, 2 in. x 4 in. lumber traveling at various speeds per the design wind speeds associated with various categorical ground wind speed tornadoes according to the EF scale. (International Code Council & National Storm Shelter Association, 2008).

There are several types of specimens categorized by their functions, such as wall and roof panels, window assemblies, and door assemblies. Windows cannot be wrapped by CarbonFlex because it will block the transparency of windows. Therefore, two specimen types, which are wall panels and door assemblies, were tested in this study. The ICC-500 requires different impact locations for both specimen types. Figure 61(a) and (b) show required impact locations for wall panels and door assemblies, respectively.

In figure 61, impact locations at the top-right (the corner) and bottom-left (3 in. from the 2 in. x 4 in. stud) represent impacts in the “shear zones” because the impact locations are near the boundaries of the studs and edges. The impact location at the center represents an impact in “bending zone” because the bending deformation most likely to occur at the center of the panel.

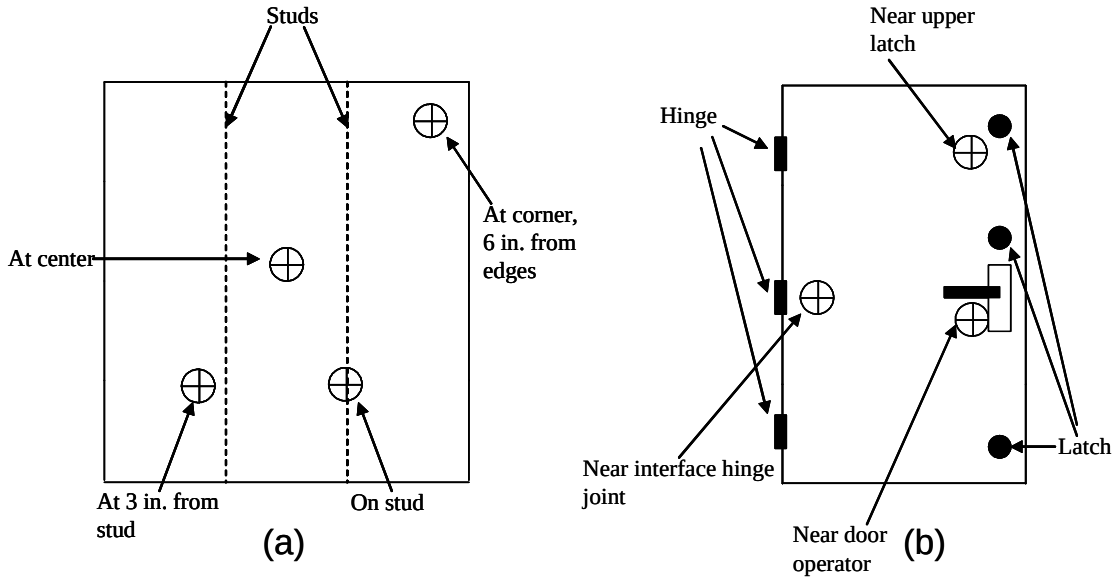

Figure 61. Impact locations for (a) a wall or roof panel, (b) a door assembly.

Pass and Fail Criteria

Words used to describe the experimental results and fail criteria for debris impact testing are defined here.

Perforation: the opening of the interior (non-impact) side of the specimen due to a missile impact.

Penetration: when a missile penetrates but do not perforate a specimen, the penetration is a distance measured from the impact tip of the missile to the outside (impact) surface of the specimen.

Permanent deformation: the permanent deformation is the distance from a straight edge held between two un-deformed points to the top of the deformation on the interior side.

Witness screen: a #70 unbleached kraft paper is used to check disengagement and spall of specimen components. The screen was installed 5 inches behind the interior side

and is intended to indicate any shards of wall that may damage the paper, thus indicating a ‘failed’ test.

According to the ICC-500, the specimen failed the test if it was perforated by a missile or had a permanent deformation greater than three inches or the witness screen behind the specimen was damaged. To pass the test, the specimen must have no perforation, no permanent deformation greater than 3 inches, and no damage on the witness screen after it was shot.

Debris Impact Specimens

The drawing AG-06 in the FEMA P-320 was chosen as a baseline for constructing the CarbonFlex specimens. The drawing AG-06 is a plan of a wood-frame safe room sheathed by steel plate and plywood sheet. In the drawing, a 14 gauge continuous steel plate was used as one of the sheathing materials. For the specimens, CarbonFlex was used in lieu of a steel plate. The drawing was selected because it is a wood-framed structure, which is relatively easier to construct than other structural types, and most construction teams are familiar with the construction of wood-framed structures. In addition, it is the cheapest construction plan provided in the FEMA P-320.

Because the specimens were to be transported from Arizona to Texas to be tested in the WiSE, a small specimen size was preferred for ease of transportation. According to the ICC-500, the smallest size for the wall panel specimens is 4 ft x 4 ft. Therefore, six–4 ft x 4 ft wall panels and three–8 ft x 8 ft door assemblies were constructed. The impact side of each wall panel specimen was wrapped by CarbonFlex having different control parameters (h_p and t_c), resulting in a spectrum of expected strengths and impact resistance. One specimen was wrapped by CFRP for comparison purposes. The

reinforcing carbon fiber fabrics that were used to manufacture CarbonFlex were aligned in 0º/90º directions. In addition, two-5 in. wide strips of carbon fiber were diagonally attached on each wall to provide a cross bracing configuration. Every wall has two– double 2 in. x 4 in. interior studs located 16 inches on center (OC); and four-4 ft long double 2 in. x 4 in. were used to form perimeter edges. This design scheme is in accordance to the ICC 500 and to FEMA 320 / FEMA 361. The expected strength and descriptions of the 4 ft x 4 ft specimens are shown in table 8. All specimens were sheathed with two layers of 3/4 inch plywood on the impact face, which were fastened with 16d common nails at 4 inches OC on the outside edges and at 6 inches OC on the interior studs. On the other (interior) face, all walls were sheathed with 7/16 inch oriented strand board (OSB.) and fastened with 8d common nails at 6 inches OC on both the interior and exterior studs.

The order of the experimental testing procedure started with the wall that was anticipated to have the largest impact resistance and highest strength to the weakest wall panel. Each specimen was shot by 15 lb, 12 ft long, 2 in. x 4 in. lumber projectile missiles. According to the ICC-500, speeds of missiles can be varied which represent a debris flying in a tornado having different wind speeds depending on the level of a tornado. For example, a missile traveling at 100 mph represents a WBD traveling in a tornado having 250 mph wind speed. The correlations of tornado's wind speed and missile speeds are shown in table 9 (International Code Council & National Storm Shelter Association, 2008).

Table 8

Descriptions of Wall Panel Specimens.

Expected strength level (1 is the highest)	Wall number	Materials on impact face	h_p (mm)	t_c (Hrs)
1	1	CarbonFlex and2-¾ plywood	5	2.5
1	2	CarbonFlex and2-¾ plywood	5	2.5
2	3	CarbonFlex and2-¾ plywood	5	3.5
2	4	CarbonFlex and2-¾ plywood	3	2.5
3	5	CarbonFlex and2-¾ plywood	3	3.5
4	6	Carbon fiber and2-¾ plywood	No	No

Note. mm = millimeter. Hrs = hours.

Table 9

Speeds of the Projectile for Debris Impact Testing.

Tornado wind speed (mph)	Speed of the missile (mph)
130	80
160	84
200	90
250	100

Note. mph = mile per hour.

Regarding the door assemblies, each 8 ft x 8 ft door panel included two main components which are the 2-ply steel door, a polystyrene in-fill, hardware (including the dead bolts), and an adjoining wall section. The wall section of each of the three door assembly panels has the same design which consists of two layers of 3/4 inch plywood sheathed with 5 mm thick and t_c = 2.5 hrs CarbonFlex on the impact face. However, the wall sections of these three door assemblies have different design from the 4 ft x 4 ft wall panels. For the wall sections, two layers of plywood sheets were attached to the studs first. Then, the Carbon fiber cloth was applied on top of the plywood sheet. After that, the polymeric compound was sprayed on top of the carbon fiber to make CarbonFlex. Thus,

the polymeric compound was sprayed only on one side of CarbonFlex unlike the 4 ft x 4 ft panels that the polymer was sprayed on both sides. Therefore, the polymer volumetric fraction in the wall sections is about 50 percent less than that in the 4 ft x 4 ft panels. In addition, CarbonFlex in the wall sections was reinforced with only one layer of carbon fiber in 0º direction while that in the 4 ft x 4 ft panels reinforced by carbon fiber in 0º/90º directions. Therefore, the amount of fiber reinforcement in the wall section is less than that in the 4 ft x 4 ft panels. On the other face, the walls are sheathed with 7/16 inch OSB. The difference between each door is the door's thickness. The descriptions of each door assembly are shown in table 10. Each door was equipped with three Sargent grade 1 commercial deadbolts (latches) and a Sargent door lock (operator) as shown in figure 62.

Table 10

Door Skin Thickness of Each Door Assembly.

Door assembly number	Thickness (gauge)
1	14
2	16
3	18

Test Strategy

Each specimen was subjected initially to the maximum missile speed of 100 mph. If the specimen failed the test, the speed would be reduced until the specimen "passed" the test. After that, the test of the next specimen, which was expected to be weaker, would start at the same speed that the previous stronger specimen had passed. For example, if the wall number 1 failed the test at missile velocity of 100 mph, the speed would be reduced to 90 mph. Then, if the wall number 1 passed the test at 90 mph, the test of the wall number 2 would be started at missile speed of 90 mph.

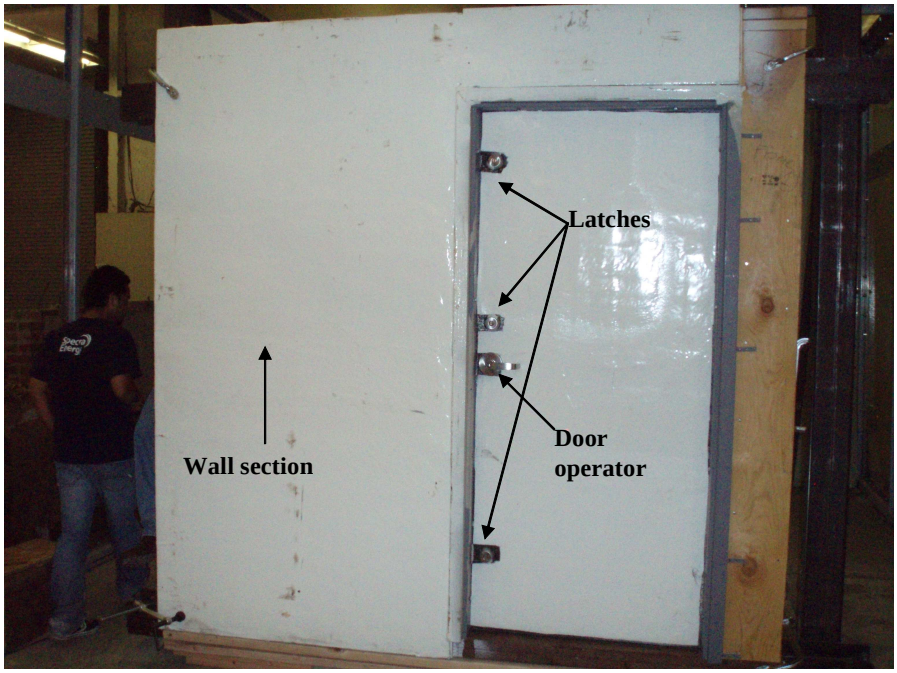

Figure 62. Components of a door assembly specimen.

Test Results

The physical observations of the test results are reported in Appendix B. However, the test results, namely the exact missile speeds, indentations, impact energies, and unit energies, are summarized in table 11. The impact energy is a kinetic energy of the missile from each shot which was calculated using equation 6.4.

$$E_k = 1/2mv_0^2 \quad (6.4)$$

Where, E_k is kinetic energy (Joule), m is a mass of the missile (kilogram), and v_0 is the velocity (meters per second). Because the exact speed from each testing impact was different and each impact created unequal indentation depth, therefore, in order to have a fair comparison, the unit energy was used which is defined as the kinetic energy of each shot divided by the indentation in the specimen created by the fired missile. The unit energy of each shot was calculated using equation 6.5.

Table 11

Summary of Debris Impact Testing Results

Wall/Panel Number	Impact number	Impact Location	Missile speed (mph)	Indentation (Inch)	Impact energy (Joule)	Unit energy (Joule/inch)
1	1	Shear	101	1.5	6935.22	4623.48
1	2	Bending	102	4.875	7073.23	1450.92
1	3	Shear	101	1.5	6935.22	4623.48
2	4	Shear	101	1.125	6935.22	6164.64
3	5	Shear	100	6-in. perforation	6798.57	—
3	6	Shear	100	8.75 in penetration with 2.5-in. perforation	6798.57	—
3	7	Shear	90	1.5	5506.84	3671.23
3	8	Bending	91	1.75	5629.89	3217.08
3	9	Shear	92	1.375	5754.31	4184.95
4	10	Shear	100	1.5	6798.57	4532.38
4	11	Bending	100	1.5	6798.57	4532.38
4	12	Shear	100	2.25	6798.57	3021.59
5	13	Shear	89	3.5	5385.15	1538.61
5	14	Bending	90	1.125	5506.84	4894.97
5	15	Shear	92	1.1875	5754.31	4845.73
6	16	Shear	102	21.125	7073.23	334.83
6	17	Bending	100	2.125	6798.57	3199.33
6	18	Shear	91	33.625	5629.89	167.43
Door 1	19	Near door operator	101	Door open (fail)	6935.22	—
Wall of Door 1	20	Stud	101	0.5	6935.22	13870.44
Wall of Door 1	21	Shear	103	Total perforation	7212.60	—
Door 2	22	Door's center	102	1	7073.23	7073.23
Door 3	23	Door's center	102	1.375	7073.23	5144.1

Note. mph = mile per hour.

$$UE = E_k/\Delta_{in} \tag{6.5}$$

Where, *UE* is unit energy and Δ_{in} is an indentation created by a missile. The unit energy implies ability to resist impact energy of specimens. For example, the specimen that has

more unit energy has better impact resistance because it required more energy to create the same (one unit) indentation.

A discussion of the results was separated into two sections. First, a brief summary of the debris impact testing results was presented, and second, the results from the wall panels were presented and analyzed. The effects of h_p and t_c to the impact of WBD were discussed by comparing the results of each panel. In addition, the influence of the impact locations (in the shear and bending zones) was pointed out. These influences specified the weak locations of the wall panels which will help improve and optimize the design of the CarbonFlex-storm shelter in the future.

A Brief Summary of Debris Impact Tests

The pass and fail impact velocities of each specimen are reported in this section, as well as a discussion of results.

Wall panel numbers 1 and 2. Both wall panels have the same h_p and t_c. Therefore, they were expected to have the same strength. A total of four impacts at 100 mph were made. Three missiles were shot to the panel number 1 and the other missile was shot on the panel number 2 (again, having the same design as panel 1). Both walls were not perforated; the maximum deformation was less than 3 inches, and the witness screen was not damaged. Therefore, the design of wall numbers 1 and 2 (2 layers of 3/4 inch plywood having h_p = 5 mm and t_c = 2.5 hrs for the CarbonFlex on the impact face, and 7/16 inch OSB on the back face of the wall panel) passed a debris impact test for a level-5 tornado having a 250 mph ground wind speed (as represented by a 100 mph 2 x 4 missile, per ICC 500 and FEMA 320/ 361).

Wall panel number 3. This panel was shot five times. The first two missiles were shot at 100 mph (representing a level-5, 250 mph ground wind speed tornado). Both impacts perforated the specimen, concluding that the specimen failed the debris impact test at 100 mph. The panel was subsequently impacted by three additional missiles having 90 mph velocity in order to rate it for a level-4 tornado (200 mph ground wind speed tornado), and the specimen indeed passed the test. Therefore, the design of wall number 3 (consisting of two layers of 3/4 inch plywood covering h_p = 5 mm and t_c = 3.5 hrs CarbonFlex on the impact face, and 7/16 inch OSB on the back face) passed a debris impact test for the tornado with 200 mph ground wind speed.

Wall panel number 4. Although the CarbonFlex that was used to design this panel has a smaller polymer volumetric fraction (corresponding to h_p = 3 mm) than wall number 3 (having h_p = 5 mm), it has a shorter critical time t_c (2.5 hrs). Per the preliminary test results that were discussed in chapter 3, the CarbonFlex specimens having a shorter t_c tended to have a higher damping ratio. Thus, this wall panel was expected to have at least the same strength level as the wall number 3. This specimen was shot three times by missiles traveling at 100 mph. The panel passed the test. Therefore, the design of wall number 4 (2 layer of 3/4 inch plywood covering h_p = 3 mm and t_c = 2.5 hrs CarbonFlex on the impact face and 7/16 inch OSB on the back face) passed a debris impact test for tornadoes having a 250 mph ground wind speed.

Even though Carbonflex in the wall number 4 is thinner (h_p = 3 mm.) than that of wall panel number 1 and 2, wall panel number 4 has the same t_c and passed the strongest tornado test as well. In addition, wall panel number 3 has a thicker CarbonFlex than wall panel number 4 but has different t_c (3.5 hrs). However, wall number 4 passed the test at

stronger level of tornado than the wall panel number 3. These results are good evidences showing that the t_c parameter affected the impact resistance of the panels more than h_p parameter.

Wall panel number 5. CarbonFlex used in this panel has the same t_c as the wall panel number 3 but less polymer's volumetric fraction than the panel number 3. Thus, the panel was expected to be weaker than the panel number 3. The specimen was shot three times with missiles having a speed of 90 mph. The panel passed the test. Therefore, the design of the wall number 4 (2 layer of 3/4 inch plywood covering h_p = 3 mm and t_c = 3.5 hrs CarbonFlex on the impact face and 7/16 inch OSB on the back face) passed a debris impact test for the tornado with 200 mph ground wind speed.

Wall panel number 6. In this panel, CFRP was used in stead of CarbonFlex. The specimen was shot three times, twice with 100 mph and once with 90 mph missiles. Although one of the missiles traveling at 100 mph did not perforate the panel because the missile hit a stud, the first and the last impacts perforated the panel. Therefore, this specimen failed both debris impact speeds. These results compared with those of CarbonFlex panels clearly indicate the tremendous energy dissipation of CarbonFlex and its ability to resist impact loads.

Without the polymeric constituent, CFRP has a brittle failure and does not have ductility which implying that the ability to dissipate energy is small. Therefore, the wall panel number 6 failed the test at both velocities. In contrast, CarbonFlex has better impact resistance, energy dissipation, and greater ductility. These great improvements came not only from adding the polymeric constituent but also having a good quality interfacial

bonding between the polymeric constituent and the epoxy which can be obtained by carefully controlled t_c.

Door assembly number 1. This specimen was shot three times. All missiles had the same velocity which is 100 mph. The first impact was aimed near the door's operator (handle). After the impact, all latches were severe damaged and the door was popped open. Therefore, this door assembly failed the test.

Moreover, two more shots were initiated, but the target, in this case, is the wall section next to the door panel. The first shot created about 0.5 inch indentation on the wall. However, the missile hit the stud. The second shot was aimed to the shear zone of the wall section. The missile perforated the wall. Therefore, the wall section also failed the test. This result indicated that the wall section has lower impact resistance than the wall panel number 1 to 5. This is because, as mentioned before, the wall section has less polymeric constituent (about 50 percent less than that in the wall panels) and fiber reinforcement.

Door assembly number 1, 2, and 3 after welded shut. Experimental results of the previous door assembly showed that the hardware (latches and door's operator) could not withstand the impact test. To further study the impact resistance of the door panels, the doors were welded to their frames before more impact tests were conducted. Each door was shot once with the 100 mph missile. The indentations are 1, 1.375, and 1.5 inches for door assembly number 1, 2, and 3, respectively. The results showed that an indentations increased when thickness of door skins decreased (the door number 1 has thickest door skin and the door number 3 has thinnest door skin see table 10).

Effect of h_p to the Impact Resistance

Wall panel numbers 1 and 4 have the same t_c but different h_p. Therefore, to study the effect of h_p to the impact resistance of CarbonFlex-storm shelter panels, the unit energies from each wall were averaged and compared. The average unit energy of the panel number 1, which has greater h_p, is 4215.63 Joule per inch which is 4.64 percent greater than that of the panel number 4.

From these results, CarbonFlex panels having greater h_p tended to have a better energy absorption which agreed with the primary testing results in chapter 3 showing that the CarbonFlex specimens having greater h_p had better ductility and damping ratio.

Effect of t_c to the Impact Resistance

The effect of t_c was shown by comparing the average unit energy of the panel number 1 and 3. The average unit energy of the panel number 1, which has shorter t_c (2.5 hrs), is 14.21 percent greater than that of the panel number 6. In addition, the effect of t_c can be clearly seen by comparing the results of the panel number 4 to those of the panel number 3. Although the panel number 4 has less polymer's volumetric fraction (less h_p), its average unit energy is 9.15 percent greater. This is because the panel number 4 has a shorter t_c which is 2.5 hrs compared to 3.5 hrs of the wall number 3. A shorter t_c means that the time between applying epoxy and spraying the polymeric constituent is also shorter resulting in having more active chemical agents in epoxy to chemically bond to the polymer. Consequently, CarbonFlex having t_c = 2.5 hrs has a better quality of interfacial bonding between epoxy and the polymer resulting in better energy dissipation.

From the results, CarbonFlex panels having a shorter t_c tended to have better impact resistance. Moreover, the resistance can be improved by properly controlling t_c.

This is a vital manufacturing parameter of CarbonFlex implying that, with fewer amounts of materials (polymer), the impact resistance of CarbonFlex could be improved by using a suitable t_c.

Effect of Impact Locations

Panels (number 1 and 3) having more polymer constituent (greater h_p) had less unit energy when the missiles hit their bending zone while the unit energies at the bending zones of panels number 4 and 5 (having less $h_{p)}$ were equal or greater than the unit energies at shear zones. This can be explained by considering the sheathing panel (on the impact side) as a slab (or a beam) having studs as its supports. CarbonFlex, which was installed behind two pieces of 3/4 plywood, acted as a tension reinforcement for the panel. According to the tensile test results shown in chapter 3, the tensile stiffness of CarbonFlex specimens decreased when the polymer's volumetric fraction increased. Therefore, the panels, which had greater h_p, were weaker in the bending zone. In addition, it is widely known that shear strength of composite materials is dominated by their matrix. Therefore, the panels that had more polymer constituent also had greater unit energies in the shear zone than in their bending zones counterparts and tended to provide greater shear resistance than the panels having less h_p.

Summary of Chapter 6

Wind-borne debris impact tests of six storm shelter wall panels and three door assemblies were conducted. Experimental results indicated that CarbonFlex had a better impact resistance than CFRP. Two designs of CarbonFlex-storm shelter wall panels passed impact testing at the highest testing velocity while other two designs passed the test at 200 mph wind speed (90 mph impact speed). In addition, the impact resistance of

CarbonFlex could be improved by properly adjusting the t_c manufacturing parameter. According to the current experimental test data, CarbonFlex having h_p equal to 3 mm and t_c equal to 2.5 hrs appears to be optimally suitable for use in storm shelter designs because it could withstand the largest impact using less material (polymer) and construction time (shorter t_c).

CHAPTER 7

Conclusion and Future Study

CarbonFlex consists of three main physical components: the carbon fiber that provides high strength, the saturant (epoxy resin), and a unique polymer that provides additional ductility and energy dissipation. However, it is the processing of CarbonFlex that affects the interfacial cohesion and interaction between the polymer and saturant epoxy and that, in turn, helps provide impact resistance, fracture toughness, and damping. As a result, some properties of CarbonFlex are functions of two parameters, which are time duration (t_c) between applying the epoxy of carbon fiber and applying the polymer constituent, t_c, which influence quality of the bonding between these two constituents. The other variable is the thickness (h_p), which is proportional to the volumetric fraction, of the polymer.

Benefits of CarbonFlex

Experimental test results indicated that CarbonFlex could enhance certain properties and redistribute damage in wrapped wood beams, through a concept called "sustainable crack growth," where the crack growth mechanism in wood beams was stabilized.

Compared to wood-framed shear walls, CarbonFlex shear walls showed a significantly improved ability to sustain strength and stiffness. These superiorities came from flexibility, high strength, and energy dissipation of CarbonFlex. In addition, some portions of energy were dissipated via CarbonFlex sheathing panel and did not concentrate at the connection between the sheathing panel and wood frames (studs) which are the weakest links in wood-framed shear walls. In addition, experimental results

indicated that, at the same story drift, CarbonFlex shear walls had a higher load level which implies that CarbonFlex shear wall systems provided a better story force distribution to the structures. Furthermore, CarbonFlex shear walls had a very high ductility (24.7) resulting in 16.86 percent greater response modification factor compared to the conventional wood-framed shear walls. Therefore, it can be concluded that CarbonFlex shear wall system is a good newly developed seismic protection system which can provide sustainable high strength, stiffness, and tremendous ductility. The risk of soft-story collapses can be reduced by using CarbonFlex shear wall system as a seismic protection method in low-rise wood-framed structures.

Moreover, CarbonFlex shear walls showed an ability to "fully" recover their stiffness after experienced high displacement demand (4.7 percent story drift). Therefore, it can protect low-rise wood-framed structures from strong aftershocks and increase safety for both victims and rescue crews/ first responders occupying the structures following seismic events.

Pioneer debris impact tests that were used to obtain useful information for future CarbonFlex-storm shelter design were conducted. Experimental test results indicated that the most efficient design of CarbonFlex used in the design of storm shelters has an h_p equal to 3 mm and t_c equal to 2.5 hrs since this design passed the highest level of tornado impact test (level 5) while using the least amount of material (polymer) and construction time. However, the wall panels having thicker CarbonFlex showed a better impact resistance in their shear zones. This is because the shear capacity of composite materials is dominated by the matrix constituent. Therefore, increasing the thickness (h_p) of CarbonFlex at the shear zone is recommended.

Preliminary Research of CarbonFlex

A series of coupon tests, namely tensile, cyclic loading, free-vibration, and flexural tests, were conducted. Results from tensile tests showed that CarbonFlex could exhibit ductile failure. Thicker polymer used to manufacture the specimens helped to increase ductility and resulted in an ultimate displacement that was 1.6 times greater following an increase in thickness (h_p) by two times. In cyclic loading tests, specimens were subjected to loads having amplitude equal to 75 percent of the ultimate tensile displacement over five consecutive loading cycles. The test results showed that the CarbonFlex behavior changed from elastic to post-yield hardening behavior to nearly-purely viscous behavior at failure. The backstress decreased with an increasing number of cycles indicating a decrease in the anelastic behavior. The damping ratios of CarbonFlex were also evaluated in free-vibration tests. The damping ratio of CarbonFlex was 4.64 percent which was 2.4 and 14 times greater than those of CFRP and steel specimens, respectively. In addition, the effects of h_p and t_c on the damping ratio were studied. By doubling the thickness of the applied polymer, the damping ratio increased by approximately 60 and 73.6 percent for CarbonFlex having t_c = 3 and 5 hrs, respectively. The results also showed that damping ratio was decreased when t_c was increased and damping ratio decreased dramatically when t_c was greater than three hours. This is the first scientific evidence showing the impact of t_c on the properties of CarbonFlex. Three point-bending tests conducted on wood beams that were wrapped by CarbonFlex were carried out. The results showed that the wrapped wood beams had greater ductility and ultimate displacement than unwrapped and CFRP wrapped beams. Moreover, the stiffness of 1/8 in thick CarbonFlex-wrapped beams (i.e., using 1/8 thick polymer)

became less negative during the increasing of the displacement after peak load. This indicated then also brought to light the concept of a composite system exhibiting "sustainable negative stiffness" and stabilized crack growth. A stress-strain relationship of CarbonFlex-wrapped wood system was proposed, and multi-linear series was used to express the stress in sustainable softening region. The numerical results showed a good correlation to the experimental test results.

Testing Results of CarbonFlex Shear Walls

According to experimental test results, the problems of conventional plywood shear wall were investigated, benefits of using CarbonFlex in the low-rise structures were shown, and the construction guidelines for manufacturing CarbonFlex-wrapped wood structures was established.

The test results showed that:

1) The failure modes of the plywood shear wall were nail pulled out and sheared off following by detaching of the plywood panel and braking of studs. This was the result of connecting rigid materials, which are plywood panels and studs, using generally weaker fasteners. When the shear walls were subjected to large displacements, the panels started to crack as nails pulled out or sheared off.
2) Following nail pull out or punch through, the plywood panels might detach from the studs resulting in a dramatic decrease in the in-plane racking strength and stiffness of the story. This caused a "soft-story" collapse of the structure.
3) The suitable wrap schematic for CarbonFlex shear walls is a full wrap. The cross-bracing schematic provided less ductility and required more time to construct. In

addition, the suddenly dropping of strength, which is undesirable behavior, was observed twice in the cross-bracing wall.

4) CarbonFlex shear walls exhibited unique hysteretic behavior which could be gathered by a combination of tension-buckling strips, buckling induced pinching, and viscoelasticity.
5) Because no damage, debonding, and detaching of CarbonFlex panel could be observed in the 8 ft x 8 ft CarbonFlex mock house, it is strongly believed that most of energy could be dissipated through the CarbonFlex "body" resulting in less energy concentration at the connection between CarbonFlex panel and studs.
6) The U- and L- wraps made from CarbonFlex did not have enough strength to resist the overturning moment of the wall. Therefore, the mechanical hold-down is preferred.
7) The strength and stiffness of the Carbonflex shear wall with openings was well predicted by using Sugiyama's shear capacity ratio when the displacement demand was less than two inches. Sugiyama's shear capacity ratio provided an under estimated strength when the displacement was greater than two inches.
8) Due to the ability to dissipate energy through the panel, CarbonFlex shear walls could sustain strength and stiffness which helped prevent the story to become a soft-story. This study is the first scientific evidence proving that using CarbonFlex can protect the low-rise structures from a soft-story collapse.
9) The strength and stiffness of CarbonFlex shear walls could be fully recovered after tested by the MPD record having maximum displacement of 3.78 inches while the stiffness of the conventional plywood shear wall degraded after the test.

This ability of CarbonFlex shear walls can reduce losses due to aftershocks and mainshock.

Construction Guideline for CarbonFlex Shear Walls

1) The structure should be fully wrapped by CarbonFlex. The carbon fabric should be stretched during attaching to studs to prevent warping. The carbon fabric can be secured to studs by using construction grade staples.
2) The 4 mm thickness (h_p) and 2.5 hrs t_c shall be used for the 8 ft x 8 ft wall subjected to the load that is not greater than 24000 lbs divided by a design safety factor.
3) Two pieces of 5 inches wide CarbonFlex strips shall be attached diagonally to form cross-bracings on the lateral force resisting wall.
4) 4 in. x 9 in. CarbonFlex strips should be placed at bottom and top of the panel in between studs to increase shear capacity of CarbonFlex panel.
5) Mechanical hold-downs shall be used at the end studs of the lateral force resisting walls.

Debris Impact Testing for CarbonFlex-storm Shelters

1) Two design categories for wall section of the shelter passed the debris impact testing for the tornado at 250 mph ground wind speed, which are:
    a. Two layers of 3/4 inch plywood covering h_p = 5 mm and t_c =2.5 hrs CarbonFlex on the impact face and 7/16 inch OSB on the back face.
    b. Two layers of 3/4 inch plywood covering h_p = 3 mm and t_c =2.5 hrs CarbonFlex on the impact face and 7/16 inch OSB on the back face.

2) Two design categories for wall section of the shelter passed the debris impact testing for the tornado at 200 mph ground wind speed, which are:
    a. Two layers of 3/4 inch plywood covering h_p = 5 mm and t_c =3.5 hrs CarbonFlex on the impact face and 7/16 inch OSB on the back face.
    b. Two layers of 3/4 inch plywood covering h_p = 3 mm and t_c =3.5 hrs CarbonFlex on the impact face and 7/16 inch OSB on the back face.
3) CarbonFlex wall panel having greater h_p and shorter t_c tended to have better energy absorption.
4) According to current available experimental information, CarbonFlex having h_p equal to 3 mm and t_c equal to 2.5 hrs is suitable to be used in the storm shelter because it could withstand the fastest impact and used less material and construction time. However, CarbonFlex panels having h_p equal to 5 mm tended to have better impact resistance at the shear zone. Therefore, the 5 mm h_p is recommended at the shear zones.

Future Study

1) The effects of temperature at the construction site at the time of manufacturing CarbonFlex to its strength and stiffness should be studied because the curing time of the saturant depends on the temperature.
2) The effects of other construction materials, such as drywall and insulation, to the behavior of CarbonFlex-wrapped structure should be investigated.
3) Several CarbonFlex shear walls having various opening sizes should be tested to establish a more reliable strength estimation method for designing purpose.
4) The pressure test of several CarbonFlex-storm shelter panels should be conducted.

5) The tests evaluating strength and stiffness of CarbonFlex panel after subjected to fire should be conducted.

REFERENCES

Akovall, G. (2001). *Handbook of composite fabrication*. Rapra Technology Ltd.

American Society of Civil Engineers. (2010). *Minimum Design Loads for Buildings and Other Structures (ASCE 7-10).* American Society of Civil Engineers.

American Wood Council. (2008). *2008 Wind and Seismic, Special Design Provisions for Wind and Seismic.* American Forest & Paper Association, INC.

APA – The Engineered Wood Association. (2001). *Diaphragms and Shear Walls Design/ Construction Guide*. APA – The Engineered Wood Association.

APA – The Engineered Wood Association. (2007). *Introduction to Lateral Design*. Tacoma Washington: The Engineered Wood Association.

Ashley, S. (2012, August 27). Oak Ridge collaborates for cheaper carbon fiber. Retrieved March 29, 2013, from http://www.sae.org/mags/aei/11104

ASM International. (1990). *ASM handbook* (10th ed.). Materials Park, OH: ASM International.

Astaneh-Asl, A., (2000). Steel Plate Shear Walls. Proceeding U.S.-Japan Partnership for Advanced Steel Structures, U.S.-Japan Workshop on Seismic Fracture Issues in Steel Structures, February 2000, San Francisco, CA.

Astaneh‐Asl, A. (2008). STEEL SHEAR WALLS, BEHAVIOR, MODELING AND DESIGN. *AIP Conference Proceedings*, *1020*(1), 5–18. doi:doi:10.1063/1.2963889

ASTM Standard, D143-09. (2009). Standard Testing Method for Small Clear Specimens of Timber. *ASTM International*, West Conshohocken, PA. www.astm.org.

ASTM Standard, D3039/D3039M. (2009). Standard Testing Method for Tensile Propertiesof Polymer Matrix Composite Materials. *ASTM International*, West Conshohocken, PA. www.astm.org.

Applied Technology Council (ATC) 29-2. (2003). Seminar on seismic design, performance, and retrofit of nonstructural components in critical facilities. October 23-24, Los Angles, CA.

Attard, T.L. (2004). Optimal Damping and Higher-Mode Control in Nonlinearly Degrading Shear Buildings for a Ground Acceleration. *International Symposium on Network and Center-Based Research For Smart Structures Technologies and Earthquake Engineering*, SE04, Osaka, Japan.

Attard, T. L. (2005). Post-Yield Material Nonlinearity: Optimal Homogeneous Shear-Frame Sections and Hysteretic Behaviors. *International of Solids and Structures*, *42*(21-22), 5656-5668.

Attard, T.L. (2007). Controlling all Inter-Story Displacements in Highly-Nonlinear Steel Buildings using Optimal Viscous Damping. *Journal of Structural Engineering*, *133*(9).

Attard, T.L, Dansby, R., and, and Marusic, M. (2007). Optimal Nonlinear Structural Damage Control for Kinematically Strain Hardened Systems using an Evolutionary State Transition. *ECCOMAS Thematic Conference on Computational Methods* in Structural Dynamics and Earthquake Engineering, COMPDYN 2007, Rethymno, Crete, Greece.

Attard, T.L., & Dansby, R.E. (2009). Evolutionary Structural Control of Elastic and Inelastic Strains using Rehabilitative Algorithms in Damaged Steel Buildings.*Journal of Mechanics of Materials and Structures*. *4*(3), 413 - 424.

Attard, T. L., & Mignolet, M. P. (2008). Random Plastic Analysis using a Constitutive Model to Predict the Evolutionary Stress-Related Responses and Time Passages to Failure. *Journal of Engineering Mechanics*, *134*(10), 881-891.

Bachman, R. (1998). Building code seismic design provisions for nonstructural components. *Report No. ATC 29-1, Proc. Seminar on seismic design, performance, and retrofit of nonstructural components in critical facilities*, ATC, Redwood City, CA, p.1-74.

Bachmann, H. (2003). *Seismic Conceptual Design of Buildings – Basic principles for engineers, architects, building owners, and authorities*. Swiss Federal Office for Water and Geology, Swiss Agency for Development and Cooperation, BWG, Biel.

Balaguru, P. N., Giancaspro, J., & Nanni, A. (2009). *FRP composites for reinforced and prestressed concrete structures*. Taylor & Francis.

Beall, F., Li, J., Breiner, T., Wai, J., Machado, C., Oberdorfer, G., & Mosalam, K. (2006). Small-Scale Rack Testing of Wood-Frame Shear Walls. *Wood and Fiber Science*, *38*(2), 300–313.

Berman, J. W. & Bruneau, M. (2004, August). *Plastic Design and Testing of Light-Gauge Steel Plate Shear Walls*. Paper presented at the 13th World Conference on Earthquake Engineering, Vancouver, BC, Canada.

Berkeley Seismological Laboratory, (2003). http://www.seismo.berkeley.edu/seismo/hayward/

Berkowitz, B. (2012, March 3). Deadly tornadoes create huge insured loss risk. *Reuters*. Boston. Retrieved from http://www.reuters.com/article/2012/03/03/us-insurance-tornadoes-idUSTRE8220LJ20120303

Campbell, F. C. (2010). *Structural composite materials*. ASM International.

Cassidy, E. D. (2002, December). *Development and Structural Testing of FRP Reinforced OSB Panels for Disaster Resistant Construction*. The University of Maine.

Chuang, T. J., & Mai, Y. W. (1988). Flexural Behavior of Strain-Softening Solids. *Journal of Solids Structures, 25*(12), 1427-1443.

Chui, Y. H., & Ni, C. (1997). Load Embedment Response of Timber to Reversed Cyclic Load. *Wood and Fiber Science, 29*(2), 148-160.

Dansby, R.E., & Attard, T.L. (2007). Controlling nonlinear vibrations in steel structures using an evolutionary gain formulation to optimally satisfy performance objectives. *Sixth International Conference on Earthquake Resistant Engineering Structures*, ERES2007, Bologna, Italy

Dhiradhamvit, K. (2009, May). *Using Structural Health Monitoring Data To Evaluate Performance of Rapid-Set® Concrete and Using Lead-Core Rubber Base Isolator to Protect Highway Bridges*. California State University, Fresno.

Dhiradhamvit, K., Attard, T. L. & Hongyu, Z. (2011). Development of a New Lightweight "Rubberized-Carbon" Composite for Wood Home Protection. In *1st International Conference on Construction*. Athens, Greece: Architecture and Engineering.

Diani, J., Fayolle, B., & Gilormini, P. (2009). A review on Mullins Effect. *European Polymer Journal, 45*, 601-612.

Dolan, J. D., & Johnson, A. C. (1996). Monotonic Test of Long Shear Walls with Openings. (Report No. TE-1996-001, The American Forest & Paper Association, Washington, DC).

Eamon, C., Jensen, E., Grace, N., & Shi, X. (2012). Life-Cycle Cost Analysis of Alternative Reinforcement Materials for Bridge Superstructures Considering Cost and Maintenance Uncertainties. *Journal of Materials in Civil Engineering, 24*(4), 373–380. doi:10.1061/(ASCE)MT.1943-5533.0000398

Elgaaly, M. (1998). Thin Steel Plate Shear Walls Behavior and Analysis. *Thin-Walled Structures, 32*, 151-180.

Evans, E., & Ritchie, K. (1997). Dynamic Strength of Molecular Adhesion Bonds. *Biophysical Journal, 72*, 1541-1555.

Fakhouri, M. Y., & Igarashi, A. (2012). Multiple-Slider Surfaces Bearing for Seismic Retrofitting of Frame Structures with Soft First Stories. *Earthquake Engng Struct. Dyn., 42*, 145-161.

Falk, R. H., & Itani, R. Y. (1987). Dynamic Characteristics of Wood and Gypsum Diaphragms. *Journal of Structural Engineering, 113*(6), 1357–1370. doi:10.1061/(ASCE)0733-9445(1987)113:6(1357).

Falk, R. H., & Soltis, L. A. (1988). Seismic behavior of low-rise wood-framed buildings. *The Shock and Vibration Digest, 20*(12), 3–7.

Federal Emergency Management Agency. (1994). *Reducing the risks of nonstructural earthquake damage: A practical guide*. Federal Emergency Management Agency. September 1994.

Federal Emergency Management Agency. (2008). *FEMA P-320 Taking Shelter From the Storm: Building a Safe Room For Your Home or Small Business* (3rd ed.). Federal Emergency Management Agency.

Filiatrault, A., Isoda, H., & Folz, B. (2003). Hysteretic damping of wood framed buildings. *Engineering Structures, 25*(4), 461–471. doi:10.1016/S0141-0296(02)00187-6.

Gangone, M. V., Kroening, R. A., Minnetyan, L., Janoyan, K. D., & Grimmke, W. F. (2005). Evaluation of FRP Rebar Reinforced Concrete Bridge Deck Superstructure. *American Society for Non-Destructive Testing (ASNT).*

Glickman, T. S., & American Meteorological Society. (2000). *Glossary of meteorology*. Boston, Mass: American Meteorological Society.

Grazulis, T. P. (2001). *The tornado: Nature's ultimate windstorm*. Norman: University of Oklahoma Press.

Hoa, S. V. (2009). *Principles of the manufacturing of composite materials*. DEStech Publications, Inc.

Homeland Security Department, Federal Emergency Management Agency. (2006). *Homebuilders Guide to Earthquake Resistant Design and Construction*. Government Printing Office.

Holmes, J. D., Baker, C. J., & Tamura, Y. (2005). Tachikawa number: A proposal. *Journal of Wind Engineering and Industrial Aerodynamics, 94*, 41-47.

Hota, G., & Liang, R. (2011). Advanced Fiber Reinforced Polymer Composites for Sustainable Civil Infrastructures. In *International Symposium on Innovation & Sustainability of Structures in Civil Engineering*. Xiamen University, China.

Howard, J., Tracy, C., & Burns, R. (2002). Comparing Observed and Predicted Directivity in Near-Source Ground Motion. *Earthquake Spectra, 21*(4), 1063-1092.

Huang, X. (2009). Fabrication and Properties of Carbon Fibers. *Journal of Materials, 2*, 2369-2403.

International Risk Management Institute, IRMI, 2003. http://www.irmi.com/Expert/Articles/2003/Gould01.aspx

International Code Council. (2006). *2006 International Building Code*. International Code Council, INC.

International Code Council. (2007). *2007 California Building Code*. California Building Standards Commission.

International Code Council. (2009a). *2009 International Building Code*. International Code Council, INC.

International Code Council. (2009b). *2009 International Residential Code® for One- and Two-Family Dwellings*. International Code Council, INC.

International Code Council, & National Storm Shelter Association. (2008). *ICC-500 ICC/NSSA Standard for the Design and Construction of Storm Shelters*.

Jones, R. L., & Chandler, H. D. (1986). Chemical corrosion of E-glass fibres in neutral phosphate solutions. *Journal of Materials Science, 21*(6), 2175–2178. doi:10.1007/BF00547966.

Kalsbeek, E. C., & Bruining, W. J. (2012). European Patent Number EP 2205781 B1: Method for Spinning and Washing Aramid Fiber and Recovering Sulfuric Acid. European Patent Office.

Kircher, C. A. (2003). It makes dollars and sense to improve nonstructural system performance. *Proc. of Seminar on Seismic Design, Performance, and Retrofit of Nonstructural Components in Critical Facilities*, Applied Technology Council, ATC 29-2, p. 109-119, Newport Beach, California, October 23-24, 2003.

Kobori, T., Takahashi, M., Nasu, T., Niwa, N. & Ogasawara, K. (1993). Seismic response controlled structure with active variable stiffness system. *Earthquake Engineering and Structural Dynamics*, *22*, 925-941.

Lebeda, D. J., Gupta, R., Rosowsky, D. V., & Dolan, J. D. (2005). Effect of Hold-Down Misplacement on Strength and Stiffness of Wood Shear Walls. *Practice Periodical on Structural Design and Construction*, *10*(2), 79–87. doi:10.1061/(ASCE)1084-0680(2005)10:2(79)

Lee, S. M. (1993). *Handbook of composite reinforcements*. VCH.

Li, H., Yan, M., Qi, D., Zhang, S., Ding, N., Cai, X., … Deng, J. (2011). Corrosion of E-glass fiber in simulated oilfield environments. *Journal of Petroleum Science and Engineering*, *78*(2), 371–375. doi:10.1016/j.petrol.2011.06.006.

Li, M., Foschi, R. O., & Lam, F. (2012). Modeling Hysteresis Behaviors of Wood Shear Walls with a Protocol-Independent Nail Connection Algorithm. Journal of Structural Engineering, *138*(1), 99-108.

Liberto, J. (2012, August 29). Hurricane Isaac damage estimate could top $1.5 billion. *CNNMoney*. Retrieved October 12, 2012, from http://money.cnn.com/2012/08/29/news/economy/hurricane-isaac-damage-estimates/index.html

Lin, N., Holmes, J. D., & Letchford, C. (2007). Trajectories of Wind-Borne Debris in Horizontal Winds and Applications to Impact Testing. *Journal of Structural Engineering*, *133*(2), 274-282.

Lin, N., & Vanmarcke, E. (2008). Windborne debris risk assessment. *Probabilistic Engineering Mechanics*, *23*, 523-530.

Line, P., & Douglas, B. K. (1996). Perforated Shearwall Design Method. *In Proceeding of the International Wood Engineering Conference, 2*, (pp.345-349). Madison, WI.

Lyons, M. A. (1998). *Seismic Retrofit Training for Building Contractors and Inspectors*. Association of Bay Area Governments.

Martin, Z., Skaggs, T. D., & Keith, E. L. (2005). *Using Narrow Pieces of Wood Structural Panel Sheathing in Wood Shear Walls* (Report No. T2005-08, APA – The Engineered Wood Association).

McDonald, B., Bozorgnia, Y., & Osteraas, J., J. (2000). Structural Damage Claims Attributed to Aftershocks. *Proceedings Forensic Engineering.* San Juan, Puerto Rico.

McDonald, J. R. (2001). T. Theodore Fujita: His Contribution to Tornado Knowledge through Damage Documentation and the Fujita Scale. *Bulletin Of The American Meteorological Socirety, 82*(1), 63.

McDonald, J. R., & Mehta, K. C. (2004). *A recommendation for an Enhanced Fujita Scale (EF-Scale).* Lubbock, Texas, Wind Science and Engineering Center.

MCEER, ATC-29 (2004). MCEER's Research on Nonstructural Components Featured at ATC-29-2 Seminar. Bulletin of the *Proc. of Seminar on Seismic Design, Performance and Retrofit of Nonstructural Components in Critical Facilities*, ATC-29, Redwood City, CA.

McKevitt, W.E., Timler P.A.M., & Lo, K.K. (1996). Nonstructural damage from the Northridge earthquake. *International Journal of Rock Mechanics and Mining Sciences and Geomechanics Abstracts, 33*(1), 39A-39A(1).

Middleton, D. H. (1990). *Composite materials in aircraft structures*. Longman Scientific & Technical.

Miranda, E. & Taghavi, S. (2005). Approximate Floor Acceleration Demands in Multistory Buildings. I: Formulation. *Journal of Structural Engineering, 131(*2), p. 203-211.

Misam, A., & Mangulkar Madhuri, N. (2012). Structural Response of Soft-story-High Rise Buildings under Different Shear Wall Location. *International Journal of Civil Engineering and Technology, 3*(2), 169-180.

Miyagawa, H., Jurek, R. J., Mohanty, A. K., Misra, M., & Drzal, L. T. (2006). Biobased epoxy/clay nanocomposites as a new matrix for CFRP. *Composites Part A: Applied Science and Manufacturing*, *37*(1), 54–62. doi:10.1016/j.compositesa.2005.05.014.

Miyauchi, K., & Murata, K. (2007). Strain-Softening Behavior of Wood Under Tension Perpendicular to the Grain. *Journal of Wood Science, 53*, 463-469.

NAHB Research Center, Inc. (2001, March). Wood Shear Walls with Corners. U.S. Department of Housing and Urban Development, Office of Policy Development and Research.

Nigg, J. M., & Mileti, D. S. (1998). The Loma Prieta, California, Earthquake of October 17, 1989-Recovery, Mitigation, and Reconstruction. *U.S. Geological Survey Professional Paper*, *1553-D*.

Patton-Mallory, M., Wolfe, R. W., Soltis, L. A., & Gutkowski, R. M. (1985). Light-Frame Shear Wall Length and Opening Effects. *Journal of Structural Engineering*, *111*(10), 2227-2239.

Petak, W., & Elahi, S. (2000). The NORTHRIDGE EARTHQUAKE, USA and its ECONOMIC AND SOCIAL IMPACTS. *Euro Conference on Global Change and Catastrophe Risk Management Earthquake Risks in Europe, IIASA, Laxemburg, Austria*.

Petrie, E. M. (2007). *Handbook of adhesives and sealants* (2nd ed.). McGraw-Hill.

Primeaux II, D. J. (1989). Spray Polyurea Versatile High Performance Elastomer for the Polyurethane Industry. In *Proceeding of the 32nd annual technical/marketing conference* (pp. 126–130). Presented at the San Francisco.

Qu, B., Bruneau, M., Lin, C. H., & Tsai, K. C. (2008). Testing of Full-Scale Two-Story Steel Plate Shear Wall with Reduced Beam Section Connections and Composite Floors. *Journal of Structural Engineering*, *134*(3), 364-373.

Residential Building Committee. (2006). Cripple Wall Fact Sheet. Earthquake Engineering Research Institute. Retrieved from http://eerinc.org/old/quake06/best_practices/fact_sheets/cripple_wall.pdf

Rihal, S.S. (1992). Performance and behavior of non-structural building components during the Whittier Narrows, California (1987) and Loma Prieta, California (1989) earthquakes: selected case studies. *Report No. ATC-29, Proc. seminar and workshop on seismic design, performance of equipment, and nonstructural elements in buildings and industrial structures*, ATC, Redwood City, CA, 33-38.

Risk Management Solutions, Inc. (2011). *Estimating Insured Losses from the 2011 Tohoku, Japan Earthquake and Tsunami* (RMS Special Report).

Rosato, D. V. (2004). *Reinforced plastics handbook* (3rd ed.). Oxford□; New York: Elsevier Advanced Technology.

Salenikovich, A. J., & Dolan, D. J. (2003) The Racking Performance of Shear Walls with Various Aspect Ratios. Part I. Monotonic Tests of Fully Anchored Walls. *Forest Products Journal*, *54*(10), 65-73.

Salenikovich, A. J., Dolan, D. J., & Easterling, W. S. (1999). *Monotonic and Cyclic Tests of Long Steel-Frame Shear Walls with Openings* (Report No. TE-1999-001, The American Iron and Steel Institute, Washington, DC).

Sankaranarayanan, R., & Medina, R.A. (2006). Evaluation of peak acceleration demands of nonstructural components exposed to near-field ground motions. *Proc. 1st European Conference on Earthquake Engineering and* Seismology, Genva, Switzerland, Paper 1248.

Seaders, P., Miller, T. H., & Rakesh, G. (2009). Performance of Partially and Fully Anchored Wood-Frame Shear Walls Under Earthquake Loads. *Forest Products Journal*, *59*(5), 42.

Serrette, R., Encalada, J., Hall, G., Matchen, B., Nguyen, H., & Williams, A. (1997). *Additional Shear Wall Values for Light Weight Steel Framing* (No. LGSRG-1-97). Santa Clara, California: Steel Framing Alliance.

Shishkin, J. J., Driver, R. G., & Grondin, G. Y. (2009). Analysis of Steel Plate Shear Walls Using the Modified Strip Model. *Journal of Structural Engineering*, *135*(11), 1357-1366.

Singh, M.P., Moreschi, L. M., Suarez, L. E., & Matheu, E.E. (2006). Seismic Design Forces. I: Rigid Nonstructural Components. *Journal of Structural Engineering*, *132*(10), 1524-1532.

Singiresu, S. R. (2003). *Mechanical Vibration. 4th ed*. Prentice Hall, New Jersey.

Sinha, A. & Gupta, R. (2009). Strain Distribution in OSB and GWB in Wood-Frame Shear Wall. *Journal of Structural Engineering*, *135*(6), 666-675.

Soong, T.T., Yao, G.C., & Lin, C.C. (2000). Near-fault seismic vulnerability of nonstructural components and retrofit strategies. *Earthquake Engineering and Engineering Seismology*, *2*(2), 67-76.

Spencer, B.F. & Nagarajaiah, S. (2003). State of the art of structural control. *Journal of Structural Engineering*, *129*(7), 845-856.

Symans, M. D., & Constantinou, M. C. (1999). Semi-Active Control System for Seismic Protection of Structures: a State-of-the-Art Review. *Engineering Structures*, *21*, 469–487.

Tachikawa, M. (1983). Trajectories of Flat Plates in Uniform Flow with Application to Wind-Generated Missiles. *Journal of Wind Engineering and Industrial Aerodynamics*, *14*, 443-453.

Taerwe, L. (1995). Non-metallic (FRP) reinforcement for concrete structures: Proceedings of the second international RILEM symposium (FRPRCS-2), Ghent, 23-25 August 1995. London: E. & F.N. Spon.

Tamura, Y. (2009). Wind-Induced Damage to Building and Disaster Risk Reduction. *Proceeding of the Seventh Asia-Pacific Conference on Wind Engineering, November 8-12, 2009*. Taipei, Taiwan.

Thippeswamy, H. K., GangaRao, H. V. S., & Craigo, C. (2000). Review of Bridge Decks Utilizing FRP Composites in the United States. In *Condition Monitoring of Materials and Structures* (pp. 110–119). American Society of Civil Engineers. Retrieved from http://ascelibrary.org/doi/abs/10.1061/40495%28302%299

Thorburn, J. L., Kulak, G. L., & Montgomery, C. J. (1983). Analysis of Steel Plate Shear Walls. *Structural Engineering Report No. 107*, Department of Civil Engineering, University of Alberta, Edmonton, Alberta, Canada.

Timler, P. A. & Kulak, G. L. (1983). *Experimental Study of Steel Plate Shear Walls* (Structural Engineering Report No. 114, Department of Civil Engineering, The University of Alberta, Edmonton, Alberta).

Tuakta, C. (2005, June). *Use of Fiber Reinforced Polymer Composite in Bridge Structures*. Massachusetts Institute of Technology.

Tuomi, R. L., & McCutcheon, W. J. (1978). *Racking Strength of Light-frame Nailed Walls*.

Van de Lindt, J. W. (2004). Evolution of Wood Shear Wall Testing, Modeling, and Reliability Analysis: Bibliography. *Practice Periodical on Structural Design and Construction*, *9*(1), 44–53.

Van Den Einde, L., Zhao, L., & Seible, F. (2003). Use of FRP composites in civil structural applications. *Construction and Building Materials*, *17*(6–7), 389–403. doi:10.1016/S0950-0618(03)00040-0.

Villaverde, R. (1996). Earthquake resistant design of secondary structures: a report on the state-of-the-art. *Proc. 11th World Conference on Earthquake Engineering*, Paper No. 2013.

Villaverde, R. (1997a). Method to improve seismic provisions for nonstructural components in buildings. *Journal of Structural Engineering*, *123*(4), 432-439.

Villaverde, R. (1997b). Seismic design of secondary systems: state-of-the-art, Method to improve seismic provisions for nonstructural components in buildings. *Journal of Structural Engineering*, *123*(8), 1011-1019.

Villaverde, R. (2005). Approximate Procedure for the Seismic Nonlinear Analysis of Nonstructural Components in Buildings. *Journal of Seismology and Earthquake Engineering, 7*(1), 9-24.

Villaverde, R. (2006). Simple method to estimate the seismic nonlinear response of nonstructural components in buildings. *Engineering Structures, 28*(8), 1209-1221.

Weineman, S. A. & Rajagopal, K. R. (2000). Mechanical Response of Polymers: An Introduction. *The Press Syndicate of the University of Cambridge*, Cambridge, United Kingdom.

White, K. B. D., Miller, T. H., & Gupta, R. (2009). Seismic Performance Testing of Partially and Fully Anchored Wood-Frame Shear Walls. *Wood and Fiber Science, 41*(4), 396-413.

Xu, X., & Mishra, S. K. (2004). Structural control with emphasis on nonstructural components. In *Seminar on Seismic Design*. Presented at the Performance and Retrofit of Nonstructural Components in Critical Facilities.

Yin, Y., &Li, Y. (2011). Loss Estimation of Light-Frame Wood Construction Subjected to Mainshock-Aftershock Sequences. *Journal of Performance of Constructed Facilities, 25*(6), 504-513.

Zhang, Y., & Iwan, W. D. (2002). Active Interaction Control of Tall Buildings Subjected to Near-Field Ground Motions. *Journal of Structural Engineering, 128*(1), 69-79.

APPENDIX A

OBSERVATIONS FROM CARBONFLEX SHEAR WALL TESTS

Walls Subjected to Loads Perpendicular to the Walls (PPW)

No severe damage could be observed from all specimens. However, studs of the wall sheathed by plywood were pulled out a little bit from both top and sill plates. The plywood sheathed wall provides the least maximum load and the CarbonFlex fully wrapped wall provides the highest maximum load. However, the 1 ft CarbonFlex joint wraps provided the maximum load capacity per square inch of CarbonFlex material. Therefore, the 1 ft joint wraps should be used in the wall subjected to the perpendicular loads.

Walls Subjected to Loads Parallel to the Walls (PLW)

Dummy wall. After the MPD test, a few nails at both bottom corners were pulled out. The plywood panels were not detached from the wall. After the HPD test, severe damages were observed. Most of the nails at the sill plate were pulled out. One of the plywood sheets was detached.

Plywood shear wall number 1 (PW1). In the LPD test, no major damage could be observed. However, the rotation of all plywood sheets could be seen as well as nails at the corners of each sheet. Rotation of the plywood and the nails enlarged diameter of the nails' holes by about 1/16 inch. Some nails at the middle of the wall were pulled out about 1/4 inch. The MPD record created a lot of damages and rotation of plywood sheets. One of the Simpson HTT5 hold down was completely pull out. Three nails at the center of the wall were pulled out. Four nails at the bottom right corner (the far edge from the actuator) were also pulled out. One of them was pulled out completely. At this corner, the twenty four inches long crack parallel to the sill plate could be seen on the plywood sheets. The wall was also tested be the HPD record. Severe damages could be observed

especially at the bottom corner near the actuator. Both Simpson HTT5 hold downs were completely pulled out at the wall drift about 4.9 inches following by lifting up and then pulling out of couple studs near the actuator. Half of the sill plate (actuator side) was broken resulting in more nails pull out at the sill plate. The peak load from the test is 9023.4 lbs. This results indicating that the better anchoring method for the hold downs would be needed and the lag screws were not proper for the hold downs.

Plywood shear wall number 2 (PW2). No major damage could be observed from the LPD test. However, some nails at the bottom edges were pulled out about 1/4 inch. There was no damage at both hold downs. For the MPD test, the sill plate was dramatically damaged. Because the hold downs (concrete blocks) were anchored to the sill plate, the over turning moments were transferred to the sill plate instead of the ground. Large bending occurred at both ends of the sill plate following by the broken of the sill plate. After sill plate broken, most of the nails at the bottom edge were pulled out. The maximum displacement and load of this wall are 3.721 inches and 8312.5 lbs, respectively.

CarbonFlex strip bracing wall (CFSBW). No damage could be observed from the LPD test. For the MPD test, two of the strips were broken resulting in the suddenly dropping of the load. The uplift of the sill plate at hold down locations was observed.

CarbonFlex strip bracing with plywood wall (CFSPW). For the LPD test, no damage or nail pulled out could be detected. For the MPD test, one of the strips was broken at the bottom corner of the wall. Some nails along the sill plate were pulled out. For the HPD test, three more strips were broken near the sill plate. Three studs near the actuator were pulled out. The bottom plywood panel was detached from the sill plate.

CarbonFlex fully wrapped wall number 1 (CFFW1). The wall was not damaged in the LPD test. For the MPD test, after the peak load, the wall could sustain the load at higher level than the plywood shear wall. In addition, couple studs were pulled out. The sill plate was broken due to the high over turning moment that transferred to the sill plate. Therefore, the method to transfer the load to the strong ground was needed.

CarbonFlex fully wrapped wall number 2 (CFFW2). No damage could be observed from the LPD test. For the MPD tests, there were some short cracks occurred at studs and the panel along the diagonal lines. For the HPD test, severe damages occurred at the top corner far away from the actuator. A 34 inches long crack of CarbonFlex could be seen at the bottom corner near the actuator. The double top plate was shear off from three studs. Two interior studs were broken at the top. CarbonFlex panel detached from the studs along the diagonal line. A lot of wood stuck with the CarbonFlex panel at the detached areas.

CarbonFlex fully wrapped wall number 3 (CFFW3). There was no damage from the LPD test. For the MPD test, end studs were lifted up a little bit. However, U and L-wraps at the studs could hold the studs. After the test, there was no damage at U and L-wraps, no stud was pulled out. Although some locations of CarbonFlex panel detached from interior studs, from observation, there were some wood attached to the CarbonFlex panel at the detaching locations. This indicated that the failure occurred at the wood level not at the bonding between CarbonFlex and wood. The maximum detachment length was about 3 ft For the HPD test, The U and L-wraps at the end stud near actuator were broken and the end stud was pulled out. After that, CarbonFlex panel and U-wrap at interior studs were sheared off at the bottom edge of the wall. Three more interior studs were

pulled out. This indicated that the U and L-wraps were not strong enough to hold the studs and the Simpson hold downs would be needed.

CarbonFlex fully wrapped with plywood wall (CFPW). There was no damage from the LPD test. However, the wall failed in the MPD test. Large cracks could be seen at the top of three middle studs. Nails attaching plywood to three studs at the top of the panel near actuator were pulled out. Plywood and CarbonFlex were broken and detached from the wood frame at the top corner near actuator. The crack length is about 32 inches long. The double top plate was shear off from four studs.

CarbonFlex fully wrapped with opening wall (CFOW). No damage could be observed from both LPD and MPD tests. For HPD test, a lot of tension and buckling strips could be seen on the panel. CarbonFlex detached from two middle studs. One of the studs was broken at the top. The frame members of the opening had a lot of rotation during the test. However, no damage was seen around the opening after test. The top plate was shear off from three studs at the far side from actuator. Cracks were seen at the CarbonFlex panel at the top of the wall. There was no damage at the sill plate and the bottom of the panel.

The common failure mode that occurred in CFFW2, CFPW and CFOW is the top plate shear off. This might be the result of adding CarbonFlex strips in between studs at the bottom of the wall. Therefore, the bottom of the panel is stronger than the top. Hence, CarbonFlex panel broke at the top first. When the top of CarbonFlex panel broke, the exceeded energy was dissipated through the nails connecting top plate to studs causing the top plate pulled out and sheared off. Therefore, CarbonFlex strips should be required at both top and bottom of the wall.

Wood-Framed Structures

Plywood house. No damage could be observed from the LPD test. For the MPD test, nails at the top and middle of the side-wall were pulled out. The maximum pulled out length was about one inch which created gaps between plywood sheets and studs at the nails pulled out areas. For the window-wall, most of the damages occurred at the middle of the wall. Nails at the bottom corner of the top plywood sheet were pulled out resulting in the detachment of the sheet.

After the MPD test, the house was tested by the HPD record. As expected, more damages were observed from both side and window walls. On the side-wall, more nails were pulled out resulting in almost fully detachment of the top plywood sheet. After detaching of the top plywood sheet, the bottom plywood sheet provided a rigid support for the studs. Therefore, the top part of studs acted more like cantilever beams resulting in severe damages (broken) at the top part of studs

On the window-wall, the top plywood sheet also detached. Most of damages occurred along the edges of the plywood sheets. In addition, more damages were observed along the edges of the window. Both stiffness and load capacity were decreased dramatically after partially detachment of the top plywood sheet and pulling out of the nails on both side and window-walls. Therefore, after large displacement, the plywood shear wall cannot sustain the load which might lead to the “soft-story” problem. After the displacement of 5 inches, more nails were pulled out and more detachment of plywood occurred resulting in 64 percent decreasing of the load. Subsequently, the studs were broken at displacement about 6.2 inches resulting in 80 percent decreasing of the load compared to the first cycle.

CarbonFlex-wrapped house. Due to the high load capacity of CarbonFlex-wrapped house, it could be tested only by the LPD and MPD records (the load exceeded the capability of the actuator when the displacement was greater than 4 inches). Initially, the stiffness of the house was high and the load reached the capacity of the actuator (24000 lbs) at displacement about 3 inches.

To decrease stiffness so that the house could be tested, the quasi-static test was conducted. The quasi-static test consists of 36 cycles. After five cycles, the stiffness was reduced. Then, the maximum displacement was increased from the previous cycles until the maximum displacement of 3.78 inches could be reached in the 33^{th} cycle. After that, the house was tested with the sin wave having 3.89 inches amplitude for three more cycles. Although the house was subjected to 36 cycles having high-load, the house still be very strong and could sustain a very high strength. No debonding, detaching, and damage of CarbonFlex panel could be observed. After 36 cycles of quasi-static test, the MPD test was conducted. The results show that stiffness of CarbonFlex house was little to none decreased. This is evidence showing that CarbonFlex helps sustain strength of the structure. Moreover, there was no detaching occurred at the interface between CarbonFlex and the studs and a lot of tension and buckling strips occurred on the CarbonFlex. This implies that energy was dissipated through the body of CarbonFlex resulting in less energy dissipated through the connectors, such as nails, as in the conventional plywood shear walls. Consequently, CarbonFlex can help prevent the soft-story problem for the low-rise building during the seismic events.

APPENDIX B

OBSERVATIONS FROM DEBRIS IMPACT TESTS

Wall Panel Number 1

The wall was shot 3 times with projectile missiles traveling at 100 mph. The first missile was shot to the upper right corner of the wall (6 inches from the top and 14 inches from the right edge of the wall) which is considered as a shear zone. The missile penetrated 1.5 inches into the wall and bounced back. Some 8d nails on the OSB. on the right edge stud (close to the target) popped out. The second target was located at the middle of the wall (24 in. from the top and 24 in. from the right edge) which is considered as a zone that maximum bending occurs. The missile created a 4.875 inches indentation on the wall but did not perforate the wall (no penetration through the OSB. layer). There was no damage on the witness paper. More 8d nails on the back side were popped out. The last missile was shot to the target near lower left corner (8 inches from the left edge and 28 inches from the top). The missile penetrated about 1.5 inches into the wall and bounced back. More 8d nails on the OSB were popped out, especially on the left edge stud. No major damage was observed on the back side of the wall. The witness paper was not damaged. After 3 missile shootings, the wall passed the impact test for maximum tornado speed.

Wall Panel Number 2

The wall number 2 which has the same properties as the wall number 1 was shot by the projectile at 100 mph. The target was located at about 3 inches away from one of the interior studs (13.5 inches from the left edge, 12 inches from the top). The missile penetrated into the wall but did not penetrate through the CarbonFlex layer. Because the target was close to the stud, the stud hit the back sheathing material generated a permanent displacement and fracture on the OSB. However, the displacement was less

than 3 inches and no damage was observed on the witness paper. Therefore, the wall "passed" the impact test.

Wall Panel Number 3

The wall was shot two times by the missiles at 100 mph. The first target location was 1 ft from the left edge and 1 ft from the top. The missile stuck out about 6 inches from the OSB. The second impact was also shot at 100 mph. The target was located at the upper right corner of the wall in the shear zone. The missile perforated the wall and passed the OSB. about 2.5 inches. Therefore, the wall failed the test at 100 mph missile speed.

After the second shot, the wall was shot again by a lower missile speed (90 mph). The third shot was located at the lower right corner of the wall (31.5 inches from the top and 6 inches from the right edge). The missile penetrated 1.5 inches into the wall but did not penetrate through CarbonFlex layer. Some nails on OSB. popped out. The forth missile was shot to the bending zone (25 inches from the top and 22 inches from the right edge). The missile penetrated 1.75 inches into 3/4 inch plywood. No damage of CarbonFlex layer could be seen from the outside. More 8d nails on the OSB. popped out. The fifth missile was aimed to the lower left corner, near the left interior stud (30 inches from the top and 15 inches from the left edge). The missile penetrated into the wall about 1.375 inches deep and then bounced back. Cracks and a permanent deformation were observed on the OSB. near the interior stud. The damages occurred because some parts of the missile hit the stud and the load was transferred directly to the OSB. After 3 shots at 90 mph, no major damage was observed on the back side. The witness paper behind the wall was not damaged. Although there was a permanent deformation on the back

sheathing material, the deformation was smaller than 2 inches. No missile perforated the wall. Therefore, this wall passed a debris impact test for the tornado with 200 mph ground wind speed.

Wall Panel Number 4

This wall was shot by 3 missiles at 100 mph. The first missile was shot to the left shear zone of the wall. The missile penetrated 1.5 inch into the wall. A small deformation was observed at the OSB. The second impact was aimed to the bending zone of the wall. The missile penetrated 1.5 inch into the wall. Three 8d nails popped out about 1/4 inch from the OSB. No damage or deformation was detected on the back side of impact location. The third impact was located at the upper right corner of the wall. The missile penetrated 2 inches from the impact face. No damage was found on the back side. Two 8d nails on the right edge stud popped out about 1/2 inch from the OSB. After three impacts, there was no major damage. The permanent deformation from the first impact was less than 2 inches. The witness paper was not damaged. No missile perforated the wall. Therefore, the wall passed a debris impact test for the tornado with 250 mph ground wind speed.

Wall Panel Number 5

This wall has the same t_c but thinner than wall number 3. Therefore, the strength of this wall was expected to be lower than that of wall number 3. Therefore, the wall was shot by three missiles at 90 mph. The first missile was shot to the shear zone near the right edge of the wall. The missile penetrated 3.5 inches creating a small permanent deformation on the OSB. From observation, the CarbonFlex layer was damaged. In addition, three 8d nails popped out about 1/4 inch from the OSB. The second impact hit

in the bending zone of the wall. The missile penetrated 1 inch into the wall and bounced back. No damage on the back side and CarbonFlex layer was observed. The third missile was shot to the area near the left interior stud. The missile bounced back. Three 8d nails on the interior stud popped out. No major damage could be seen neither on the OSB. nor witness paper. Therefore, the wall passed a debris impact test for the tornado with 200 mph ground wind speed.

Wall Panel Number 6

In this wall, carbon fiber was used instead of CarbonFlex. The first and second impacts were shot at 100 mph and the third impact was shot at 90 mph. The first missile was aimed to the upper left corner in the shear zone. The missile perforated the wall and stuck out 15.625 inches from the OSB. The second shot was aimed at the middle of the wall in the bending zone. The missile penetrated 2.125 inches into the wall but did not perforate the wall. The third missile was shot to the upper right corner of the wall in the shear zone. The missile perforated the wall and stuck out 28.125 inches from the OSB. Many of carbon fibers were pulled out with the missile. The wall was severe damaged.

Door Assembly Number 1

The first impact was shot to the wall near the handle (41.5 inches from the top of the door and 8.5 inches. from the handle). After the impact, the door was opened. All hardware (3 deadbolts and a handle) were severe damaged. The top and the bottom deadbolts were bent more than the middle one. In addition, the strike plates on the door frame were severe damaged. 2 inches permanent deformation was also observed on the back of the door at the impact location. Because the door opened after the impact, this door assembly failed the missile impact test.

The wall section of the door assembly was also shot. The first missile was shot to the upper left corner of the wall in the shear zone at 100 mph. The missile bounced back. The impact created 1/2 inch permanent deformation on the impact face but not perforated the wall. There was no damage on the back side. However, from the observation, the missile might hit one of the interior studs. Therefore, the other impact was shot to the bending zone of the wall at 100 mph. The missile perforated the wall and went through the whole length. From this test results, it could be concluded that, for the impact resistance design, CarbonFlex needs at least 2 layers, 0º/90º directions of the reinforcement. In addition, the CarbonFlex layer should be attached to the studs and covered by 2-3/4 inch plywood. This allows the polymer constituent of CarbonFlex to be sprayed on both sides providing more energy dissipation and ductility.

Door Assembly Number 2

The door was welded to the door frame so that the improvement of the door assembly could be evaluated and the future strategy of using CarbonFlex with the door could be studied. The door skin was made from 16 gauge steel. This door was preliminary tested by the manufacturer without CarbonFlex. The results showed that the missile perforated and stuck with the door.

In this test, the door was shot at the middle point. The missile traveled at 100 mph. The missile created 1 inch permanent deformation at the impact location. No perforation was observed. This shows the great energy dissipation of CarbonFlex. However, the delamination of CarbonFlex was observed near the middle hinge of the door.

Door Assembly Number 3

This door was also welded to the door frame. The door skin was made from 18 gauge steel. The door was shot at the middle point. The missile created 1.375 inches permanent deformation at the impact location. Greater delamination than that of door assembly number 2 was observed in the same area. In addition, a 7 inches long horizontal crack of the CarbonFlex could be seen at the delamination location.

APPENDIX C

A CALCULATION EXAMPLE OF RESPONSE MODIFICATION FACTOR (R-FACTOR) FOR CARBONFLEX SHEAR WALLS

Figure C1 shows the force-displacement curve from the test of fully wrapped CarbonFlex shear wall. The yielding of the wall occurred at 1339.84 lbs as shown in figure C1. The results were simplified and shown in figure C2.

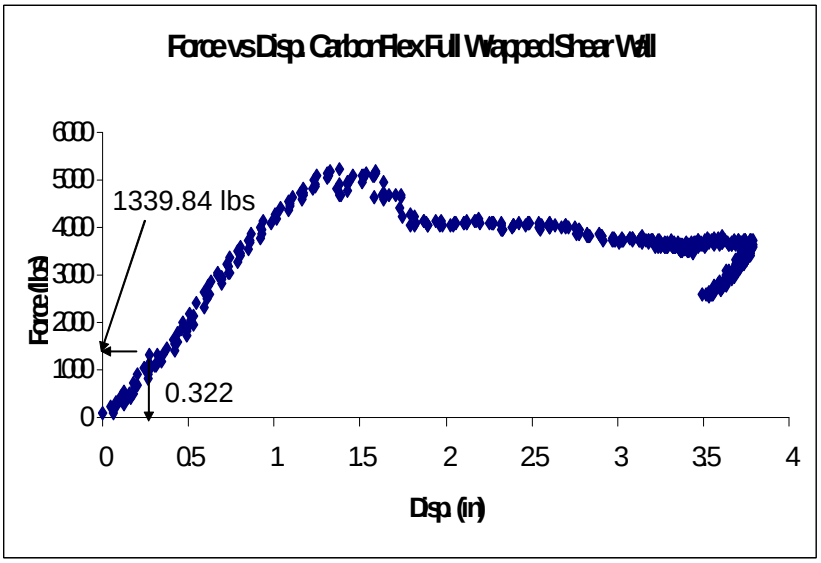

Figure C1. Force-displacement curve of CFFW1.

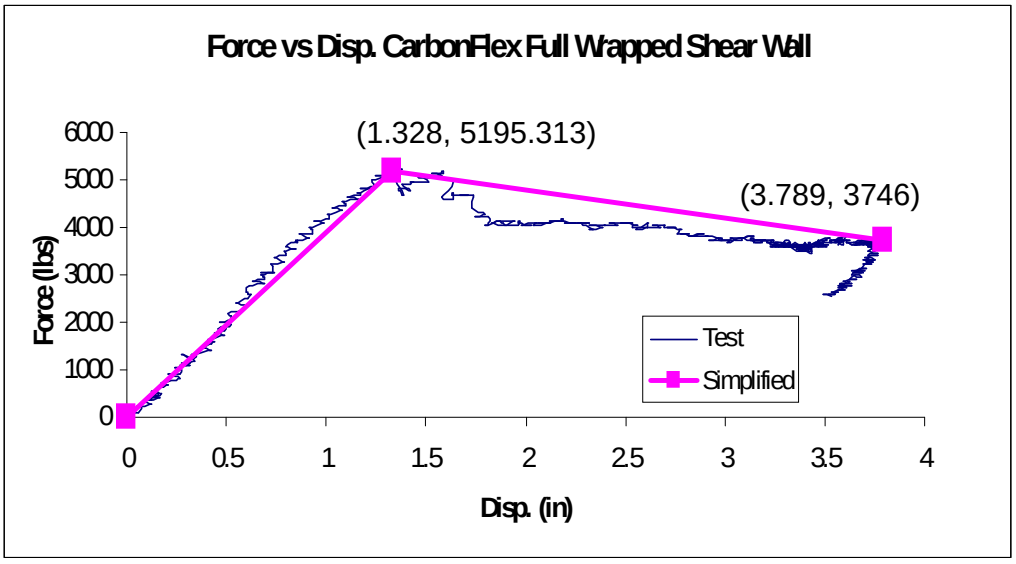

Figure C2. Simplified test results.

As mention earlier, F_u needs to be calculated before R-factor. Fu can be calculated by equating area OAB to area OCDE as shown in figure C3.

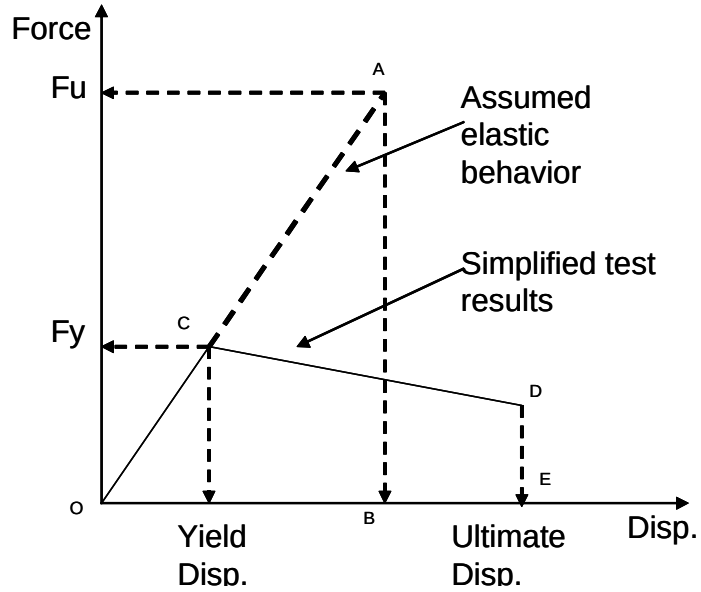

Figure C3. Calculation of F_u.

Area OAB = ½ x F_u x OB. There are 2 unknowns which are F_u and OB. However, from Fy/yield Disp. = F_u/OB, therefore, OB = F_u x yield disp./F_y. From figure C2, the area under the simplified curve can be calculated as:

1/2 x (5195.313x1.328) + ½ x (3.789-1.328) x (5195.313+3746) = 14451.97

By setting area OAB = area OCDE, 1/2 x Fu^2 x yield disp./F_y = 14451.9

$$F_u = \sqrt{\frac{14451.97 * F_y * 2}{yielddisp.}} = \sqrt{\frac{14451.97 * 1339.844 * 2}{0.322}} = 10966.75$$

From $R = \frac{F_U}{F_y}$, R = 10966.75/1339.844 = 8.185

Therefore, according to equal energy method, the R-factor for CFFW1 is 8.185. By using the same method, R-factor of CFFW2 is 8.25.